2008

# The Development of an in Vivo Spinal Fusion Monitor Using Microelectromechanical (Mems) Technology to Create Implantable Microsensors

Lisa Anne Ferrara
*Cleveland State University*

**Abbreviated Title:**

**AN IN VIVO SPINAL FUSION MONITOR USING (MEMS) TECHNOLOGY**

# THE DEVELOPMENT OF AN IN VIVO SPINAL FUSION MONITOR USING MICROELECTROMECHANICAL (MEMS) TECHNOLOGY TO CREATE IMPLANTABLE MICROSENSORS

**LISA A. FERRARA**

Bachelor of Science in Biology
Bridgewater State College
June, 1985

Bachelor of Science in Electrical Engineering
University of Lowell
June, 1989

Masters of Science in Neuroscience
Syracuse University
December, 1996

Submitted in partial fulfillment of requirements for the degree

**DOCTORATE OF ENGINEERING IN APPLIED BIOMEDICAL ENGINEERING**

at the

Cleveland State University

May, 2008

This dissertation has been approved

for the Department of **CHEMICAL AND BIOMEDICAL ENGINEERING**

and the College of Graduate Studies by

Thesis/Dissertation Committee Chairperson, *Shuvo Roy, Ph.D.*

Department of Biomedical Engineering, Cleveland Clinic

*Aaron Fleischman, Ph.D.*

Department of Biomedical Engineering, Cleveland Clinic

*Brian Davis, Ph.D.*

Department of Biomedical Engineering, Cleveland Clinic

*George Chatzimavroudis Ph.D.*

Department of Chemical and Biomedical Engineering, Cleveland State University

*Kathleen Little, Ph.D.*

Department of Health, Physical Education, Recreation and Dance

Cleveland State University

*This work is dedicated to my two best friends, my mother and my husband, for giving me the strength, support, and unconditional love to complete this.*

**ACKNOWLEDGEMENTS**

1. **The Committee Members**
2. **The Biological Resources Unit at The Cleveland Clinic**
3. **The BioMEMS Laboratory at The Cleveland Clinic**
4. **Thomas Bauer, M.D., Ph.D.**
5. **Edward Benzel, M.D., F.A.C.S.**
6. **Marie Bondea, M.A.**
7. **Maddy Coquillette**
8. **Stan Dannemiller, D.V.M.** and **Jori Leszczynski, DVM, DACLAM**
9. **Jeremy Dunning, M.S.**
10. **Bacem Georges from DePuy Spine, Inc.**
11. **Vijay Goel, Ph.D.**
12. **Illya Gordon, B.S.**
13. **Ryan Milks, B.S.B.E.**
14. **Kimberly Powell, Ph.D.**
15. **Richard Schlenk, M.D.**
16. **Daisuke Togawa, M.D., Ph.D.**
17. **James Wickersham, B.S.M.E.**
18. **Christopher Zorman, Ph.D.**

**THE DEVELOPMENT OF AN IN VIVO SPINAL FUSION MONITOR USING MICROELECTROMECHANICAL (MEMS) TECHNOLOGY TO CREATE IMPLANTABLE MICROSENSORS**

**LISA A. FERRARA**

## ABSTRACT

Surgical fusion of the spine is a conventional approach, and often last alternative, to the correction of a degenerative painful spinal segment. The procedure involves the surgical removal of the intervertebral disc at the problematic site, and the placement of a bone graft that is commonly harvested from the patient's iliac crest and placed within the discectomized space. The surrounding bone is expected to incorporate and remodel into the bone graft to eventually provide an immobilized site. Spinal instrumentation often accompanies the bone graft to provide further immobility to the targeted site, thus augmenting the fusion process. However, the status of a fusion and the incorporation of bone across a destabilized spinal segment are often difficult for the surgeon to assess. Radiographic methods provide static views of the fusion site that possess excessive limitations. The radiographic image cannot provide the surgeon with information regarding fusion integrity when the patient is mobile and the spine is exposed to multiple motions. Fortunately, technological advances utilizing microelectromechanical system technology (MEMS) have provided insight into the development of miniature devices that exhibit high resolution, electronic accuracy, miniature sizing, and have the capacity to monitor long-term, real-time *in vivo* pressures and forces for a variety of situations. However, numerous challenges exist with the utilization of MEMS devices for *in vivo* applications.

This work investigated the feasibility of utilizing implantable microsensors to monitor the pressure and force patterns of bone incorporation and healing of a spine fusion *in vivo*.

The knowledge obtained from this series of feasibility test using commercially available transducers to monitor pressures and forces, will be applied towards the development of miniature sensors that utilize MEMS technology to monitor real-time, long-term spine fusion in living subjects. The packaging, and radiographic, and sterilization characteristics of MEMS sensors were evaluated for the future application of long-term human implantation for real-time, accurate measurement of the loads during bone healing.

## TABLE OF CONTENTS

## LIST OF TABLES

### CHAPTER III



### CHAPTER IV



### CHAPTER V



### CHAPTER VI



### CHAPTER VII

## LIST OF FIGURES

### CHAPTER II



### CHAPTER III

**CHAPTER IV**

**Chapter 5**

**CHAPTER VI**

**CHAPTER VII**



**CHAPTER VIII**

# CHAPTER I

# INTRODUCTION

## 1.1 The Spinal Market

Back pain is the second most common medical condition for which individuals seek treatment, accounting for more than 50 million physician office visits annually in the United States (U.S.) [52] It is estimated that more than 75% of the entire U.S. population will be affected by low back pain over the course of their lifetime. The spinal market in the U.S. is a $12 billion market, with spine implants comprising approximately a $3 billion sub-segment.[52] In 2006, more than $1.8 billion was spent on spinal fixation and dynamic stabilization devices in the U.S.[52,78] Sales of these products are expected to grow at a compound annual rate of 10.4% reaching more than $3.2 billion in the year 2012. Although back pain requiring spinal fusion is not life threatening, and the resulting surgical caseload is small when compared to the percentage of back pain patients, it is a major cost burden on the American healthcare system.[77,78]

## 1.2 Clinical Relevance

Spinal surgery is often a final alternative to spinal stabilization and relief of pain. Bone graft fusion with accompanying spinal instrumentation systems is a conventional surgical technique used to stabilize the spine. The eventual goal of this bone graft and spinal

instrumentation construct is to create a balanced environment where the spinal instrumentation is used to initially function as the load bearing element that immobilizes the fusion segment during the early unstable stages of bone grafting and healing.[6,7,59,83] However, the success of a fusion across a destabilized spinal segment is often difficult for the surgeon to assess. Numerous *in vitro* and *in vivo* studies have been conducted to biomechanically assess the surgical fusion procedure and bone fusion integrity.[6,7,34,59,92,121] Currently, conventional methods to examine bony incorporation include radiographic evaluation of the fusion, Magnetic Resonanic Imaging (MRI) and Computed Tomography (CT), and patient history. Yet, discrepancies exist between radiographic evidence and more direct means of fusion assessments, such as operative exploration, biomechanical testing, and histological techniques that will stain for newly developed bone. The disadvantage of these direct methods is that they can only be used postmortem. Previous studies[11,14] have shown that mechanical and histological maturation of the fusion mass occurs much earlier than what has been demonstrated radiographically. Kanayama et al.[59] reported maturation of a posterolateral fusion mass to occur at approximately 8 weeks in sheep, whereas radiographic and histological evaluation determined maturation to occur at 16 weeks. Histological evidence indicated the fusion site to contain mainly woven bone at 8 weeks and entire trabeculation at 16 weeks. Contrary to this observation was the biomechanical evidence, which demonstrated the ability of the fusion mass to bear sufficient load at 8 weeks, indicating that mechanical strength had been achieved prior to full mineralization. Blumenthal and Gill[11] confirmed that plain radiographs often led to a 20% underestimation of the fusion grade. Furthermore, Brodsky et al.[14] reported that the accuracy of radiographic techniques to determine fusion status decreased with multiple spinal levels. These authors also discovered that on surgical examination, the fusion mass moved independent of the underlying vertebrae, indicating a non-union at the vertebral endplates.[11,14] Thus, the use of conventional radiographic techniques cannot provide the surgeon with the dynamics of the fusion mass, adequate visualization of bone incorporation into the host bone (i.e. vertebral

endplates), the mechanical strength capability of the fusion mass, and the real-time bone remodeling scenario. Radiographic measures are greatly limited in fusion assessment by providing a discrete snapshot of the fusion to the surgeon, which, in turn, may provide a false positive or false negative.

Bony incorporation of the fusion graft usually occurs within 4-6 months after surgery in the human spine. However, a patient's post-operative assessment typically occurs at 2-3 month intervals. These intermittent patient evaluations, which are often accompanied by plain radiographs of the fusion site, cannot provide the physician with sufficient knowledge of the bone ingrowth across the fusion graft during the course of the bone healing, and are frequently misleading. Radiographic imaging of bone healing provides a static solution to a dynamically evolving process. Often the patient's recurring pain post-operatively may not correlate with the radiographic assessments conducted by the radiologist and surgeon. If a patient returns with post-operative pain, a pseudarthrosis (non-fusion) may exist, but may not be detectable via plain radiographs. Possible ramifications of a pseudarthrosis include an increased risk of early failure and loss of fixation due to excessive stress and bending moments placed onto the load-bearing instrumentation. Placement of the patient in flexion and extension for radiographic imaging still limits the surgeon from viewing the dynamics of the fusion, especially at the host bone interface. Furthermore, numerous variables factor into the patient's well being following surgery. Since pain is quite subjective and radiographic imaging techniques cannot provide the entire story of the post-surgical status, diagnostic and therapeutic solutions may be inaccurately prescribed to alleviate the patients pain, resulting in further unnecessary repeat surgical stabilization procedures. Therefore, it is understandable that under these circumstances, uncertainty regarding fusion status usually prevails. If fusion status could be assessed continuously during the postoperative course, the process of determining the need for a second surgical procedure is simplified. Finally, knowledge of the biomechanics of the entire fusion construct, that is the spinal

instrumentation systems and bone graft, would further enhance the surgical strategy for the patient and improved patient outcome, while minimizing additional surgical costs due to second and third surgical revision procedures.

Unfortunately, *in vitro* biomechanical testing using cadaveric tissue cannot provide the continuous healing scenario of remodeling bone. Currently, *in vitro* biomechanical testing, where cadaveric tissue is prepared and tested under various axial and torsional loading parameters on a hydraulic testing apparatus has been the gold standard for providing biomechanical data. However, the use of non-living tissue introduces discrepancies in results that cannot be translated to the scenario in actual spine patients. A cadaveric spine lacks surrounding musculature, and a circulating fluid environment, with a constant exposed temperature, and has begun decomposing with cellular lysis. The lack of surrounding musculature cannot accurately simulate the spinal column during physiological loading paradigms. Hence, there is a multitude of challenges that exist with current diagnostic technologies used for fusion determination that directly limits the information available to the surgeon for proper surgical strategic planning. The ability to measure biomechanical parameters such as load, stress, strain, acceleration, and displacement *in vivo* would greatly advance current medical diagnostic tools and could in turn, provide highly accurate real-time information specific to each patient. Biomechanically speaking, contact pressures obtained at the bone graft interface would yield healing pressures related to the actual loading paradigms that included mechanical contribution from the surrounding musculature and ligamentous tissue.

The ability to monitor fusion real-time *in vivo* would greatly advance the medical treatment of spinal disorders. Although many factors contribute to a successful fusion, such as lifestyle, gender, age, and tissue integrity of the patient, sensors could monitor the progression at individual etilolgies and fusions pre and post-operatively. Monitoring fusion could accurately provide information regarding the bone graft used for fusion and the spinal

instrumentation that often accompanies the bone graft for added stability and immobility to allow for bony incorporation during the initial stages of healing and remodeling. If a fusion is unsuccessful due to a pseudarthrosis at the bone graft site, the spinal instrumentation is at risk of early failure and loss of fixation due to excessive stress and bending moments placed onto the load-bearing instrumentation. Catastrophic implant failure and/or loss of fixation could cause neurologic damage to surrounding tissues. The eventual goal of the bone graft and spinal instrumentation is to create a balanced environment where the spinal instrumentation is used to initially function as the load bearing element that immobilizes the fusion segment during the early unstable stages of bone grafting and healing. If the instrumentation is too rigid, it will shield the necessary stress that the bone graft needs to initiate osteoblastic activity for new bone formation and may result in resorption of the graft.[55,131] If the instrumentation lacks adequate rigidity and applies excessive micromotion across the bone graft site, a pseudarthrosis may be inevitable. The ideal amount of micromotion necessary for a bone graft to endure for successful bony incorporation is still a mystery to surgeons and researchers.

## 1.3 Research Objectives and Study Hypotheses

### *1.3.1. Research Objective*

The objective of this research is to investigate the feasibility of using implantable microsensors to monitor the pressure and force patterns of bone healing at a fusion site *in vivo*. Conventional methods to monitor healing of the spine after surgery are based on a combination of patient history and imaging tools such as x-rays, MRI and CT. Unfortunately, these "snapshot" techniques cannot provide the patient and surgeon with accurate real-time

information on the fusion status or the possibility of spinal instrumentation failure, and can often lead to “false positives” or an inaccurate assessment of healing status.

The overall goal would be to employ microelectromechanical systems (MEMS) technology to develop a miniature, non-invasive, real-time, continuously monitoring, spine fusion status assessment system. However, initial studies using conventional transducers are required to establish a model to quantify biomechanical parameters that will contribute to the future design of a MEMS-based fusion assessment system. This study will use commercially available pressure sensors and strain gauges to obtain the essential *in vivo* pressure and force data from a bone graft and spinal instrumentation recorded during the course of bone healing.

Consequently, our **short-term** goal and focus of this dissertation is to initially determine the feasibility of implantable pressure and force sensors to monitor the changes in pressure at a bone graft interface and the forces transmitted through a stabilizing spinal implant during the bone healing process in a caprine cervical spine model. Our future **long-term** goal is to extend the sensor technology to the human spine for real-time evaluation of the bone fusion status through the development of minature, implantable wireless MEMS sensors that can be injected into the spine.

The preliminary fusion assessment system will utilize a conventional pressure transducer within a catheter and load transducers using strain gauge technology for the *in vivo* physiological measurements of the healing status at the bone graft site and the forces experienced by the spinal instrumentation used to stabilize the fusion site. The data from the implanted pressure sensors and strain gauges will be obtained telemetrically, and will determine the pressure range and trends incurred during bone incorporation of the fusion graft, and the load variations that occur with the transition from a load-bearing device to a load-sharing device.

Therefore the study hypotheses are:

(1) Load transmission along a ventral cervical spine plate and a bone graft can be measured to monitor healing status.

(2) Pressure measured at the bone graft and vertebral body endplate interfaces at a fusion site in the cervical spine will provide a mechanism to detect altered biomechanical markers during bone healing. The pressure trends during bone fusion healing will reflect the status of bone incorporation.

(3) The basic MEMS materials used to construct microsensors will prove to be safe and efficacious materials that can be sterilized and housed within a living body without incurring toxic foreign body responses.

## 1.4 Specific Aims

### *1.4.1 Specific Aim 1:* To establish a model that will potentially assess the feasibility of monitoring force transmission along a ventral cervical spine fixation system and pressure changes at the bone graft interface during fusion healing in a caprine cervical spine.

We propose to use existing commercialized sensor technology in a cadaveric caprine (goat) model to establish the feasibility of measuring force transduction transmitted along an implanted spinal plate during cervical spine fusion and the contact pressures at a bone graft interface. An *in vitro* biomechanical study was conducted to simultaneously monitor the forces along a ventral cervical plate and the pressures at a bone graft site. Ventral plating across a bone graft site is conventionally used to promote spinal fusion for stabilization of the degenerative cervical spine. Commercially available sensors were utilized in this biomechanical model to measure the force and pressure along the ventral plate and the bone graft interface. High resolution conventional strain gauges were purchased from vendors and configured as a force transducer to operate with a

commercially available telemetry system to monitor the forces transmitted across a ventral cervical spine fixation plate during bone fusion healing. The strain gauges were mounted onto conventional cervical spine instrumentation (DOC cervical spinal plate fixation system, DePuy Acromed Inc., Raynham, Massachusetts) prior to surgery and coated with Silastic (HiTec Corp., Westford, MA) and Parylene (Specialty Coating Systems, Amherst, NH). Parylene was chosen as an ideal coating as it can be applied in thin layers and is biocompatible.[60,61,63] The output leads from the strain gauges were attached to separate subcutaneously placed implanted telemetry systems (1 for the pressure transducer, and 1 for the strain gauges), which will wirelessly transmit the data to an external computer. The pressure was measured using a commercially available telemetric pressure sensor (Dataquest A.R.T. 2.2 Telemetric Pressure Catheter, Data Sciences International, St. Paul, MN) housed at the bone graft and vertebral endplate interfaces. Early bone healing was simulated in an *in vitro* manner using bone cement at the bone graft interface and the forces and pressures measured under physiological loading of the cadaveric goat spine fusion model.

### *1.4.2 Specific Aim 2:* **To apply the established load (force and pressure) detection model to a living system to determine actual performance of telemetric sensors within the harsh environment of a living system.**

The system that was developed and established through the *in vitro* study as discussed in Specific Aim 1, and was then incorporated into a living system for long term implantation and evaluation. A caprine model of similar breed and size to those used in the *in vitro* study were used to evaluate the behavior and performance of the load sensing devices during long term implantation across a fusion site of the cervical spine. Six goats were implanted with force sensors and/or pressure transducers to monitor the forces along a cervical plate and pressures at the bone graft interface during bone healing.

Both parameters were monitored immediately post-operatively and on a regular basis for a period up to 6 months. This data provided the pressure ranges and force changes that occur *in vivo* during the course of bone remodeling and fusion incorporation in the cervical spine. The optimal outcome will be the ability to measure and predict the status of bone healing through altered biomechanical parameters along the spine.

### *1.4.3 Specific Aim 3:* To assess the site-specific biocompatibility, biofunctionality, packaging and sterilization of MEMS pressure sensors and the materials used to fabricate MEMS devices through implantation into the cervical spine.

Once a feasible model had been established and it demonstrated that changes in forces and/or pressures along a bone grafted spine could be correlated with bone healing, a novel microsized biosensor employing microelectromechanical fabrication (MEMS) techniques were evaluated for safety and functionality after conventional sterilization techniques in the spine. MEMS uses silicon wafers with conventional etching processes and lithography to construct multiple microscopic devices on one wafer. However, implantation of silicon based devices into a living system has not been evaluated in the spine. The site-specific biocompatibility of silicon and related materials that are commonly used to construct MEMS pressure sensors were evaluated after implantation in the caprine cervical spine. After autopsy, gross examination, radiography, microscopy, and histological techniques were used to characterize local tissue response and possible material degradation. The functionality of microsized MEMS pressure sensors (GE Novasensor, Fremont, CA) after sterilization were evaluated before implantation in the cervical spine. Tissue responses to the pressure sensors post-implantation were evaluated and the sensor structure was examined for mechanical damage. The optimal outcome will be that the materials used to construct MEMS pressure sensors exhibit minimal degradation and do not illicit unfavorable tissue response or sensor migration.

# CHAPTER II

# BACKGROUND

## 2.1 The Mechanics of Bone Healing

Bone is a responsive viscoelastic tissue that forms in response to increased stresses, and resorbs in response to decreased stresses. This summary of Wolff's Law best describes bone remodeling as that of form following function.[131] Furthermore, the anisotropic nature of bone in the vertebral bodies of the spine is caused by new trabecular bone coinciding with the principal stress trajectories.[23,131] It has long been known that bone healing is directly related to mechanical stimulation that can induce fracture, induce fusion, or alter its biological pathway.[13,22,88,131] For example, bone hypertrophy is often the result of repetitive loading under small strain and high frequency motions.[44] However, the exact regulatory cellular mediators of bone formation and resorption, as a result of mechanical stimuli, still remain a mystery. Knowledge of these factors could provide the missing link towards bone regenerative therapies.

Bone will repair and remodel in response to favorable loading conditions.[23,24,44,76,82,131] Unfavorable loading conditions can lead to bone atrophy and non-unions, often forming fibrous tissue in lieu of bone formation. Carter et al. proposed that the type of stress applied to immature or undifferentiated tissues can dictate the fate of the tissue formation (Figure 2.1).[18] The establishment and application of controlled biophysical stimuli (i.e. loading

paradigms) to selectively differentiate immature tissue cells into viable fibrous or bone tissue could lead to a new frontier in tissue engineering. However, if applied loading paradigms can alter the ultimate outcome of an immature cell (mesenchymal cell), this suggests that the cells can respond to such stimuli by altering their mechanical parameters, such as force or pressure, during various stages of development. Simply put, if immature cells respond to mechanical stimuli, they may also elicit detectable responses to mechanical stimuli. Thus, mechanical parameters could potentially be used to monitor bone healing performance. **Figure 2.1** demonstrates the proposed stress and loading paradigms that alter the fate of a cell. Compressive shear stresses applied intermittently will lead to endochondral ossification, while constant compressive loads lead to the formation of cartilage.

| | | |
|---|---|---|
| Intermittent compressive or shear stresses | ➡ | Endochondral Ossification |
| Tensile stress | ➡ | Intramembranous Ossification |
| Constant compressive stress | ➡ | Cartiliage |
| High shear stress | ➡ | Fibrous Tissue Formation |

**Figure 2.1.** Proposed stress and loading paradigms with their respective fate of immature cell differentiation.

Although the mechano-cellular interactions involved with bone healing and repair are not fully understood, there has been numerous research that furthers the evidence that biophysical stimulation can elicit cellular responses to form or resorb bone. According to Wolff's Law, mechanical loading elicits an osteogenic response in bone, causing bone to form in regions of increased stress.[131] However, there is an optimal degree of stress that will favor bone formation. Sarmiento *et al*. demonstrated that controlled weight bearing under functional braces had a positive effect on tibial fracture healing.[107] Meadows *et al.* continued to demonstrate that loading was proven to be a permissive factor for bone defect repair.[76] In essence, cells respond to particular biophysical stimuli and can be monitored. Ideally, improvements in biomaterials, electronics, and packaging systems will be needed to create

a sensing system that can provide long-term, real-time accurate recordings of cellular responses. Currently, existing technology is lacking with respect to an implantable monitoring system that could record cellular responses with wireless data transmissons over the course of a few weeks to months. Additionally, the molecular indicators of bone repair are not well understood.

Numerous researchers have attempted to directly measure the various biomechanical parameters within the spine and in various orthopedic applications to provide a better understanding of the bone responses and healing mechanisms involved with daily stress exertion, as well as, surgical intervention and fixation that may be used to immobilize and stabilize bony segments. Bone deformation or strain, fluid pressure, intradiscal pressure, and forces acting upon a bony element or internal orthopedic fixation device have been investigated by a multitude of researchers.[1,16,17,32,50,66,68,75,80] However, numerous challenges and limitations exist with previous published research.[16,17,32,40,50,66,68,91-101,114,115,117,131]

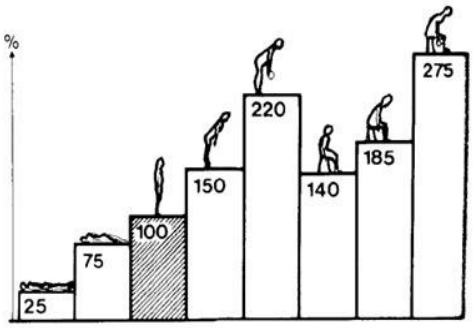


**Figure 2.2a.** A diagrammatic comparison of the *in vivo* loads (in terms of disc pressures) in the third lumbar disc during various activities. The sitting pressures are greater than standing pressures.[80]

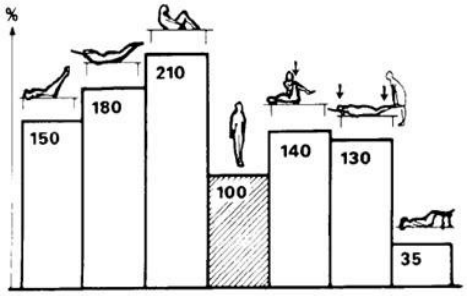


**Figure 2.2b.** Comparison of disc pressures *in vivo* at L3 during various exercises and positions. Pressures during sit-up with legs bent, hyperextension exercises, and back lying with the hips and knees flexed are greater than standing pressures.[80]

The earliest *in vivo* work was conducted by Nachemson and colleagues[32,79] in the late 1960s and early 1970s monitoring intradiscal pressures of the human spine for a variety of spinal loading motions (standing, sitting, flexed, etc..). **(Figure 2.2a & 2.2b.)** Later, the same group of researchers investigated spinal forces in the scoliotic patient after surgical intervention by instrumenting a Harrington Rod system with wire-connected, built-in strain gauges which converted strain into force

transmission along the rods.[79] However, the wires were brought out through skin incisions, making it difficult to obtain long-term stress and strain data from the instrumentation due to technical difficulties such as wire breakage and infection.

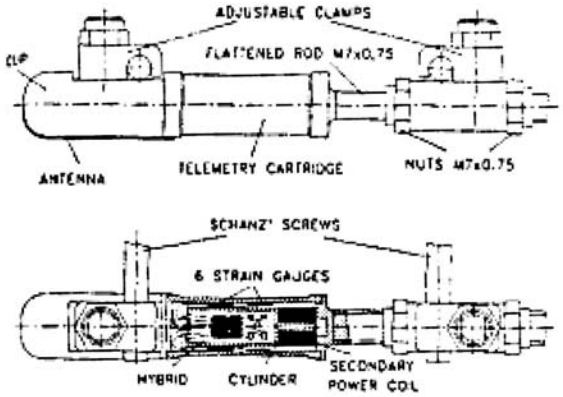


**Figure 2.3**: External and internal view of the telemeterized spinal fixation device (AO Fixator) used by Rohlmann et al. [92] to measure the loads acting on the internal spinal fixation device. A measuring cartridge integrated into the longitudinal threaded rod containing six semiconductor strain gauges as load sensors, and eight-channel telemetric unit and an inductive coil for power. The cartridge is hermetically sealed.

More recently, Rohlman et al. have reported the development of telemeterized spinal fixators that can be used to measure forces and moments on the spine *in vivo*.[101] A conventional AO spinal fixateur interne device was modified to study the effects of different spinal destabilization modes on implant performance. A hermetically sealed cartridge housed strain gauges and an inductively powered telemetric unit that were integrated into the threaded portion of the implant formed this sensor, **(Figure 2.3)**.[101] The strain gauges acted as force sensors and the wire coil was used to inductively couple power from an external source to the implanted signal processing electronics. In addition, the wire coil acted as an antenna for telemetric transmission of the data from the strain gauges to an external monitoring console. The fixators were used to correlate loading of the spinal implants with postures associated with various activities. Rohlman has published numerous reports based on the loads measured by implantable force sensing spinal implants used to quantify the spinal forces during walking, sitting, use of walking aids, and carrying weights.[91-101]

To date, the only work that has attempted to examine *in vivo* loading of spinal instrumentation during the course of fusion was reported by Ledet et al., where strain gauges

were mounted onto interbody fusion devices and implanted into the disc interspace of the baboon lumbar spine **(Figure 2.4)**.[68] The strain gauges were connected by wires to a subcutaneously implanted telemetric unit that transmitted the data to an external console. The system was used to correlate real-time *in vivo* loads with radiographs of the fusion sites. The implant-load cell in the baboon spine demonstrated dynamically changing loads during various activities, with the highest loads during extreme activities exhibiting loads in excess of 2.8 times the body weight. The main shortcoming of the system was its limited functionality lifespan (16 weeks or less) due to corrosion of the strain gauges and breakage of wires as the two primary failure modes.[68] However, this study clearly demonstrated that the changes in loads (force) may be used to indicate performance demands on the spinal construct (implant and bone).

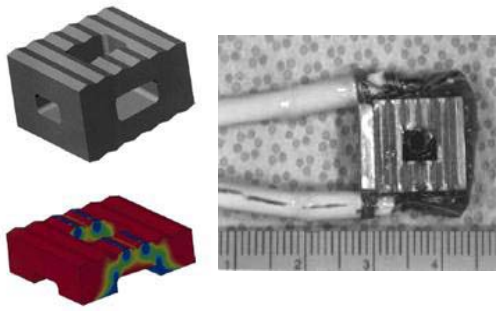

**Figure 2.4.** The interbody fusion device used by Ledet et al.[67] incorporated strain gauges to make load sensors to telemetrically measure the in vivo loads transmitted across the interbody fusion site.

The concept of utilizing pressure and force to measure changing conditions in the spine is not a novel one. There have been successful *in vivo* demonstrations of the pressure and force changes associated with the intervertebral disc and the loads transmitted through posterior spinal instrumentation, yet the complications that have occurred with these technologies have outweighed their success.[29,79,80,91-101] The benefit of these studies have been their contribution of insight towards the possibility of using these parameters in a manner that will provide a real-time long-term *in vivo* status of tissue healing without the risk of wire breakage, electronic failures, implant rejection, and bulky hardware. Therefore, the goal of the present study was to devise an implantable spinal construct (consisting of an active implant and/or spinal bone) that will further determine which parameter (pressure at the bone graft stie or force along a spinal implant) is the optimal choice for the indication

of a bone healing at a fusion site. Both pressure and force were investigated in an initial biomechanical *in vitro* study to determine their feasibility for monitoring altered biomechanical changes.

### *2.1.1 In Vivo Intradiscal Pressure*

Nachemson and colleagues[32,79] initiated some of the early *in vivo* work in the late 1960s and early 1970s by assessing intradiscal pressures of the human spine for a variety of spinal loading motions (standing, sitting, flexed, etc..), and later, investigated spinal forces in the scoliotic patient after surgical intervention by instrumenting a Harrington Rod system with wire-connected, built-in strain gauges. However, the wires were brought out through skin incisions, making it difficult to obtain long-term stress and strain data from the instrumentation due to technical difficulties such as wire breakage and infection. Post-operative measurements were successfully made in one patient for a period of one day only. In 1973, Elfstrom and Nachemson revamped this experimental method by designing an intravital wireless telemetric Harrington distraction rod capable of measuring the axial forces through the instrumentation during daily spinal loading post-operatively.[32,79] The wireless technology greatly improved the monitoring duration capabilities to a maximum of two weeks post-operatively for a number of commonly used positions, maneuvers, and physical exercises in eleven patients.

Furthermore, Nachemson was instrumental in providing vital *in vivo* intradiscal pressure for various body positions.[80] His work examined the pressure variations *in vivo* within different regions of intervertebral discs using a pressure sensor mounted inside a spinal needle. He demonstrated that a bending moment was induced on the spine by holding a 20kg mass a certain distance from the center of rotation as measured by using a pressure sensor mounted inside a spinal needle and correlating the data to the condition of the discs

(healthy or degenerate) through electromyography. The pressure sensor revealed that this particular exercise increased the intradiscal pressure of the L3-4 lumbar spinal segment to three times the weight of the whole body, thus overstressing that particular spinal level. However, the inconvenience associated with the insertion of a spinal needle into the patient along with increased infection risk associated with a dangling wire connection to an external electronics console ensured that this approach to pressure measurement was not adopted for routine clinical assessment**.** To date, with respect to bone healing, there are no reports of any previous work that has been directed towards measuring pressure fluctuations within bone grafts during vertebral fusion.

### *2.1.2 In Vivo Force (Strain) on Spinal Instrumentation*

More recently, Rohlman et al. have reported the development of telemeterized spinal fixators that can be used to measure forces and moments on the spine *in vivo.*[94] A conventional AO spinal fixateur interne device was modified to study the effects of different spinal destabilization modes on implant performance. A hermetically sealed cartridge housed the strain gauges and inductively powered telemetric unit that were integrated into the threaded portion of the implant.[94] The strain gauges acted as force sensors and the wire coil was used to inductively couple power from an external source to the implanted signal processing electronics. In addition, the wire coil acted as an antenna for telemetric transmission of the data from the strain gauges to an external monitoring console. The fixators were used to correlate loading of the spinal implants with postures associated with various activities. Rohlman has published numerous reports using this implant design to quantify load measurements for walking, sitting, comparing *in vitro* test measurements to *in vivo* measurements, walking with walking aids, and load carrying.[91-101] From a clinical perspective, there are two major disadvantages to Rohlman's approach. First, the bulkiness of the telemetric spinal device could interfere with the bone fusion process. A bulky spinal device

may interfere with the bony surfaces and reduce the surface area available for fusion.[34,59] Furthermore, the entire data acquisition system accompanying the telemetric device was quite large and non-portable, which limits its use to specialized research subjects. Finally, it is not common practice in the U.S. to perform two consecutive spinal surgical procedures, where the initial surgery incorporates the force measurement implant, followed by the second surgery that provides surgical correction. The ideal spinal stabilization construct would house implantable sensors that could monitor the *in vivo* stresses along a spinal implant and at the site of the bone graft for an extended period of time until the bone graft has fully incorporated.

As previously discussed, the only work that has attempted to examine *in vivo* loading of spinal instrumentation during the course of fusion was reported by Ledet et al., where strain gauges were mounted onto interbody fusion devices.[68] These interbody implants were filled with bone graft and inserted into disc spaces to induce vertebral fusion. The strain gauges were connected by wires to a subcutaneously implanted telemetric unit that transmitted the data to an external console. The system was used to correlate real-time *in vivo* loads with radiographs of the fusion sites. The main shortcoming of the system was its limited functionality lifespan (16 weeks or less). Corrosion of the strain gauges and breakage of wires were two primary failure modes.

## 2.2 Research Motivation

The concept of pressure measurements recorded at the host bone and graft interface is quite novel. The majority of previous research has focused on either the stresses or strains placed upon spinal implants as a correlate to bone healing, or the pressure within the confines of an intact intervertebral disc to identify the stresses imposed on the human spine for a variety of loading paradigms. Knowledge of the *in vivo* intradiscal pressures may provide

insight to the degenerative cascade of the intervertebral disc, as well as potential sources of disc injury. However, the examination of the stresses and strains that may be imposed on spinal instrumentation during fusion or motion introduces many assumptions and errors to the model. Pressure is based on the contact pressures at the bone interface that may provide valuable information of the biomechanical changes that may occur with bone incorporation or resorption during fusion healing. The force measured on the spinal implant itself may not correlate to the extent of bone healing or fusion rate, but when used in combination with pressure sensors in other surrounding tissues can provide a biomechanical landscape for bone healing or fusion status. Since all spinal implants differ in design and may differ in their degree of force transmission along the spinal column, combining this implantation with pressure sensors in the surrounding bone will provide information specific to the implant design and its interaction at the bone healing interface.

Biomedical telemetry, the introduction of wireless data transmission, has contributed to the refinement of *in vivo* measurement techniques by minimizing complications seen with wired systems and providing the user with longer periods of monitoring within the human body.[15,19,30,40,53,54,87,101,110,115] For any implanted device, protrusion of the wires through the skin, wire breakage, infection, accuracy of the transmitted data, biocompatibility, and implant rejection are all challenges and risks faced with any foreign body placed into a living system. The portability that could be provided by an implantable wireless MEMS pressure and force sensors are necessary features that need to be factored into implantable sensor design.

The novelty of MEMS technology lends numerous questions with respect to the safe and efficacious use of MEMS materials in a living system. Previous investigators have assessed the biocompatibility of MEMS materials utilizing standard cytotoxicity protocols.[64] Kotzar et al.[63] examined a series of materials commonly used in the fabrication and packaging of standard MEMS devices for cytotoxicity using the ISO 10993 biocompatibility testing standards. The material set comprised of; 1) silicon (Si, 500 um-thick), 2) silicon dioxide

(SiO2, 0.5 um-thick), 3) silicon nitride (Si3N4, 0.2 um-thick), 4) polycrystalline silicon (polysilicon, 0.5 um-thick), 5) silicon carbide (SiC, 0.5 um-thick), 6) titanium (Ti, 0.5 um-thick), and 7) SU-8 (50 um-thick). Except for the silicon substrates, all the other materials were formed by thin film deposition using standard techniques onto 100-mm diameter, (100) silicon wafers, which were procured from a vendor. Cytotoxicity tests that were performed followed the ISO 10993-5 standard: "Test for Cytotoxicity – *In Vitro* Methods". A single extract of the test article was prepared using single strength Minimum Essential Medium (1X MEM) supplemented with 5% serum and 2% antibiotics. Each test extract was then placed onto three separate confluent monolayers of L-929 mouse fibroblast cells which had been propagated in 5% $CO_2$. Test well contents were also examined for confluency of the monolayer, and color as an indicator of resulting pH. Results were scored on a scale of 0-4, where 0 represented the best case - no adverse reaction whatsoever - and 4 represented the worst case - complete cell lysis. A score of 2 or below was considered acceptable for many implantable applications. This study indicated that the cytotoxicity testing revealed that all of the MEMS materials were graded 0, which was as good as the negative control. The data from this evaluation suggested that MEMS materials serve as suitable candidates for the development of implantable medical devices. However, further testing will still be required to validate MEMS devices for specific applications, such as in vertebral bone. Overall, the scope of this dissertation will establish that monitoring pressure and force variations are suitable parameters for determining bone healing status and that MEMS sensors designed to monitor these parameters will be acceptable for implantation into the spine.

In summary, the future development of a Smart Spinal System that would incorporate MEMS technology to measure *in vivo* bone healing involves a multitude of factors that must be investigated prior to final implantation into a human spine for the long term monitoring of a bone fusion status. Once an *in vitro* human cadaveric model is established that will validate the feasibility of using pressure and force as parameters to measure bone healing, the feasibility of sterilization and packaging of these sensors must be assessed

prior to implantation into a living system. Once implanted, the biocompatibility of MEMS sensors and the radiographic imaging potential of these sensors can be evaluated for their interaction within a living system. **Figure 2.5** provides an overview of the areas of research necessary for the development of a MEMS based smart spinal system.

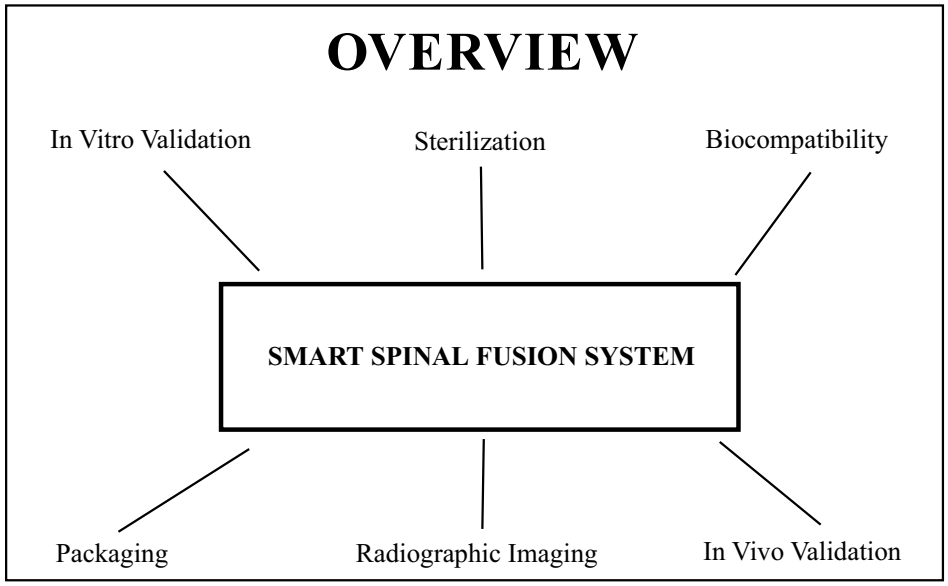


**Figure 2.5:** Overview of the necessary areas of research for the development of a smart spinal system capable of monitoring the *in vivo* biomechanical responses related to bone healing.

# CHAPTER III

# ESTABLISHING *IN VITRO* STUDY TO ASSESS THE FEASIBILITY OF USING PRESSURE AND FORCE TO MONITOR BONE HEALING

## 3.1 Study Overview

The first step towards the development of a smart spinal sensor that can monitor the forces along a spinal implant and the contact pressures related to bone healing involved proof of concept study to determine the feasibility of measuring these biomechanical parameters during bone healing. This will provide the basis to establish a smart bone healing biosensor model that can be incorporated into a living system. Therefore, an *in vitro* cadaveric biomechanical study was conducted to determine the feasibility of monitoring forces along a spinal implant and the contact pressures at the bone graft interface during a simulated bone healing process.

## 3.2 Introduction

Bone graft incorporation and fusion usually occur within four to six months after interbody fusion in humans. Unfortunately, it is often difficult to interpret. Conventional imaging techniques provide subjective and often inaccurate information regarding the

qualitative and quantitative aspects of the fusion process and can have a high percentage of false positives.[11,14] In addition, they do not provide the surgeon with information regarding bone incorporation into the vertebral endplates, nor can they provide information regarding the mechanical strength of the bone graft-endplate mortise interface.[11,14] Clearly, a more precise method for determining these parameters is desirable.

Using sensors to monitor dynamic biomechanical parameters of the spine, such as those associated with bone healing, could serve as an ideal alternative to conventional imaging techniques. The novel concept of monitoring pressure at the host bone and graft interface in order to assess the spine fusion process is proposed in this chapter.[5,8,105] The choice of pressure as the assessment/monitoring parameter is based on precedent. First, pressure is a well defined physiological assessment parameter, particularly in the cardiovascular arena.[53,54] Second, it has been investigated and shown to be of significant utility in orthopedic applications.[86,87,95,96,97,98,99]

Biomechanical parameters are quantifiable and dynamic in nature.[21,28,29,42,103,127] Many authors have attempted to examine *in vivo* loads applied to spinal implants during the course of healing, but few have examined pressure at the bone graft-mortise interface.[28,86,91-101,130] Unfortunately, with the *in vivo* implantation of electronic load measurement systems, multiple technical difficulties arise. These include limited functional 'lifespan' (typically 16 weeks or less) of the implantable recording devices, corrosion of the transducers, fracture of wires, infection, the need for extensive data processing equipment, and the need for large external and bulky monitoring systems that affect compliance. Others have investigated, via *in vitro* biomechanical analyses, the loads and pressures placed on an interbody cervical spine bone graft in the pre- and post-instrumentation states.[29,41,126,127] These studies demonstrated load transfer through the bone graft, thus implying that biomechanical parameters, such as load and pressure, could serve as viable parameters that could be used to quantify the biomechanical alterations that are associated with bone healing (i.e. fusion),

as well as fusion failure. These biomechanical parameters, however, have not yet been determined nor quantified.

The long-term goal of the research presented herein was to establish the feasibility of developing miniature telemetric biosensors to assess the process of bone healing; in this case, spine fusion.[5,8,73,105] Such technology has been proposed, but is not yet available. For example, implantable wireless pressure sensors based on microelectromechanical systems (MEMS) could, in principle, be inserted during fusion surgery, and subsequently monitor changes in load (forces and pressures) during the fusion process. This information would be transmitted to the surgeon to augment clinical imaging technology to guide patient care. However, the feasibility of measuring such parameters along with the ranges of physiological pressure and load changes must first be established. Therefore, preliminary proof of concept studies using conventional pressure transducers, were conducted to provide the necessary information that will be used to design and develop implantable biosensors that may employ wireless MEMS technology

The present study is a preliminary investigation that was designed to evaluate the use of pressure and load as biomechanical determinants of bone healing in an *in vitro* model for the future input towards the development of MEMS-based implantable telemetric microsensors. In order to accomplish this, *in vitro* pressures at the bone graft-endplate mortise interfaces and *in vitro* loads transferred through a ventrally placed cervical plate during a simulated fusion were monitored during physiologic compressive loading.

## 3.3 Materials and Methods

### *3.3.1 Overview*

Single level interbody fusions were performed on a series of six cadaveric goat cervical spines obtained from a slaughterhouse. The goat model was chosen as the interbody fusion model of choice because of its loading characteristics and inter-specimen anatomical

and biomechanical consistency.[117] Although a challenging mechanical model, the upright posture of the upper cervical spine of the goat during standing exposes the cervical spine to an axial loading environment that is comparable to that of humans.[117,135-137] The load transmission along a ventral cervical plate and the contact pressure response at the bone graft and vertebral endplate interface of a fusion site were measured during loading for each goat spine under five conditions (Table 3.1):

Condition (1) - intact (DISC)

Condition (2) - with an intervertebral bone graft (GRAFT)

Condition (3) - with an intervertebral bone graft with a ventral cervical plate (PLATE)

Condition (4) - with an intervertebral bone graft with the ventral plate and polymethylmethacrylate (PMMA) to simulate early stage bone healing (PMMA)

Condition (5)- with an intervertebral bone graft after removal of the ventral cervical plate (REMOVAL)

The data and associated analysis presented herein represent a preliminary feasibility study, designed to investigate the use of pressure assessment as a clinically useful metric following spine fusion surgery. The number of specimens used was small, therefore statistical analysis, for the most part, was foregone.

### *3.3.2 Specimen Preparation and Study Design*

A total of six cadaveric caprine (goat) C2-C5 cervical spines were prepared for biomechanical testing, as this was the minimum required for a preliminary evaluation. All specimens were denuded of surrounding musculature, leaving the ligamentous and bony tissues intact. In preparation for biomechanical testing, each C2-C5 spinal segment was thawed at room temperature, embedded into customized testing fixtures using a polyester styrene polymer, and allowed to cure for 24 hours prior to testing. To minimize dehydration

during testing, each segment was wrapped in saline soaked gauze during preparation. Biomechanical testing was conducted on each specimen for each of the five treatment groups, in the sequence portrayed in **Table 3.1**.

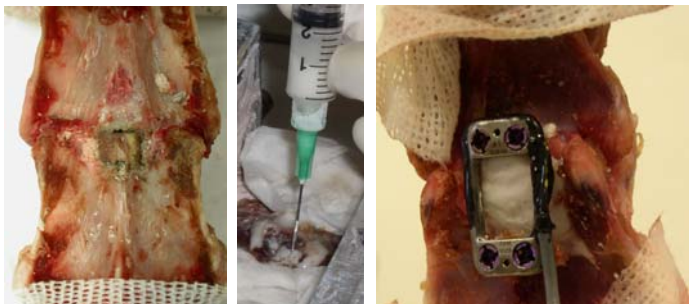

**(a)** **(b)** **(c)**

**Figure 3.1:** Preparation of the graft site at C3-C4 with PMMA prior to inserting the bone graft (a) PMMA was injected into the host site, the graft was gently impacted into this and the graft was further sealed with additional PMMA (b). The force sensing plate was secured over the graft site for additional testing (c).

All specimens were first non-destructively tested in their intact state (Condition 1), without the ventral plate or pressure transducers which would allow only stiffness to be calculated. Following intact testing, a ventral cervical plate (28 mm, DOC ventral cervical rigid plate, DePuy Spine, a Johnson and Johnson Subsidiary, Raynham, Massachusetts) that was configured as a force transducer, was placed across the intact disc to obtain the load transmission along the plate. Since bone healing properties were to be assessed by using pressure, as well as the load along the plate, the catheters were not inserted into the intact disc. Once this testing was completed, the plate was removed and a discectomy was then performed at the C3-C4 interspace and an autologous bone graft was obtained from the dissected C6 or C7 vertebral body. This involved using a 1 cm osteotome to create a cube-shaped cortico-cancellous bone graft (one cortical surface). The cube-shaped bone graft was carved into similar dimensions resembling the osteotomized void at C3-C4, and was gently impacted into the fusion site. Biomechanical testing was then conducted for the grafted state (Condition 2), followed by the addition of the 28mm DOC™ ventral cervical rigid plate with 4mm X 16mm divergent fixed angle screws used to immobilize the C3-C4 motion segment after bone graft placement. Biomechanical testing was repeated for this condition (Condition 3). The simulation of a fusion was then accomplished by the addition of 2 cc of polymethylmethacrylate (PMMA) into the graft

site. This stiffens and strengthens the interface, as would likely occur during the early phases of the bone incorporation process. Injection of the PMMA involved removal of the plate and bone graft, followed by injection of the liquid PMMA into the host site, followed by gentle reimpaction of the graft into this region forming a mortise of PMMA surrounding the graft. Additional PMMA was injected around the periphery of the bone graft and allowed to cure to further seal cracks and voids around the graft and served as a stiffening agent that circumferentially surrounded the bone graft **(Figure 3.1a and 3.1b).** The DOC™ Cervical Plate was then implanted across the C3-C4 site treated with PMMA **(Figure 3.1c)** and biomechanical testing was then repeated (Condition 4). Finally, the cervical plate was removed and the testing repeated (Condition 5).

### *3.3.3 Pressure and Load Transducers*

The pressure transducer consisted of two pressure sensing catheters that were inserted at both bone graft-endplate mortise interfaces (ie. superior and inferior interfaces). A two channel Dataquest A.R.T. 2.2 Telemetric Pressure transducer, (Physiotel Multiplus Implant, TL11M3-D70-PCP Data Science International, St. Paul, Minnesota) with two silicone elastomer catheters each (1.2 mm in diameter) with a full scale range of 40 MPa, and an accuracy of 0.1kPa was used. The battery was rated a nominal lifespan of 3.5 months of continuous use and was housed with the transmitter. The silicone elastomer catheters were used for contact pressure recordings at the bone graft and vertebral endplate interfaces. Each was housed within a circular canal at the bone graft and vertebral endplate interface and filled with a proprietary gel at the tip and an incompressible fluid along the catheter to transmit contact pressures from the fusion site to the sensing region of the pressure transducer **(Figure 3.2)**. Each catheter served as an independent channel and the data was analyzed separately. The pressure sensors were activated by a magnet and the data recorded continuously during simulated physiological loading.

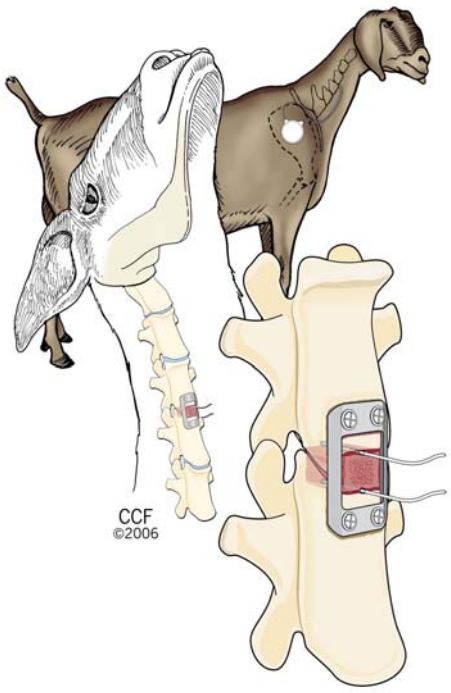


**Figure 3.2** Pressure catheters inserted at the bone graft interfaces of the goat cervical spine to record pressures continuously during axial loading.

Prior to testing, the linearity and tracking behavior of the pressure transducer was measured against the compressive loading applied by the Instron test apparatus. This was accomplished by applying six cycles of a known compressive load to each transducer and the pressures continuously acquired. A sinusoidal load at a frequency of 0.1 Hz and a maximum compressive load of 200N were applied to the pressure catheters under load control using the servohydraulic materials test apparatus (Instron 8874, Instron Corp., Canton, Massachusetts). These pressure measurements provided an evaluation of the applied cyclical load and its relationship with the measured pressures. The compressive loading cycles applied by the testing apparatus were mapped against the measured pressure cycles to assess the transducers' performance with respect to phase lags and/or non-linearities in response to the compressive loading **(Figure 3.3)**. A linear regression was conducted to statistically analyze the linearity of the pressure transducer and the phase lag was quantified in response to the compressive loading. Finally, the deformation at the minimum and maximum peaks was recorded with the pressures and loads applied. Configuration

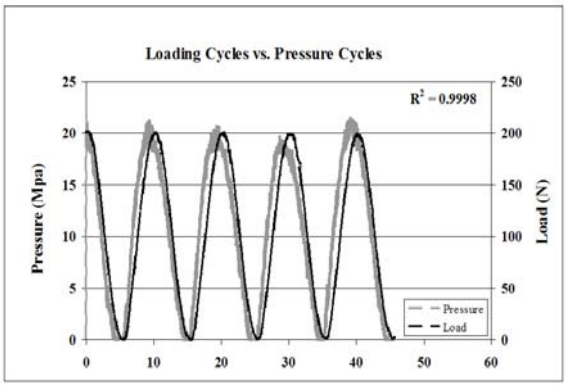


**Figure 3.3:** Correlation of the pressure transducer with a 200N applied load from the Instron testing apparatus. A sinusoidal waveform input from 0N to 200N in pure compression at a rate of 0.1Hz was applied for five cycles of loading. A linear correlation was observed between pressure and the applied load, $R^2$=0.9998. The observed phase lag between the load applied and the pressure recorded was less than 1 second and could be attributed to the compliancy of the catheters or the hydraulic delay within the Instron testing apparatus.

and operation of the pressure transducers utilized Dataquest A.R.T. Version 2.3 software (DSI™ Data Science International, St. Paul, Minnesota) to sample and analyze all of the recorded pressures at a sampling rate of 500 Hz.

The cervical plate functioned as an active load transducer, using conventional strain gauge technology. Load was monitored along the DOC™ cervical plate across the C3-C4 bone graft site using two independent channels to measure axial load along the plate during loading. Two linear strain gauges (120W) were mounted along the longitudinal axis of the plate, wired into one leg of a four-arm Wheatstone Bridge, and combined with a commercially available telemetric strain sensing system that transmitted signals via radio transmission to a stationary receiver (ATi 2000, ATi, Spring Valley, Ohio). The load transmitted through the plate was calculated by inserting the Young's Modulus, E, for titanium alloy and the cross-sectional area of the plate into the following equation:

Young's Modulus states; $E = \frac{\sigma}{\varepsilon}$ ;

where σ is the load divided by the cross-sectional area, and ε is the strain or change in the length due to deformation divided by the original length. To determine the normal load or in this case, the longitudinal load along the axial plane; $F_n = \in_n * E * A$ ; where $F_n$ is the normal load, $\in_n$ is the normal strain that is measured during loading of the DOC plate system, and A is the cross-sectional area of the plate system where the strain gauge is mounted.

Due to the low profile geometry of the DOC™ plate, as well as the limited space for mounting strain gauges, loads along the ventral plate were examined for compression only during the biomechanical testing. The pressure and load assessments were associated with different controls. The pressure measurements were paired with the bone graft (Condition 2; GRAFT) as a control and the load measurements were paired with the plate across an intact disc (Condition 1; DISC) as a control. The relative changes in pressures and loads were statistically compared between treatment groups to identify biomechanical differences related to simulated fusion.

### *3.3.4 Biomechanical Testing*

Non-destructive physiological loads were applied to each cervical spine using an Instron 8874 biaxial servo-hydraulic materials testing apparatus. Pressure at the bone graft-vertebral endplate interfaces and load transmission along the ventral cervical plate were assessed **(Table 3.1)**. In preparation for testing, each spine was embedded at C2 and C5 into customized gripping fixtures and mounted onto a servohydraulic biaxial testing apparatus (Instron 8874). Each spine was preconditioned for twenty repetitive compressive loading cycles at 200N to achieve uniformity in the tissue responses prior to sampling the pressures. At the time of testing, each cervical segment was secured to the Instron testing apparatus prior to biomechanical testing. The upper jig that was housing the rostral C2 vertebra was allowed to rotate during loading. The angles were recorded using a ±1V rotational potentiometer mounted to the testing fixtures. The center of rotation was located by applying a 200N maximum compressive load to the upper jig. The load was reapplied until no angular motion was detected by the upper rotational potentiometer. The lower jig was stationary and rigidly affixed to the testing apparatus. Once the center of rotation (COR) was determined through this process for each specimen tested, this position for each specimen was reflected onto the mounting fixtures and clearly marked. The COR location specific to each specimen was maintained throughout

**Table 1**

| Condition | Group | Pressure (Measured with pressure catheters - Megapascals) | Load (Measured along the ventral cervical plate - Newtons) |
|---|---|---|---|
| 1 | DISC | No pressure measurements | Intact disc - No load measurements |
| 2 | GRAFT | Bone graft only – Pressure measured | Bone graft only – no plate, therefore no load measured |
| 3 | PLATE | Bone graft with ventral plate – Pressure measured | Bone graft with ventral plate – Load measured |
| 4 | PMMA | Graft, plate, and PMMA added to graft site – Pressure measured | Graft, plate, and PMMA added to graft site – Load measured |
| 5 | REMOVAL | Removal of plate – Pressure measured | Removal of plate - No load measurements |

**Table 3.1:** Treatment groups listed for each measurement parameter. Pressures at the bone graft-endplate mortise interfaces and loads along a ventral cervical plate were measured during biomechanical testing of each cervical spine. Physiologically relevant loads were applied to each spine specimen and the pressures and loads were measured for the intact, grafted, plated graft, PMMA augmented, and plate removal scenarios.

the course of testing in each specimen. Following the preconditioning and alignment phases, each cervical spine was non-destructively cycled under load control in compression for six continuous cycles at a data sampling rate of 50Hz. A 200N pure compressive load was applied to each specimen using a sinusoidal waveform input at a frequency of 0.1Hz.[135-137] The rostral mounting fixture was free to rotate, while the caudal fixture remained rigidly attached to the Instron platform. Load and deformation data was sampled and analyzed at a rate of 50 Hz. The mean pressures were calculated for all six cycles of axial compressive loading for each group The pressure and load data acquisitions were conducted on two different computer systems (Pressure: Dataquest A.R.T. 2.2, Data Science International, St. Paul, Minnesota and Load: ATi 2000, ATi , Spring Valley, Ohio) that were synchronized with the Instron testing apparatus.

The segmental stiffness was determined for C3-4 by calculating the slope of the elastic portion of the load-deformation curve, with the corresponding pressures measured at the bone graft-vertebral endplate interfaces at C3-4 and the load along the ventral cervical plate.

Ventral and dorsal motion was measured across the C3-4 motion segment using a Nikon Coolpix 4.0 Megapixel digital camera with a resolution of 320 x 240 pixels at a sampling rate of 14Hz, and MaxTRAQ v1.41 software image analysis system (Innovision Systems, Inc., Lapeer, MI). This technique was employed to quantify graft settling or subsidence. Descriptive statistics were used to gather the means and standard deviations of the acquired data for all of treatment groups. An analysis of variance with a repeated measures technique was used to detect statistical differences between treatment groups.

## 3.4 Results

### *3.4.1 Accuracy of the Pressure Transducer*

**Figure 3.3** depicts the accuracy of the pressure transducers while cyclically loaded from 0N to 200N in pure compression by the Instron test machine. The 200N compressive load correlated with a mean deformation on the catheter of 1.37 ± 0.04mm and approximately 20MPa of pressure. A subsidence of 0.25 ± 0.10mm was measured across the fusion site. A linear regression and statistical correlation was conducted on the load versus pressure yielding an $R^2$ of 0.998, indicative of the high linearity of the pressure transducer. There was very little phase lag (<1 second) between the Instron load cycles and the pressures measured at the bone graft interface **(Figure 3.3)**. The small lag could be attributed to the delay in the actual hydraulics of the Instron testing apparatus in combination with the delay in the viscoelastic response of the pressure catheters due to compliance with the polymenic material and accompanying gel.

Fortunately, each pressure transducer housed two independent recording catheters, such that the extrusion of a single catheter did not significantly affect the pressure monitoring process. The pressures measured from the lower catheter located at the caudal interface of the bone graft and vertebral endplate are presented in this study. The lower catheter pressure data was consistently greater than the upper catheter readings to an accuracy less than 10% for all of the goats.

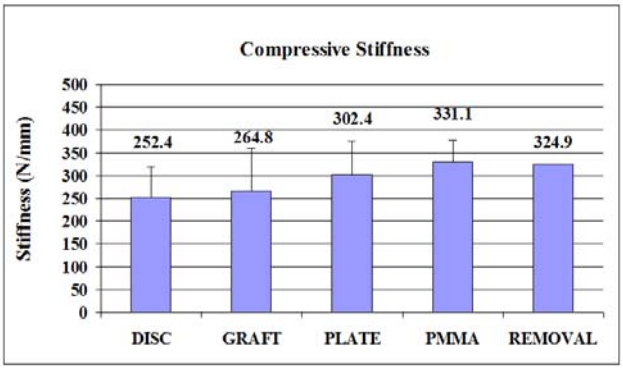


**Figure 3.4:** Compressive Stiffness for all of the testing scenarios (DISC, GRAFT, PLATE, PMMA, REMOVAL). A 200N compressive load at 0.1Hz was applied to each C2-C5 spinal segment with grafting occurring at C3-C4.

### *3.4.2 Stiffness*

Each cervical spine segment was observed to exhibit a progressive increase in compressive stiffness with the addition of the graft (Condition 2;

GRAFT), cervical plate (Condition 3; PLATE), and PMMA (Condition 4; PMMA) **(Figure 3.4)**. The stiffness ranged from 252.4 N/mm (Condition 1; DISC) to 331.1 N/mm (Condition 4; PMMA), with the greatest stiffness observed for Condition 4; PMMA and intermediate stiffnesses recorded for Conditions 2 and 3. These observations correlate with stiffness augmentation by both surgical strategies (Conditions 2 and 3; GRAFT and PLATE) and simulated healing (Condition 4; PMMA). Once the plate was removed (Condition 5; REMOVAL) and the specimens retested, the stiffness decreased, but remained greater than Condition 2; (GRAFT), due to the added rigidity achieved with the addition of the PMMA. The amount of graft settling (subsidence) across C3-4 for a total of 50 cycles was a mean of 0.25 ± 0.10 mm.

### *3.4.3 In Vitro Pressures at the Bone Graft and Vertebral Endplate Interfaces*

The mean graft interface pressures for compression loading are depicted in **Figure 3.5**. There was a linear increase in pressure from Condition 2 (GRAFT) to Condition 5 (REMOVAL) ranging from 0.64 to 1.03 MPa, with the greatest pressure observed for the plate removal state (Condition 5; REMOVAL). The addition of the ventral DOC™ plate (Condition 3; PLATE) increased the graft interface pressure over that observed in the GRAFT state (Condition 2; GRAFT), thus implying that an increased load was borne by the bone graft after the addition of the ventral plate (Condition 3; PLATE). PMMA injection into the mortise resulted in an even greater increase in the pressure measured

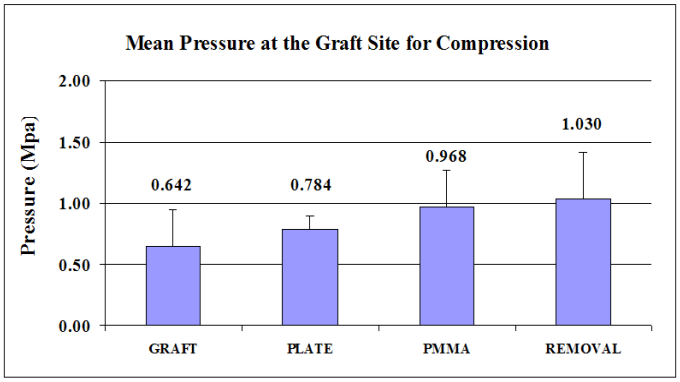


**Figure 3.5:** Mean pressures in compression at the bone graft and vertebral endplate interface measured for each test group. There is a steady increase in the pressures at the bone graft and endplate interface after plate implantation and further with PMMA augmentation.

at the interface (Condition 4; PMMA), followed by further increase in the pressure at the graft-endplate interface after plate removal (Condition 5; REMOVAL).

### *3.4.4 In Vitro Compressive Loads through the DOC™ Cervical Plate*

The mean compressive loads through the DOC Cervical Plate are depicted in **Figure 3.6** for two loading conditions (Conditions 3 and 4; PLATE and PMMA, respectively). This correlates with the stability acquired via the natural process of bone fusion (biomechanically simulated with PMMA insertion in this case).

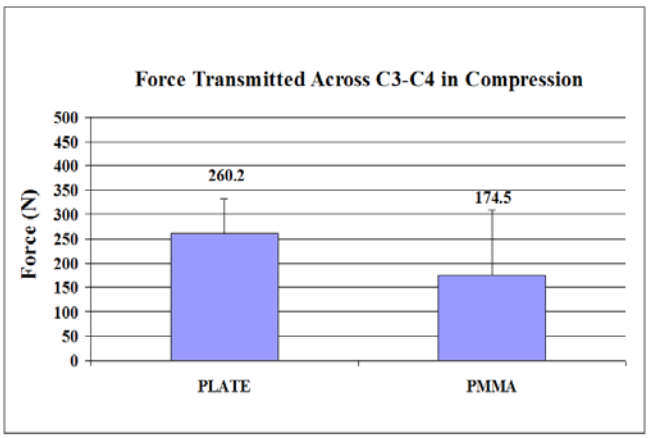


**Figure 3.6:** Mean load transmission along the DOC™ ventral cervical plate measured at the C3-C4 fusion site.

## 3.5 Discussion

### *3.5.1 Compressive Stiffness*

In the model presented here, the stiffness was greatest for the specimens with the bone graft augmented with PMMA (Conditions 4 and 5). The specimens associated with the least stiffness were in the Condition 1 group (DISC). This is expected due to the greater mobility and reduced elastic modulus of the intervertebral disc versus a bone graft. The grafted group (Condition 2; GRAFT) was observed to be associated with marginally greater stiffness than the DISC (Condition 1) group. The etiology of this is multifactorial, but may in large part be due to the lack of support from the anterior longitudinal ligament, which was obligatorily removed during bone graft insertion. Furthermore, the removal of an intact

disc involves disruption of the supportive annulus fibrosus and vertebral endplates. Once the connection between the nucleus pulposus, annulus fibrosus, and endplate interfaces are disrupted and the anterior longitudinal ligament is compromised, a decrease in spinal stability is expected. Additionally, the placement of an interbody bone graft, does not achieve a 100% surface area of contact between the vertebral endplates and the bone graft interface. These factors neutralized much of the expected increase in stiffness associated with grafting. This is most likely so in the human clinical situation as well (i.e., the attainment of only a modest increase in stiffness in the early time frame following anterior cervical discectomy and fusion without plating).

The addition of a rigid plate, on the other hand, increased the stiffness of the grafted motion segment (Condition 3; PLATE). Additional augmentation with PMMA, a material that possesses a higher modulus of elasticity than bone, increased the overall stiffness of the grafted and plated construct even further. The addition of PMMA created a scenario that simulates a maturing fusion at the vertebral endplate-graft interface, thus increasing the stability in compression by minimizing the motion across the graft site and increasing the surface area of contact at the endplates. In the *in vivo* fusion situation, the contact surface area increased, motion was reduced, and the overall global stiffness increased as the bone fusion process ensued and the bone graft began to incorporate and remodel into the adjacent vertebral bodies. The addition of PMMA in this experimental model (Condition 4) appears to appropriately replicate the biomechanics of early bone healing of this scenario. At such a point in the postoperative period, the construct can adequately resist compressive and tensile loads. This process, as demonstrated herein, can be characterized and quantified via the assessment of pressure.

### *3.5.2 In Vitro Pressures at the Bone Graft Interface and Load Transmission along the DOC™ Plate*

The assessment of the mean graft interface pressures **(Figure 3.5)** demonstrated a steady increase for each consecutively applied condition, although the increase from the GRAFT group (Condition 2) to the PLATE group (Condition 3) was minimal. The loading and unloading of a bone graft has a direct impact on the pressures measured at the bone graft-endplate interface, as well as the loads transmitted along a ventral cervical plate. Taking this into consideration, the addition of a rigid plate should unload the interbody graft in compression, shielding the pressure catheters at the graft-endplate interfaces from additional loading.[29,126] A small amount of graft settling or subsidence (0.25 ± 0.10 mm) was observed after the 20 preconditioning cycles prior to testing, followed by the added cycles during compression testing. The cause of the increase in graft site pressure after ventral plate application (the slight increase observed from Condition 2 to Condition 3) could be attributed to two factors. First, the aforementioned subsidence of the graft most certainly resulted in further compression on the pressure catheters. A second rationale is that the application of the ventral plate with sagittally divergent screws is known to compress the spine locally (bringing, in this case, C3 and C4 vertebral bodies closer together) via the triangulation effect the screws that are divergently placed in the sagittal plane. This results in a compression force vector that, in turn, translates into greater graft interface pressures.

Subsidence, or the settling of a bone graft, has been consistently observed after fusion surgery in humans. It consists of both axial and angular components. As the process of subsidence evolves, the surrounding vertebrae settle onto the surface of the bone graft, the bone graft shortens, and a loss of vertical height is observed. The spine deforms due to the effects of gravity and repetitive axial impulse loading of the spine during ambulation, even in the presence of interbody grafts. In humans, within 1 to 2 weeks after surgery, there exists a mean subsidence of 1.4 mm with anterior cervical fusion using autologous bone. Even rigid ventral plating does not eliminate subsidence of the cervical spine.[119,120] This is

in spite of the fact that a rigid implant should result in less load transmitted to the bone graft and hence, less subsidence.[119] Subsidence has been shown to be less of a concern in animals due to the dense nature of bone and the rapidity at which the bone fusion process transpires. It has been experimentally demonstrated in cadaveric bovine spines that the extent of subsidence is small and the majority of settling (mean of 0.1 mm of subsidence) occurred within the first one hundred cycles of loading, which is consistent with the findings observed in the presented study.[49]

Bone graft loading and the resulting subsidence was obviously not completely shielded by ventral plate fixation. Since subsidence occurs regardless of plate fixation,[9,119] a significantly biomechanical effect of the plate may be expected in the early phases of bone healing in the clinical setting, or biomechanical testing as performed here (Conditions 1-3). This graft subsidence along with the ventral plate loading of the graft may explain the increase in the graft site pressures after the addition of the ventral plate (Condition 3). In addition, the increase of graft site pressure may be further explained by a ventral shifting of the center of rotation (COR) caused by the plate and the manner in which the specimen was loaded via the experimental design.[29,41,126] The serial repetitive loading paradigms of the spine may have caused the COR to shift more ventrally as the spine continued to settle, than during the preconditioning phase of the experiment.

PMMA was added to simulate early fusion healing (Condition 4). The load borne by the ventral plate decreased following the addition of PMMA, while the graft site pressure rose. These findings are consistent with those expected during early bone fusion incorporation following surgery. Load sharing with a redistribution of the loads along the ventral spinal column can be implied with this finding. With the simulated maturation of the fusion mass using PMMA, the load borne by the ventral plate was diminished, while greater load was absorbed by the graft in the form of increased pressure. In other words, a greater portion of the load was borne by the simulated early fusion (bone healing), which simultaneously

offloaded the plate. Subsequently, as the fusion further matures in vivo, greater loads are transmitted through the bony mass and the woven bone solidifies into organized remodelled bone. Simultaneously, a reduction in the load transmitted through the ventral plate is expected and, in fact, was observed here.

The scenario presented herein most likely simulates an early to intermediate phase of healing from a biomechanical perspective. With the cyclical loading of a simulated fusion mass (Condition 4; PMMA), subsidence or settling of the fusion mass continues to occur. More importantly, after plate removal, greater pressures continue to be observed at the graft site due to continued subsidence and greater load borne by the graft. The load sharing provided by the plate had been removed, thus shifting the entire load to the graft. This is reflected in a further increase of graft site pressure. It can be hypothesized, that had a dynamic plate been incorporated for fixation in this study (in lieu of the rigid ventral plate) greater subsidence would have been observed and thus, greater pressures at the graft site would have been expected.

### *3.5.3 Implications of Experimental Findings*

It appears, from the data presented herein, that the assessment of bone graft-endplate mortise pressure and implant loads can be used to assess the progression of fusion acquisition in the *in vivo* state. The utilization of the PMMA simulated the early to intermediate stages of bone healing in this study, as demonstrated by previous researchers.[3,21,130] Due to the difficulty of obtaining precise *in vivo* biomechanical data in humans, methods must be employed in an *in vitro* study to simulate clinical relevancy. Thus, the application of PMMA in this study represented the early to intermediate stages of bone healing after fusion surgery.

Overall, this preliminary study supports further investigations to determine feasibility of using pressure at the graft site and the simultaneous loads along a ventral plate to assess bone fusion status. The observation that pressure very closely parallels load **(Figure 3.3)**

lends significant credence to the use of pressure as a metric for the clinical assessment of biomechanical parameters. Use of these biomechanical parameters to quantify a biological phenomenon, such as bone healing, could lead to the future development of implantable biosensors to achieve similar information in an *in vivo* human clinical environment. Theoretically, MEMS technology could be applied to produce miniature biosensors that could be implanted at fixation and fusion sites to monitor healing progressions *in vivo*. This would provide an accurate real-time assessment of fusion status. Further work, however, is required. At the very least, the potential feasibility of using such measurements clinically has been shown.

### 3.6 Conclusion

In summary, this preliminary assessment demonstrated the biomechanical sequelae of load sharing during the acquisition of simulated arthrodesis. The alterations of pressure at the bone graft-endplate interface and the loads along the ventral plate were altered by various loading paradigms and construct conditions that simulated the early to intermediate fusion healing. Both graft site pressure and implant loading varied with different loading conditions. It appears that both pressure and load can serve as indicators for bone healing and fusion incorporation. The knowledge of these variables in the clinical situation, combined with appropriate clinically derived information, could greatly enhance the spine surgeon's postoperative assessment capabilities. In essence, graft site pressure and implant load evaluation serve as relevant biomechanical indicators of biological phenomenon, such as bone fusion acquisition. Accordingly, we have stated that our study is preliminary and that future investigations will be necessary to establish statistical significance.

# CHAPTER IV

# *IN VIVO* EVALUATION TO MONITOR THE CONTACT PRESSURES DURING BONE HEALING UTILIZING A GOAT MODEL

## 4.1 Study Overview

This study utilized a goat model to validate the ability to monitor contact pressures during bone healing at an interbody bone graft interface. The previous chapter concluded that it was conceivable to monitor the pressures at a bone graft interface and the forces along an active telemetric ventral cervical plate during bone healing. However, there were significant challenges that plagued monitoring cervical plate forces in vivo, in particular long-term coating of the plate and wiring system could not withstand long-term implantation into the harsh fluid environment of a living system. This was demonstrated by a trial implantation of a telemetric active cervical plate into a goat model. Within two weeks, there was significant cracking of the parylene and silastic coating of the wiring and electronics, leading to rapid failure of the active plate. Pressure posed to be an ideal parameter to monitor bone healing, as it directly measured the pressures at the bone graft site, which is the point of bone incorporation.

## 4.2 Introduction

Postoperatively, the status of a fusion and the incorporation of bone across a destabilized spinal segment can be difficult to assess and has led to a 20% underestimation of the fusion

grade.[11,14] In addition, conventional imaging techniques are limited in utility and cannot provide the surgeon with information regarding the dynamics of the fusion mass, adequate visualization of bone incorporation into the host bone (ie, vertebral endplates), mechanical integrity of the fusion mass, and the real-time bone remodeling scenario. An alternative mechanism for assessment with greater accuracy would be desirable.

We propose the novel concept of pressure measurement at the host bone and graft interface to monitor the spine fusion process. This choice of pressure as the monitoring parameter is based on some precedent. First, pressure is a well-defined physiological assessment parameter, particularly in the cardiovascular arena. Second, pressure measurement has been investigated for other areas in medicine, including the orthopedic arena.[19,40,80,87,105,113] For example, many researchers and clinicians have examined the relationship between intradiscal pressure and pain or the extent of motion segment degeneration.[19,69,86] Nevertheless, there is a dearth of research exploring the relationship between pressure and bone healing.

Telemetric transmission of biomechanically derived information for *in vivo* healing and implant behavior assessment is not a novel concept.[69,86,95,99,113] Researchers have attempted to employ strain gauges on spinal implants, using telemetric data transmission for *in vivo* serial monitoring of loads following fusion during daily activities.[99,101] Unfortunately, these systems were plagued with complications. The telemetric unit was bulky, and internal wire breakage was a common occurrence. Consequently, long-term measurements (> 4-6 months) of *in vivo* axial loads on implants and bone healing were not accomplished. In our study, we used a commercially available implantable telemetric transducer with two gel-filled catheters that were implanted at the graft and vertebral endplate interface at the bone graft site in the goat cervical spine. These transducers housed all of the electronic components within a hermetically sealed chamber and used the two gel-filled catheters for pressure transmission. Therefore, there was little risk of internal wire breakage and loss of signal transmission.

*In vivo* animal studies are often used to investigate the effects of altered biomechanical parameters and their association with evolving biological events. The goat's cervical spine has greater bone density than that of humans, shows less variability within the species, is kinematically different, and possesses anatomical differences from that of humans.[117] Nevertheless, several factors make the goat a suitable model for measurement of interbody bone graft pressure. The upright posture of the goat's cervical spine is ideal for interbody fusion studies because the cervical spine is axially loaded.[117,137] In addition, although the cervical disc interspace of a goat spine is essentially a ball and socket joint and the human disc interspace is elliptically shaped, the range of motion is similar.[132]

This preliminary study was designed to assess the *in vivo* healing status of the spine, with an overall goal to demonstrate thatchanges in the *in vivo* biomechanical parameters (ie, pressure in this scenario) can be measured over time. The basic concept of the study was to establish the feasibility of using telemetric pressure sensors to assess the process of bone healing in vivo. Information generated from studies like this could contribute to future development of implantable microsized biosensors using microelectromechanical systems (MEMS) technology for *in vivo* chronic monitoring of orthopedic implant performance and tissue healing.[5,8,38,105] However, this technology is not yet commercially available, and the ability to actually monitor the *in vivo* bone healing and to sense a change in biomechanical parameters must be addressed before the technology can be developed. Therefore, preliminary proof-of-concept studies using conventional pressure transducers are required to provide the necessary information to design and develop implantable biosensors that might employ novel technologies such as MEMS. Once it is deemed a feasible concept to investigate further, the potential of such a technology is infinite. Possible applications include incorporation of microsized implantable biosensors onto orthopedic implants to detect early migration of the implant, loss of fixation at the bone and implant interface, and changes in tissue performance based on these measurements.

A goat cervical interbody fusion model was employed in this study to address the feasibility of using pressure measurements to monitor the process of bone healing by differentiating between the successful initial acquisition of fusion and the development of a pseudarthrosis during the early postoperative period. Therefore, we focused on the use of pressure as an indicator of changes in healing patterns that can be indicative of fixation loss and pseudarthrosis.

### 4.3 Materials and Methods Overview

A goat cervical interbody fusion model was employed. Pour study groups were analyzed. Six male castrated Alpine goats underwent a ventral fusion operation at C3-C4, following discectomy. Iliac crest autograft, with an accompanying ventral cervical fixation plate (DOC; Depuy-Acromed, Raynham, Massachusetts), was employed. Five of the goats were implanted with a dual-channel telemetric pressure transducer and were sacrificed at either 4 (Group A) or 6 (Group B) months **(Table 4.1)**. The remaining goat functioned as an operative control in which telemetric hardware was not placed, but a bone graft at C3-4 was placed (Group C). This goat was sacrificed at 4 months. *In vivo* contact pressure at the bone graft and vertebral endplate interface was assessed in each goat in Groups A and B three times daily. At the termination of the study, each goat was euthanized, and the spines were harvested for further evaluation of the fusion status via non-destructive biomechanical testing, histological sectioning, or micro-CT imaging.

**Table 4.1.** Study Group Composition and Fusion Status Assessments Conducted

| | Group A | Group B | Group C | Group D |
|---|---|---|---|---|
| **Composition** | Goats 1,2,3<br>Euthanized at 4 months<br>(n=3) | Goats 4,5<br>Euthanized at 6 months<br>(n=2) | Control<br>No pressure transducer<br>(n=1) | Cadaveric cervical spines<br>for *in vitro* testing<br>(n=6) |
| **Fusion Status Assessments** | Histology (n=1)<br>Biomechanical (n=2)<br>MicroCT (n=1) | Histology (n=1)<br>Biomechanical (n=1)<br>MicroCT (n=2) | Histology (n=1) | Biomechanical (n=6) |

### *4.3.1 Pressure Transducer and Calibration Procedure*

Prior to surgical implantation, the calibration of the DSI dual-channel, telemetric pressure transducer (Physiotel Multiplus Implant, TL11M3-D70-PCP Data Science International, St. Paul, Minnesota) was evaluated by placing a manual contact load onto each catheter following the configuration of the device once *in vivo*. Each transducer had an accuracy of ± 0.1 kPa and a maximal pressure shift of 2%, with two independent catheters used to monitor *in vivo* contact pressure at the bone graft interface site in the goat spines **(Figure 4.1)**. The battery was rated at a nominal lifespan of 3.5 months for continuous use and was housed with the transmitter. Two 1.2-mm-diameter silicone, elastomeric, close-ended, compressible tube catheters with pressure sensors housed at the proximal end of the fluid-filled tubes were used to measure pressure at the bone graft and vertebral endplate interfaces under compressive loading. Each closed catheter was affixed within a circular canal at the bone graft and vertebral endplate interface and transmitted the contact pressure measurements from the bone graft to the pressure sensor sealed within each catheter.

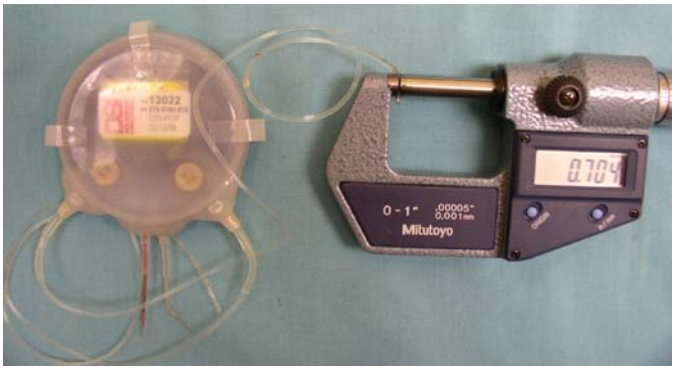


**Figure 4.1:** The DSI telemetric pressure transducer housing two pressure sensors within the fluid-filled catheters, with one catheter being compressed to a measured displacement to demonstrate the catheter compliancy.

Prior to implantation of each pressure transducer, the linearity and tracking behavior of each pressure transducer was measured against the compressive loading applied by the Instron test apparatus. This was accomplished by applying six cycles of a known compressive load to each transducer and comparing it to the pressure measurements acquired. A sinusoidal load at a frequency of 0.1 Hz and a maximum compressive load of 200 N were applied under load control using the servohydraulic materials test apparatus (Instron 8874, Instron

Corp., Canton, Massachusetts) to the pressure transducer. To do so, the catheter was restrained within a semicircular canal and directly compressed by the Instron testing apparatus. The compressive loading cycles applied by the testing apparatus were mapped against the measured pressure cycles to assess the transducers' performance with respect to phase lags, accuracy, and/or nonlinearities in response to the compressive loading **(Figure 4.2)**. The maximum catheter deformation under compressive load for each sample was also measured. A linear regression analysis was conducted to assess the linearity of the pressure transducer and the phase lag in response to the compressive loading. The configuration and operation of the pressure transducers was by Dataquest A.R.T. version 2.3 software (DSI) to sample all of the recorded pressure at a sampling rate of 500 Hz. Finally, the subsidence across the C3-C4 motion segment was quantified by measuring the ventral and dorsal motion during cadaveric biomechanical testing for six of the cervical spine specimens using the MaxTRAQ version 1.41 software image analysis system (Innovision Systems Inc., Lapeer, Michigan).

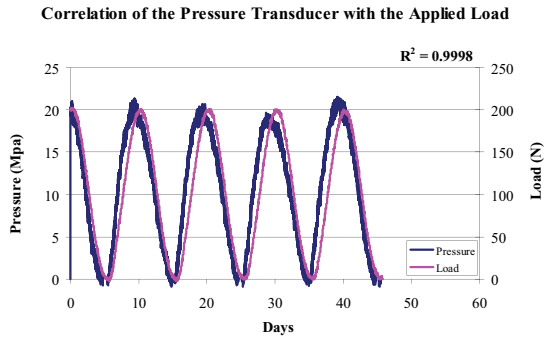


**Figure 4.2:** Correlation of the pressure transducer with a 200-N applied load from the instron testing apparatus. A sinusoidal waveform input from 0 N to 200 N in pure compression at a rate of 0.1 Hz was applied for five cycles of loading. The accuracy of the transducers is demonstrated by the linear correlation between pressure and the applied load, $R^2$=0.9998.

### *4.3.2 Surgical Procedure for the Cervical Interbody Fusion*

An incision was made ventral to the stenocleidomastoid muscle (SCM). The spine was approached between the strap muscles, esophagus, and trachea medially and the carotid sheath and SCM laterally. After the longus coli muscle was retracted laterally, a ventral discectomy was performed at the C3-C4 segment after localization with fluoroscopy. An osteotome was used to craft mortises by cutting out a box-shaped region (1.3 $cm^3$) for placement of the bone graft **(Figure 4.3)**. Autogenous bone was harvested from the goat's


**Figure 4.3** Cuboid-shaped autogenous bone graft crafted from the iliac crest of the goat. The dimensions closely matched that of the host sites at C3-C4.

iliac crest, properly sized, and gently impacted into the C3-C4 disc space **(Figures 4.3 and 4.4)**. Each bone graft for all five goats was reproducible in size to an error of less than 10%. A 2.8-cm DOC ventral cervical rigid plate (DePuy Spine, [J&J subsidiary], Raynham, Massachusetts), with 4-mm-by-16-mm divergent fixed angle screws, was used to immobilize the C3-C4 motion segment once the bone graft was in place **(Figure 4.4)**. The telemetric pressure transducer was implanted after the bone grafting procedure by insertion of each catheter above and below the bone graft into two pre-awled locations at the bone graft-vertebral endplate interfaces and sutured into place **(Figure 4.4)**. Each pressure-sensing catheter was seated into a circular channel that was created at the bone graft-vertebral endplate interface to provide localized containment of the catheters for the transmission of contact pressures. The transmitter and battery portions of the transducer were implanted in a submuscular pocket created in the dorsolateral region in each goat's neck.

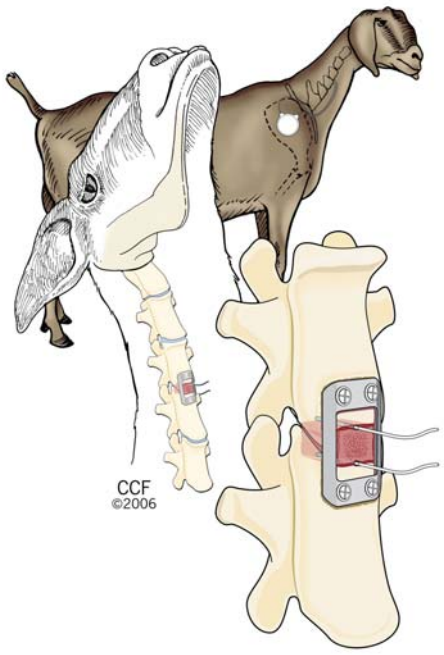


**Figure 4.4** An illustration of the two catheter placements from the DSI pressure transducer into the goat cervical spine. The catheters were inserted approximately 1 cm in depth at the superior and inferior bone graft and vertebral endplate interface.

The goats were monitored daily for signs of infection and distress for the duration of the study

(4-6 months). This time frame has been used successfully for cervical interbody fusion in goats.[135-137] One of the six original goats demonstrated early signs of wound infection and was dropped from the study analysis. Pressure was recorded three times daily for a duration of 2 minutes per trial while the goats stood idle with their necks in an upright position. Efforts were made to calm each animal prior to sampling pressure data to ensure minimal physical activity during data sampling. At the end of 4 to 6 months, the goats were euthanized with an overdose of pentobarbital (75 mg/kg) using a standardized protocol that is compliant with the Animal Review Committee for the Cleveland Clinic.

### *4.3.3 Histological Preparation*

Two goats (one each in Groups A and B) were used for histological evaluation. Tissue samples were fixed in 70% ethanol and rough-cut with a band saw to remove adherent soft tissue and the spinous processes. Tissue blocks were then slowly dehydrated without decalcification in a graded series of ethanols and embedded in methylmethacrylate (MMA) using a vacuum chamber at 2°C to 8°C over a 23-day period. Without removing the fixation hardware, sagittal cuts were made using an Exakt diamond saw (EXAKT, Appartebau, Germany), in three sections (central, medial, and lateral) of each C3-C4 level. Each section was ground to a final thickness of 10 to 40 mm and stained with Villanueva's mineralized bone stain (Poly Scientific, Bay Shore, New York). With this staining technique, the mineralized bone stains green, osteoid seams stain magenta, and the remaining tissue stains blue and pink. Once the sections were stained, a board-certified pathologist meticulously assessed each slide for signs of new bone growth and adverse tissue reactions.

### *4.3.4 Biomechanical Testing*

An *in vitro* biomechanical evaluation of the fusion status for three of the Group A and B goats was conducted and compared to the biomechanical behavior of six cadaveric goat

spines implanted with a bone graft and ventral cervical plate at C3-C4 (Group D) to assess the status of the fusions in the implanted goat spines postmortem. Group D consisted of six cadaveric goat cervical spines obtained from a local slaughterhouse and implanted with bone grafts and ventral plates, just prior to the time of biomechanical testing. In these Group D specimens, snug bone-on-bone contact was achieved with an accompanying overlying ventral plate. This position resembles the clinical situation that exists immediately after surgery, when healing and arthrodesis have not yet begun. Variations in contact pressure at the graft interface were examined for possible relationships to fusion status.

Nine goat spines were used for the biomechanical evaluation of the fusion site to determine whether a fusion was present. Three spines were harvested from Groups A and B **(Table 4.1)**. Six additional spines (Group D) were obtained from a local slaughterhouse vendor and used as a biomechanical comparison for the immediate nonfused grafted situation at C3-C4.

In preparation for testing, the spines were embedded at C2 and C5 into customized gripping fixtures and mounted onto a servohydraulic biaxial testing apparatus (Instron 8874). Each spine was secured to the Instron testing apparatus in a cantilever loading fashion and preconditioned for 20 cycles to 200 N in compression. The center of rotation was located by applying a 200-N maximum compressive load to the upper jig and reapplied until no angular motion was detected by the upper rotational potentiometer. Following the preconditioning and alignment phases, each cervical spine was nondestructively cycled under load control in compression to 200 N at 0.1 Hz for six continuous cycles at a data sampling rate of 50 Hz.[25,135-137]

### *4.3.5 Micro-CT Imaging*

Micro-CT images of three of the five goats (Three out of five goats were chosen for MicroCT examination, as this procedure was conducted on the specimens allotted for

biomechanical testing. The remaining two specimens were prepared for histology prior to MicroCT.) from Group A and B specimens **(Table 4.1)** were obtained by collecting one hundred and eighty 512-by-512 twelve-bit projection radiographs at 1° intervals around half of the entire specimen.[67] The images were collected at 90 kVp, 28mA, and with a 1-second exposure time with the image intensifier operating in 7-inch mode and at twice the magnification. Off-line image corrections of the x-ray projection data were conducted following the protocol of Grass et al.[46] The micro-CT images provided high-resolution x-ray imaging of the fusion sites for each goat specimen and provided details of the trabecular structure.

| Group | Goat Number | Relative Change in Pressure (Normalized to Day 0) (%) | Fusion Status |
|---|---|---|---|
| **A** | **1** | 390 | No |
| | **2** | 410 | No |
| | **3** | 237 | No |
| | | | |
| **B** | **4** | 214 | No |
| | **5** | 333 | No |
| | | | |
| **C** | | | Yes |
| | | | |
| **D** | **1** | | No |
| | **2** | | No |
| | **3** | | No |
| | **4** | | No |
| | **5** | | No |
| | **6** | | No |

**Table 4.2:** Fusion outcomes and a summary of the relative changes in pressure within the first ten days of recording for Groups A and B.

### *4.3.6 Data Analysis*

For the pressure measurements, care was taken to capture data while each animal stood idle and was not engaged in chewing or swallowing. The relative change in pressure from the three daily trials was averaged and normalized to the pressure

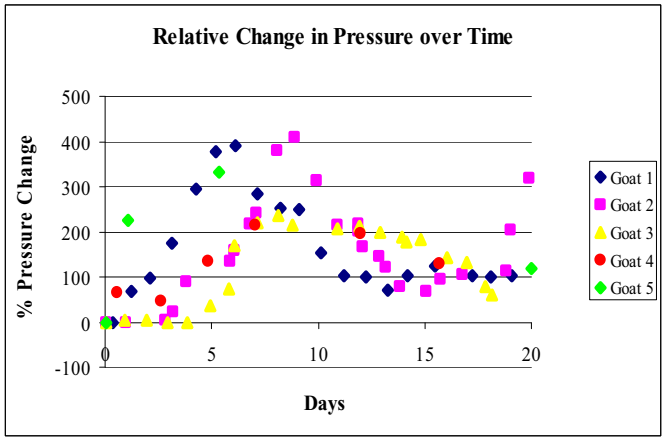


**Figure 4.5** Graphical representation of the relative change in pressure from day 0 for all of the goats. A rapid increase in pressure was observed within the first 10 days of healing with peak pressure occuring between days 6 and 9.

recorded on day 0 and then plotted against time **(Figure 4.5)**. The means and standard deviations were calculated for each daily data set and the means are presented in **Figure 4.5**. The maximum relative change in pressure within the first 10 days of pressure recordings is shown in **Table 4.2.** Due to the small sample size of the animals used for fusion in this study, the trends in relative pressure changes were examined, and a limited statistical analysis was conducted for bone graft sizing using a one-way analysis of variance (ANOVA).

## 4.4 Results

### *4.4.1 Evaluation of the Pressure Transducer*

**Figure 4.2** demonstrates the output performance of the pressure transducers while loaded from 0 N to 200 N in pure compression by the Instron test machine. The 200-N compressive load correlated with a mean deformation of 1.37 ± 0.04 mm for the catheter and approximately 20 MPa of pressure recorded from the catheter. A linear regression and correlation was conducted on the load and pressure, yielding an $R^2$ of 0.998, indicating the presence of a high degree of linearity of the pressure transducer. Very little phase lag (< 1 second) was observed between the Instron load cycles and the pressure measured at the bone graft interface. The lag is attributable to the delay in the actual hydraulics of the Instron testing apparatus and the delay in the viscoelastic response of spinal tissues.

### *4.4.2 Fusion Status*

None of the remaining five goats exhibited external evidence of infection, distress, or catheter extrusion within the first 20 days postoperatively. Long-term complications after 20 days, however, were observed in three of the goats implanted with the pressure transducers. Seroma formation and catheter extrusions were observed in these goats after 20 days. Fortunately, each pressure transducer housed two independent recording catheters. Hence, the extrusion of a single catheter did not affect the pressure monitoring process. The pressure

measurements from the caudal catheter are presented in this report. The caudal catheter pressure readings were consistently greater than the rostral catheter readings by a small margin (< 10% for all goats). This is attributable, at least in part, to the added weight of the graft and the additional load transmission to the caudal portion of the vertebral body at C3-C4.

For all 11 goat spines that were grafted **(Table 4.2)**, no significant difference was observed between the bone graft sizes for any of the goat spines (P≥0.5). None of the goats from Groups A or B, however, achieved a solid bony fusion **(Table 4.2)**. The histological and micro-CT images demonstrated a pseudarthrosis at the C3-C4 bone graft site in the goats implanted with pressure transducers **(Figures 4.6 and 4.7)**. The single goat (Group C) that did not receive a pressure transducer demonstrated histological evidence of a solid fusion at C3-C4 after four months **(Table 4.2)**.

A proprietary gel contained within the catheter was found in the surrounding tissues at the operated sites. Histologically, an inflammatory

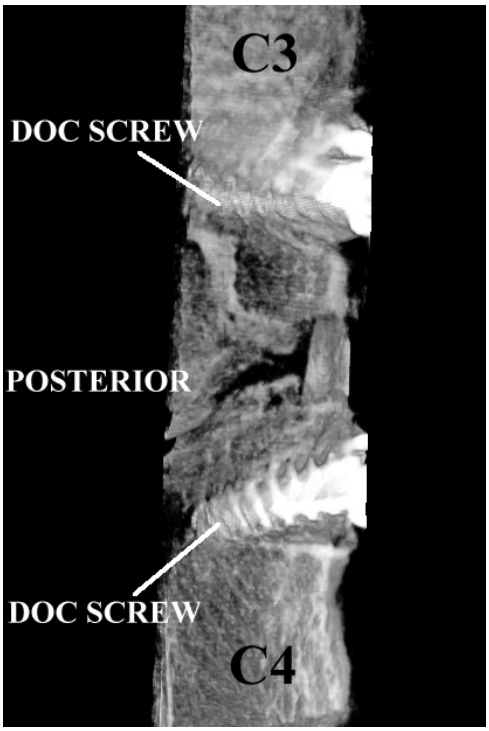


**Figure 4.6** MicroCT depicting the sagittal view through the C3-4 fusion site. A solid arthrodesis has not formed at 6 months post-operatively and bone graft remnants that have not completely resorbed, are visible.

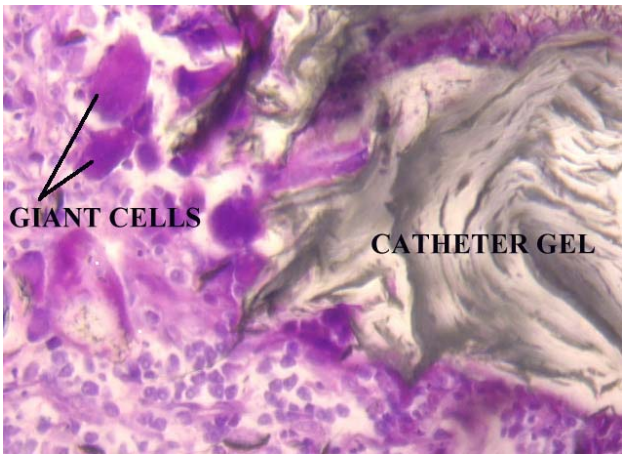


**Figure 4.7** Undecalcified histological section depicting the inflammatory response observed surrounding the gel exudates from the pressure transducer catheters.

reaction associated with this gel was present near the bone interface where the gel had egressed from the implanted catheters **(Figure 4.7)**.

### *4.4.3 Pressure*

**Table 4.2** depicts the relative maximum change in pressure for Groups A and B within the initial 10 days of recordings. The pressure measurements at day 0 ranged from 0.6 MPa (Goat 5) to 3.6 MPa (Goat 4). All of the data for each goat were normalized to day 0 for valid comparisons. Goat 2 (Group A) demonstrated the highest change in pressure, with a 410% increase within the first 10 days **(Table 4.2)**. All of the goats demonstrated consistent increases in interface pressure within the first 10 days postoperatively, ranging from a 200% to 400% increase **(Figure 4.5 and Table 4.2)**. The absolute pressure ranged from 2.5 MPa for Goat 2 to 7.6 MPa for Goat 4, with the standard deviations ranging from 0.01 to 1.00 for the average daily means among all of the goats studied. The peaks in pressure occurred between days 6 and 9 for all goats. From day 10 to day 20, all of the goats demonstrated a decline in pressure. Erratic pressure was observed thereafter. With respect to the extent of quantifiable subsidence measured during the *in vitro* biomechanical testing of the Group D specimens, a mean subsidence of 0.25 + 0.10 mm was measured across the C3-C4 bone grafted site.

## 4.5 Discussion

This preliminary study defines the pressure changes that occur during the development of a non-union after attempted cervical spine fusion. An increase in pressure during the early stages (first 10 days) correlates with an expected early graft subsidence. Postoperative subsidence increases the load borne by the graft, thus increasing the pressure observed at the interface between the bone graft and the vertebral endplate.[119] The initiation of graft instability and pseudarthrosis appears to be heralded by the appearance of erratic fluctuating pressure patterns at the bone graft-vertebral body interface. A rise in the interface pressure was consistently observed in all goats within the first 10 days of monitoring in the present

study. As previously stated, early graft settling or subsidence occurs within the first week of surgery. In humans, a mean subsidence of 1.4mm with ventral cervical fusion using autologous bone graft at 1 to 2 weeks after surgery has been reported.[6,119] It is therefore likely that the reproducible increase in pressure during this phase of healing is attributable to early bone graft subsidence at the fusion site, as validated during the *in vitro* testing conducted on the Group D spines. An interesting point to consider is that the DOC ventral cervical rigid plate used divergent fixed angled screws that by nature of design provide an anterior localized compression to the bone graft where the plate meets the bony margin of the vertebral body. This type of plating causes the center of rotation (COR) of the spine, which is naturally located halfway between the anterior and posterior vertebral margin, to shift toward the proximity of the plate fixation.[29,126] This shifting of the COR toward the plate contributed to a localized compression at the anterior portion of the vertebral body and bone graft. This would technically stress shield the posterior portion of the bone graft but provide greater stress upon the anterior and middle portion of the graft. Therefore, higher pressure would have been expected but was masked by this phenomenon.

There were some limitations to this preliminary study. The absence of fusion in this study could be attributed to the adverse reactions to the catheter and its gel, as well as the eventual seroma formation. An inflammatory reaction was found to be associated with the catheter gel in the surrounding tissue at the fusion site. Additionally, one of the disadvantages of currently available implantable telemetric units is that the bulky implants cause inflammation in the juxtaposed musculature, resulting in irritation and seroma formation.

Fortuitously, the ensuing pseudarthroses provided the opportunity to document the pressure changes associated with a failed fusion. The erratic pressure was observed following the initial subsidence phase of healing, during which interface pressure was elevated. This is intuitively associated with motion and pseudarthrosis. If stability were present, motion at the graft site would not occur and fluctuations of pressure at this site would similarly not be observed. Therefore, erratic fluctuations of pressure are consistent with pseudarthrosis,

whereas elevations of pressure are consistent with the expected subsidence that accompanies the nonpathological events that ensue during the early postoperative healing period. Nevertheless, the proof-of-concept goal of this study—that is, the ability to monitor pressure fluctuations with early bone healing-was achieved even with a small sample size. This concept can be applied further to the potential use of implant performance and tissue reaction for numerous motion-preserving and dynamized devices. However, improved clinical methods for telemetric pressure assessment are eagerly anticipated, with the hope that these improvements will facilitate the development of an implantable biosensor using MEMS technology.

# CHAPTER V

# AN *IN VIVO* BIOCOMPATIBILITY ASSESSMENT OF MEMS MATERIALS FOR USE WITH AN IMPLANTABLE MEMS PRESSURE SENSOR

## 5.1 Study Overview

The site-specific biocompatibility of silicon and related materials that are commonly used to construct MEMS pressure sensors were evaluated six months after implantation in the caprine cervical spine. After autopsy, gross examination and histological techniques were used to characterize local and peripheral tissue responses. The study involved two phases of *in situ* implantations of MEMS materials into the caprine spine. The first phase involved the insertion of silicon chips into the nucleus pulposus of multiple lumbar discs and the implantation of MEMS pressure sensors into autologous bone grafts in the caprine cervical spine. The second phase involved a more comprehensive implantation of five types of materials used for fabricating MEMS pressure sensors. Titanium is a commonly used material for orthopedic implants and served as the study control. Two castrated adult male goats were used to test for the site-specific biocompatibility of materials used in MEMS devices to determine the site-specific biocompatibility and wound-healing behavior of tissue exposed to MEMS based materials. Histological analysis of compromised spinal segments

after a six-month survival period did not reveal evidence of any adverse foreign body response by the caprine spinal tissue to the implanted MEMS materials. Furthermore, there were no signs of infection or inflammation in response to the variety of MEMS materials used in the fabrication of miniature devices.

## 5.2 Introduction

The concept of MicroElectroMechanical Systems (MEMS) has raised considerable attention for their potential use in medical devices. MEMS technology combines integrated circuit technology similar to the semiconductor industry with microfabrication processing for the development of microsized devices that can detect pressures, strains, forces, displacements, etc... However, the implantation of foreign objects into a living system, such as a device made with the materials used for the fabrication of MEMS sensors, must be evaluated with respect to tissue response and adverse tissue reactions.

The existing materials used to construct orthopedic and cardiac implants are not suitable materials for fabricating MEMS biosensors. Silicon is a common material used in the fabrication of MEMS devices which has recently entered the medical device arena. Materials such as medical grade epoxy and titanium (Ti) have been supplemented with Silicon Nitride ($Si_3N_4$) for use in dental applications.[27] Drug-delivery devices, microneedles, and immune-isolating biocapsules for long-term implantation are incorporating MEMS technology.[63,70,75,123,124] Although titanium implants within the body are biocompatible if they do not generate large doses of titanium particulate due to wear and fretting (greater than 200 mg of particulate)[26], the processing techniques used in MEMS construction may pose a threat to a living system if MEMS materials are combined with titanium implants. Large doses of titanium particulate from wear debris have been shown to elicit osteolysis or bone resorption in the spine.[20,25,26,42,48,122] Combining the interaction of titanium with MEMS

materials for use as long-term implantable sensors could produce adverse tissue reactions, thus prompting further *in situ* investigation within tissue.

MEMS devices or silicon-based microelectrodes have demonstrated significant biofouling in living systems over time.[27,84,85,118] Previous work has been conducted by the authors demonstrating the inert effects of MEMS materials in the cervical spine vertebrae and lumbar intervertebral discs using a caprine model.[37,38] Further analysis was needed, however, in the form of a more comprehensive evaluation of the safety of MEMS microfabrication materials within spinal bone. Therefore, the objective of this study was to expand upon earlier work by determining the site-specific biocompatibility and wound-healing behavior of osseous and intradiscal tissue exposed to the materials currently utilized in the construction of potentially implantable MEMS devices.[37,38]

## 5.3 Materials and Methods

### *5.3.1 Phase I*

Phase I was a limited biocompatibility evaluation that investigated the base material (silicon) used to fabricate MEMS devices and actual MEMS pressures sensors. Samples of single crystal silicon (Si) and commercially available MEMS based piezoresistive pressure sensor die were selected for evaluation in a caprine model. A <100>-oriented, n-type, single side polished, 100 mm-diameter, 500 µm-thick Si wafer was diced into 1 mm-long x 2 mm-wide chips using an automated dicing saw. The pressure sensor die (Lucas NovaSensor P529B, Fremont, CA) was 0.6 mm thick with a 1 x 1 mm-wide square top surface (**Figure 5.1**). The sensor was rated for

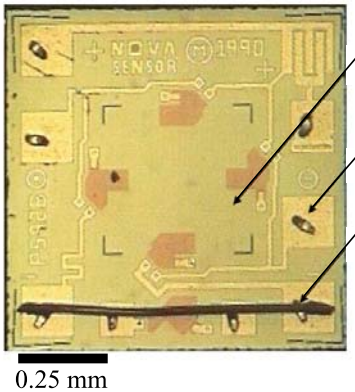


**Figure 5.1:** The Lucas NovaSensor MEMS Pressure Sensor.

absolute pressure measurement up to 350 kPa and comprised of a bulk micromachined Si membrane with 150 x 150 μm-wide aluminum contact pads. For the purpose of this study, the pressure sensors were not powered to minimize the confounding effects from wires and implanted batteries. The MEMS materials were cleaned in isopropyl alcohol and deionized water and subsequently treated by sterilization, which was conducted in a standard steam autoclave under a wrap/gravity algorithm for 25 minutes and 10 minutes dry at 121°C.

#### *5.3.1.1 Surgical Procedures*

The caprine (goat) model was selected due to the favorable anatomy of its cervical spine, which exhibits a long upright posture and axial loading characteristics[117]. The relatively long and slightly lordotic neck of a goat is exposed to daily cyclical loads and bending moments similar to the loading paradigm of the human spine.[112,117,132,135-137] The cervical and lumbar spine regions of an adult castrated 65kg male Nubian goat were chosen as the target areas for site-specific biocompatibility testing of silicon chips and the pressure sensor die.

An autologous iliac crest bone graft was implanted into the C4-5 intervertebral disc space after a complete discectomy. A MEMS pressure sensor was placed within the C4-5 bone graft close to the vertebral endplate interface. Three intervertebral discs in the lumbar spine (L2-3, L3-4, L4-5) were also selected for evaluation. The L2-3 intervertebral disc was selected as the sham control for the lumbar spine where a MEMS pressure sensor was not implanted but a surgical approach was employed. Two Si chips were implanted into the L3-4 disc and two pressure sensors were inserted into the L4-5 disc. The implantation period for the MEMS sensors and materials was six months after which the animal was euthanized and the cervical and lumbar spines meticulously harvested for subsequent evaluation.

**Cervical Spine**

The goat was prepared for surgery in accordance with an approved ARC (Animal Review Committee) protocol that complies with federal regulations for the humane treatment of animals. The goat was anesthetized with 1% isoflurane and positioned laterally on a Jackson table. A standard ventral incision was made on the cervical region of the spine in the goat neck and the surrounding musculature carefully displaced to expose the C3-C7 segments of the cervical spine. Care was taken not to stress the carotid artery, esophagus, and trachea of the animal. The organs were gently retracted laterally, to allow access to the vertebral bodies. A standard cervical discectomy was performed at the C4-5 vertebral levels using small pediatric pituitary rongeurs. The cervical intervertebral space was then prepared for the bone graft implantation. The vertebral endplates were meticulously cleaned using a curette to allow for increased vascularization, which would provide a favorable environment for enhanced bone incorporation.

A bone graft was harvested from the iliac crest of the goat (**Figure 5.2**). A small incision was made over the iliac crest and the musculature carefully dissected using a Cobb elevator. A horseshoe shaped section of bone (approximately 21 mm-wide x 32 mm-deep x 10 mm-in height) was removed from this region using a sharpened osteotome and stored in sterile Ringer's Lactate solution until the time of

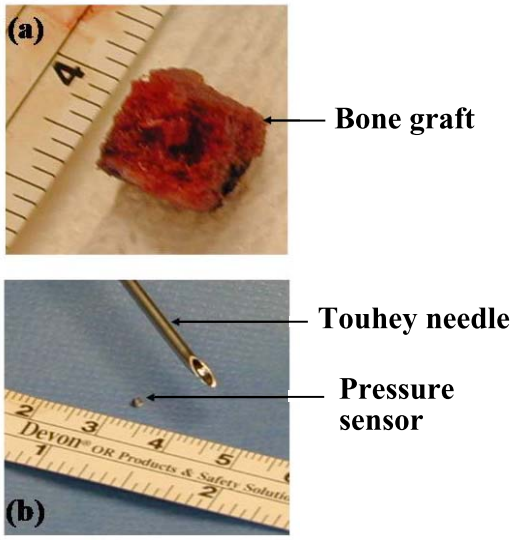


**Figure 5.2:** The upper figure (a) illustrates the cubed shape bone graft carved from the goat's iliac crest used for fusion into the C3-C4 interbody space of the cervical spine. The lower figure (b) illustrates the MEMS pressure sensor relative to the Touhey needle, used for minimally invasive insertion of the sensors into the vertebral bone and discs of the goat.

implantation. An 18-gauge Touhey needle was used to bore approximately a 1 mm-diameter x 3 mm-deep cylindrical hole into the bone graft. Afterwards, the pressure sensor was placed into this hole and packed with morselized bone. The graft was inserted into the C4-5 intervertebral space and was stabilized using a ventral DOC cervical stabilization spinal implant (DOC Ventral Rod System, DePuy Acromed (a Johnson & Johnson company, Raynham, MA).

Surgical closure was performed in a standard manner after the spinal instrumentation was in place. The musculature was closed using Ethibond (0.0) suture and single whip stitches. The skin was closed with Prolene suture (0.0) utilizing a continuous running stitch.

**Lumbar Spine**

The lumbar spine was approached through the dorsal aspect with the goat positioned in a lateral configuration. Each disc was exposed through a lateral view and the center of each disc located using 14-gauge needles. Samples of MEMS materials were subsequently introduced into nucleus pulposus regions of the L3-4 (Si chips) and L4-5 (pressure sensor) discs using an 18-gauge Touhey needle. The L2-3 disc was also penetrated with the needle without the placement of a sample material to serve as a sham control. The dorsal musculature was then closed over the exposure site and sutured with Ethibond 2.0, followed by a standard skin closure utilizing Prolene 0.0 suture with running stitches.

The stitches were cleaned with Betadine antibiotic and the animal was transported to the Intensive Care Unit for 48 hours of observation. Fluoroscopy and plain radiographs were conducted to document the surgical sites of the cervical and lumbar spines, as well as the placement and integrity of the DOC spinal instrumentation.

#### *5.3.1.2 Euthanasia and Histological Procedure*

**Figure 5.3:** Section of harvested cervical spine showing the intact DOC Ventral Rod System that was used to stabilize the fusion site.

The goat was euthanized six months post-operatively and the cervical and lumbar spine segments were harvested for histological preparation (**Figure 5.3**). An overdose of Pentobarbital was administered intravenously at a lethal dosage (75 mg/kg via intravenous injection) to ensure rapid demise with no sensation of pain or discomfort. After absence of a cardiac pulse, the cervical and lumbar spines were harvested and subsequently prepared for histological assessment. The DOC spinal system was meticulously dissected from the cervical spine with sufficient care to prevent destruction of the essential bony matrix at the fusion site. Each segment in both the cervical and lumbar regions was visually inspected for any gross abnormalities that might have resulted from adverse reactions to the MEMS materials.

Each cervical and lumbar segment were further dissected serially within the sagittal plane into smaller segments and fixed in 10% neutral buffered formalin, decalcified using a commercially prepared hydrochloric acid (HCl) based decalcifier, dehydrated through a series of graded alcohols, cleaned in xylene, and embedded in paraffin. The paraffin embedded segments were sectioned into 5 μm-thick specimens, mounted onto glass slides, and stained with hemotoxylin and eosin (H&E). A licensed pathologist supervised the histological assessment and each slide was evaluated for signs of inflammatory responses by three independent observers.

### *5.3.2 Phase 2*

This phase of the study was conducted to further address the *in situ* biocompatibility of multiple varieties of MEMS fabrication materials. Five varieties of materials used for fabricating the components of MEMS pressure sensors were implanted into various regions of the caprine cervical spine **(Table 5.1)**. One 65kg castrated adult male goat was used to test for the site-specific biocompatibility of MEMS materials used in the microfabrication of devices.

| Cervical Spine Level | Material |
|---|---|
| C2 | $Si_3N_4$ |
| C3 | Ti |
| C4 | MEMS pressure sensor |
| C5 | SiC |
| C6 | $SiO_2$ |
| C7 | Si |

**Table 5.1:** Listing of the cervical spine materials and the specific material implanted to test for site specific biocompatibility.

Six vertebral bodies (C2-C7) of the caprine cervical spine were each used to house a different set of materials as listed in Table 5.1. The materials consisted of;

1) Silicon Nitride ($Si_3N_4$),

2) Titanium particles (Ti),

3) Inactive piezoresistive MEMS pressure sensors (composed of silicon and aluminum wire bonding, - Lucas NovaSensor P529B, Fremont, California)

4) Silicon carbide (SiC),

5) Silicon dioxide ($SiO_2$),

6) Silicon (Si),

Medical grade titanium (Ti-6Al-4V, TRADCO Inc., Sullivan, Missouri) has widely demonstrated its biocompatibility when implanted into human tissue for over a decade of

use in surgical spinal implants. Multiple studies have demonstrated that medical grade titanium does not elicit adverse affects during long-term surgical implantation into living tissues. The scope of titanium spinal implants covers the gamut from rod and pedicle screw systems, interbody device systems, and dorsal and ventral plating systems. Thus, titanium is a widely accepted implant material for use in orthopedic applications and served as the study control.[4,58,109,116,133]

The materials listed in **Table 5.1**, with the exception of titanium, were prepared on silicon substrates by sputtering four inch silicon wafers with carbide, dioxide, or nitride. Each sputtered wafer was cut into multiple 1 mm x 1 mm x 0.5 mm chips, examined by microscopy for visual characteristics, and measured for approximate dimensions. The titanium alloy particles measured approximately 1-2mm in length by 0.5 mm in width and were provided by grinding medical grade titanium alloy plates. All materials were packaged and steam sterilized utilizing a wrap/gravity algorithm in a standard steam autoclave (Steris/ AMSCO, Mentor, Ohio) for 25 minutes at 121°C and 15 psi prior to implantation.

#### *5.3.2.1 Surgical and Post-surgical Procedures*

One 65kg castrated male goat was prepared for surgery in the standard ARC (Animal Review Committee) manner. The goat was anesthetized with 1% isoflurane and positioned laterally on a Jackson table. A standard ventral incision was made on the skin layer along the cervical region of the spine. The

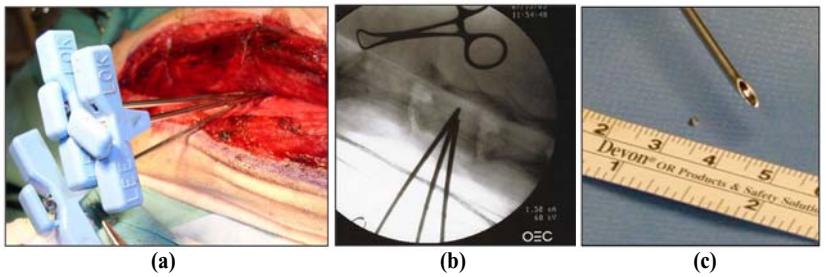


(a) (b) (c)

**Figure 5.4:** Three Lee-Lok 11-Gauge bone marrow needles placed into the anterior aspect of a cervical vertebral body, covered by the surrounding musculature (a). A fluoroscopic image demonstrating the insertion of the three Lee-Lok 11 gauge bone marrow needles into a cervical vertebral body. One cluster containing five chips of a specified material was injected via a saline-filled syringe down the needles and into the targeted bone (b). A MEMS pressure sensor and the delivery needle used in the procedure (c).

skin was carefully dissected exposing the underlying musculature. The musculature remained intact and was not displaced to avoid compromising the neck muscles and excessive bleeding. A minimally invasive anterior approach through the musculature into the targeted cervical vertebral bodies was incorporated using fluoroscopy for guiding the bone marrow needles into the vertebral bodies. A 5 mm incision was made through the musculature into the bone at each cervical spine level (C2 to C7), and three Lee-Lok 11-Gauge, 5 ½ inch long bone marrow harvesting needles were gently impacted into each vertebral body in three locations (**Figure 5.4 a,b and c**).

A saline-filled syringe containing one cluster of five chips was connected to each needle and injected into the prepared bone space through the tip of each needle. An additional 20 cc of saline was injected to ensure delivery and further chase the chips into the bone space. Three clusters of five chips were placed into each vertebral body at pre-assigned depths (anterior, mid, and posterior). The anterior location was the first 1/3 of the vertebra, the mid location referred to placement at the midline of the vertebra, and the posterior section referred to placement of the chip into the posterior 1/3 section of the vertebra. Flouroscopic imaging was used during surgery to document the surgical sites of each targeted cervical vertebral body, needle placement, and chip delivery to ensure proper placement of each chip cluster.

After completion of the material insertions into all six vertebral bodies (C2-C7), the small muscular incisions were closed with 2.0 silk suture and the skin was closed using Prolene suture in a continuous manner.

#### *5.3.2.2 Euthanasia and Specimen Retrieval*

The goat was euthanized six months post-operatively via pentobarbital administered intravenously at a lethal dosage (75 mg/kg via intravenous injection) to ensure a rapid demise with no sensation of pain or discomfort. The cervical vertebral segments were then

harvested and prepared for undecalcified histological sectioning. Each cervical vertebra was dissected and removed of surrounding musculature, and inspected for any gross abnormalities due to adverse reactions to the implanted materials or chip migration. The vertebral bodies were then placed separately into a 3:1 volume of 70% ethanol to initiate the dehydration process for histological preparation.

#### *5.3.2.3 Histology*

After a period of four weeks in 70% ethanol, each of the vertebral bodies was placed into 100% ethanol for an additional four weeks. Each specimen was dehydrated further by using five changes of 100% ethanol at ambient temperature over the course of five days. Following dehydration, the specimens were further cleared of soft tissues with three changes of xylene at ambient temperature over the course of three additional days. They were then embedded into a solution of methylmethacrylate (MMA), placed into a vacuum chamber, and kept at 2°C - 8°C over a 23-day period with three changes of MMA.

Using an Exakt diamond saw (EXAKT, Appartebau, Germany), three transaxial sections (central, medial, lateral) were made into each embedded vertebra, each measuring between 750µm -850µm in thickness. MicroCT was used to provide a detailed view of the silicon chips within each vertebra. The exact locations of the chip clusters were quantified utilizing scaled CT images and the coordinates of each chip cluster employed during histologic sectioning, so that the sections were made just shy of each chip cluster location and ground to reveal the chip clusters. Each prepared section was affixed to a glass slide and ground to approximately 125µm using an Exakt grinder with 500 grit paper. Finer grit (1000 grit) was used to grind each section to 75 microns in thickness, followed by a 2000 grit paper to grind each section to a final thickness of 10-40µm. Following grinding, each section was then stained with a proprietary mineralized bone stain. With this preparation, the mineralized bone stained trabeculae green, osteoid seams stained magenta, and the remaining tissues

stained blue and pink. Each slide was photographed, digitized, and scaled using a dissecting microscope and viewed under high magnification (400X) utilizing a light microscope. Three independent observers, two of which were bone pathologists, evaluated the slides for any signs of inflammatory responses or foreign body reactions to each material.

## 5.4 Results and Discussion

### *5.4.1 Phase 1*

The animal surgery was uneventful and all vital signs were normal. During recuperation, there were no complications related to the surgical procedures, post-operative infection, or mortality observed in the six-month survival period . Gross examination of cervical and lumbar spinal segments after harvest and dissection did not reveal any visible signs of adverse reactions to the MEMS materials including bony abnormalities, osteophytic formations, infection, or inflammation. The surrounding tissues and musculature for both spinal regions were devoid of necrosis and signs of infection.

Microscopic examination of the histological slides confirmed that there was no adverse tissue reaction to the MEMS materials either locally or peripheral to the implantation sites. The location of Si chips and the MEMS pressure sensor in the lumbar and cervical spinal regions respectively, were correlated with the series of histological sections. Examination of histological slides confirmed the absence of

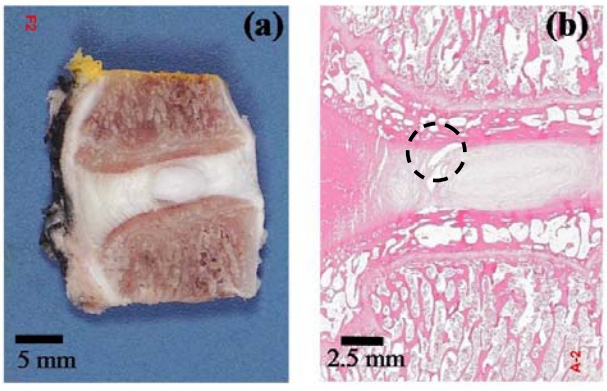


**Figure 5.5:** Gross section (a) of L3-4 lumbar spine segment where Si chips were implanted into the disc. The corresponding histological image of the disc region (b) (H&E stain) shows a void due to previous location of the Si chips and needle penetration (dotted circle). Evidence of inflammatory or infectious cellular responses is absent.

abnormal macrophage or lymphocytic cellular activity within the lumbar discs and at the cervical fusion site.

The histological sections of the lumbar disc sites indicated normal fibrous regions that lacked any evidence of inflammatory or infectious cellular responses (**Figure 5.5**). There were visible voids within the disc tissue where the MEMS materials were implanted, as confirmed during the physical dissection and sectioning of the specimen. These regions were carefully examined to confirm the absence of any adverse localized and peripheral tissue responses to the implanted materials.

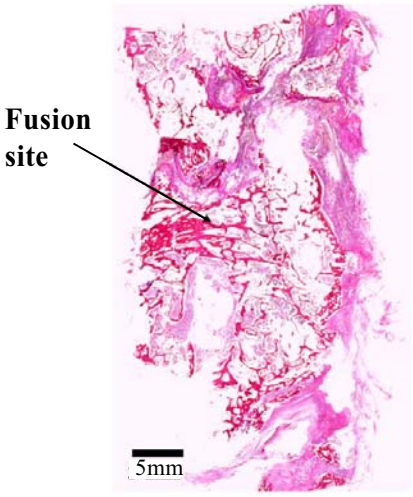


**Figure 5.6:** Histological image of the C4-5 cervical fusion site (H&E stain) that was implanted with bone graft containing a piezoresistive pressure sensor. There is evidence of vascularization and remnants of the bone graft were surrounded by healthy young bone at various stages of remodeling.

The histological sections of the cervical fusion site indicated regions of healthy remodeled bone with vascularization and viable osteoclasts and osteoblasts within the bony margins (**Figure 5.6**). The older original bone graft material exhibited osteocytes housed within multiple lacunae, an indication of remodeled healing bone. Remnants of the bone graft were surrounded by healthy young bone at various stages of remodeling. Furthermore, lines of newly mineralized bone connected the autograft to the host bone.

Previous investigations using a baseline battery of ISO 10993 physiochemical and biocompatibility tests showed that common materials used in the construction of MEMS devices including Si, silicon dioxide ($SiO_2$), and silicon nitride ($Si_3N_4$), did not exhibit cytotoxicity *in vitro* or adverse foreign body responses *in vivo* when implanted into rabbit musculature for up to 12 weeks.[63] The present study sought to build on the previous work by focusing on long-term biocompatibility of MEMS materials in specific sites relevant for a

clinical application. The preliminary results of this investigation demonstrated the site-specific biocompatibility of MEMS materials that might be utilized in the construction of a spinal fusion monitoring system. Limitations of the current investigation include the implantation of non-powered pressure sensors, limited selection of MEMS materials, and lack of biomechanical tests to validate the fusion strength of the spinal segments implanted. Nevertheless, our results from this phase demonstrated preliminary feasibility and suggest that further investigation of the *in situ* biocompatibility of additional MEMS fabrication materials for the construction of complex implantable medical devices is warranted and will be addressed in Phase 2.

### *5.4.2 Phase 2*

The animal surgery for Phase 2 was uneventful. There were no complications due to surgical procedure, post-operative infection, or mortality during the following six months of survival. Gross examination of each cervical spinal segment after harvest and dissection did not reveal any visible signs of adverse reactions to the MEMS materials including bony abnormalities, osteophytic formations, infection, or inflammation. The surrounding tissues and musculature for the cervical spine were devoid of necrosis and signs of infection. Furthermore, migration of the chips out of the vertebrae and into the surrounding tissue was not observed during dissection and histological sectioning.

#### *5.4.2.1 Macroscopic Findings*

There were no visible signs of adverse reactions to the MEMS materials or titanium during gross observation of the cervical vertebrae. No bony abnormalities, osteophytic formations, infection, or inflammation was observed for any of the cervical vertebral bodies. There was a normal appearance to all of the surrounding tissues and musculature for all vertebrae. All regions were devoid of necrosis and signs of swelling. One vertebral body,

C7, exhibited signs of malpositioning of the chip placement related to implantation at the time of surgery, where the chips were found located towards the lateral bony margin, rather than centralized within the vertebral body.

#### *5.4.2.2 Histological Findings*

Microscopic examination of the undecalcified sections through the vertebrae and implanted chips did not reveal evidence of lymphocyte and macrophage activity. For the cervical vertebrae that were implanted with silicon based MEMS materials (C2, C4, C5, C6, C7), giant cells were found along the jagged edges and corners of each chip. Although the quantity of giant cells was limited to two or three for each silicon based material ($Si_3N_4$, MEMS pressure sensor, SiC, $SiO_2$, Si), the titanium particulate had less incidence of giant cells present with fewer giant cells observed. Osteoclasts were observed along the margins of the $Si_3N_4$ chips and there was very little evidence of a fibrous tissue layer encompassing any of the silicon based materials implanted.

It was determined that there was no adverse tissue reaction to the MEMS materials and the materials composing the pressure sensors (**Figures 5.7-5.9**). There were no signs of increased macrophage or lymphocytic cellular activity within the cervical bone. However, there was an increased activity of giant cell formation along the jagged edges and corners of the Silicon based chips. Examination of the mature surrounding bone indicated regions of healthy bone with minimal osteoclastic activity. The microscopic size of the chips allowed them to

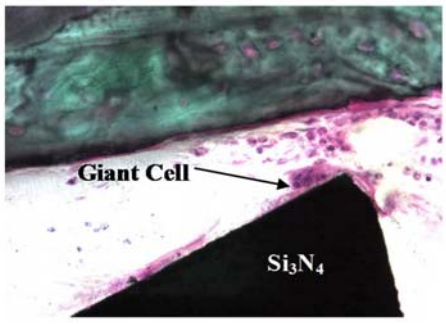


**Figure 5.7:** One cluster of $Si_3N_4$ inserted into the C2 vertebral body taken from a transaxial view. One $Si_3N_4$ chip is depicted under light microscopy at 400X magnification. Mature bone (green) surrounds the $Si_3N_4$ chip with a giant located at the jagged corner of the chip. A fibrous tissue layer has not formed around the periphery of the chip.

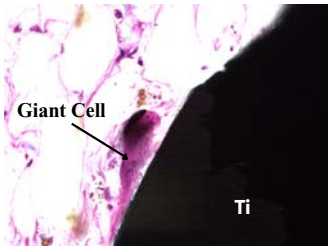


**Figure 5.8**: One cluster of titanium inserted into the C3 vertebral body, taken from a transaxial view. An irregular shard of titanium is depicted under light microscopy at 400X magnification. There is a giant cell located within the proximity of the jagged apex of the titanium matter. A thin organized fibrous tissue layer was observed to surround the titanium particles.

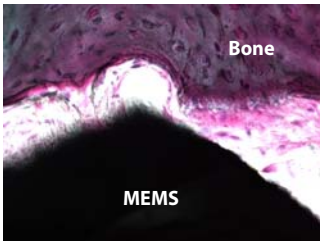


**Figure 5.9:** One cluster of MEMS pressure sensors into the C4 vertebra taken from a transaxial. One MEMS pressure sensor is depicted under light microscopy at 400X magnification. Mature bone (green) surrounds the MEMS sensor and giant cells are located to the right of the sensor. There is no fibrous tissue layer presently surrounding the sensor.

co-exist with the mature bone (stained green) without distruption of its integrity. Osteoconductive activity was significantly absent between all of the materials implanted and the surrounding native bone.

Overall, the silicon based materials used in the construction of MEMS devices did not pose infectious risk and chronic inflammatory responses to the implanted tissues of the spine. An organized layer of fibrous tissue was not observed to encompass the silicon based materials. The titanium particles did exhibit a very fine layer of disorganized fibrous tissue, where a low dose of titanium particles (<200mg) implanted into the C3 vertebra did not affect the bone integrity nor cause adverse osteolytic reactions. The titanium exhibited expected behavior, with a very thin formation of a fibrous tissue layer surrounding the titanium shards. Due to the titanium's irregularity in size and shape, there was very little osteoconductive properties and bone was not observed to have formed around the titanium particles. This can best be explained by existing wear debris literature of orthopedic implants constructed of titanium. Conventionally, once a titanium implant has been placed into the body, the wear and debris accumulation is initiated. Such particles are often less than 7-10 microns in size and are caused by micromotion, corrosion, or oxidative surface reactions.[44,111,128] Studies have shown that macrophages are the predominant cells surrounding newly implanted metal alloys and are associated with wear particles from titanium particulate. These cells are capable of differentiating into multinucleated cells exhibiting all the phenotypic features of osteoclasts, which are highly multinucleated and are responsible for

lacunar resorption.[25,44,111,128] Therefore, it is to be expected that macrophage activity is induced with the implantation of a metal alloy into a living system and can contribute to osteolysis surrounding an implant due to their osteoclastic behavior in the presence of excessive wear debris. However, if the particulates are greater than 7-10 microns, it is feasible to understand that this is beyond the phagocytic capabilities of the macrophages, resulting in less macrophage population surrounding the metal alloy and fibrous encapsulation of the particulate. Surface texture, size, and shape of the metal particulate are factors that affect the macrophage activity, phagocytic behavior, and osteolytic properties of the implant.[20,25,26,43] The titanium shards used in the present study were 1-2mm x 0.5mm or within the 1000 to 2000 micron range. These particles were larger than what is observed from wear particulate and too large to induce phagocytosis, resulting in reduced macrophage activity. Research studies have demonstrated that particulate matter greater than 50 microns in size does not excite a foreign body or phagocytic reactions unless there is a dimension on the particulate matter that is in the range of 0.1 to 1.0 μm (i.e. for long slender fibers). Ideally, particle size must be within a range of 0.1μm to 1.0μm particle size to induce phagocytosis, however particulate matter of up to 5μm can be easily phagocytosed.[10] A condition termed frustrated phagocytosis may result where large particles (entire implants or implant shards) activate phagocytosis, cannot be dissolved, resulting in an external release of lysozyme and oxidative byproducts.[10]

The concept of monitoring real-time fusion status *in vivo* using MEMS sensors is attractive for clinical implementation in spine patients undergoing vertebral stabilization surgery. However, there have been limited investigations into biocompatibility of MEMS materials for implantable clinical applications, especially where extraneous packaging must be avoided due to size constrains. Overall, this study successfully demonstrated the site-specific biocompatibility of MEMS-based materials that may be utilized in the construction of future implantable sensor technology for human implantation. Although there was some osteoclastic behavior observed for the silicon based materials ($Si_3N_4$), the materials used to

fabricate MEMS devices were relatively inert in nature. The giant body cells did illicit a foreign body response to the materials, however, signs of infection, inflammation, and adverse responses were absent *in vivo*. However, the lack of a thick fibrous tissue layer surrounding the MEMS materials is of concern. An organized fibrous tissue layer can contribute to anchoring a microscopically sized MEMS chip into a designated region. Organized fibrous tissue is representative of normal mechanical loading and a healthy environment that has resumed after tissue has been violated and has healed. It can be used to encapsulate medical devices and isolate the materials from foreign body attack, a system that occurs naturally. Although this layer was absent around the silicon based materials, there were no signs of adverse reactions to the foreign bodies implanted into cervical bone. In essence, fibrous tissue may function as a protective shield against self-attack from one's immune system and may assist in resisting implant migration.

Finally, none of the materials studied promoted osteoconduction of bone upon the surface of the materials. Although titanium promotes osteoconduction where bone will intermingle with the oxidative surface of a titanium implant, the titanium particle size used in this study did not provide an ideal environment that promoted osteoconduction.

## 5.5 Conclusion

The site-specific biocompatibility of Si chips and silicon based MEMS pressure sensors were investigated using a caprine model. Surgical procedures for the successful implantation of MEMS devices into osseous and intradiscal regions were developed. Histological analysis of the vertebral bone and intervertebral discs of the goats after a six-month survival period did not reveal evidence of any adverse foreign body response by the caprine spinal tissue to the implanted MEMS materials. Although there was an absence of thick layers of organized fibrous tissue surrounding each implanted material, none of the materials induced a severe

foreign body reaction. There were no signs of infection or inflammation in response to the variety of MEMS materials used in the fabrication of microsized devices, as well as an absence of osteoconductive properties for any of the materials implanted.

# CHAPTER VI

# STERILIZATION

## 6.1 Study Overview

The effects of steam, ethylene oxide, and gamma sterilization on the performance of micromachined pressure sensors were investigated using a variable pressure setup. These sterilization techniques are conventional techniques used for surgical applications and are conducted on all devices prior to human implantation. It is essential to determine if MEMS sensors are capable of withstanding such harsh forms of sterilization without a compromise in electronic integrity. Commercially available pressure sensor die were characterized prior and subsequent to sterilization over a 0-500 Torr pressure range. The effects of sterilization were examined as changes in sensor output voltage ($\Delta V$) at various applied pressures.

## 6.2 Introduction

Recent advances in MEMS (microelectromechanical systems) technology have resulted in an increased interest in its biomedical applications. In medicine, the incorporation of MEMS devices into clinical systems is gaining momentum as evidenced by development of micromachined disposable pressure sensors, microfluidic lab-on-chip systems, and ultrasonic imaging microtransducers[2,37,57,72,105] Miniature, implantable, physiological monitoring systems

that integrate *in vivo* sensing capabilities with wireless transmission to an external data acquisition system have also been proposed for bone fusion assessment, intracranial pressure monitoring, and detection of congestive heart failure.[5,70,81,105] However, successful translation of MEMS into implantable physiological monitoring systems must overcome challenges associated with device functionality and biocompatibility.[35,36,37,38,47,63,105]

Silicon is a fundamental material of construction for MEMS devices. This material choice is motivated by a combination of available microfabrication infrastructure and the desire to incorporate microelectronics components into the MEMS device.[56,71,89,129] However, the properties of silicon and related microfabrication materials such as silicon nitride, silicon dioxide, and aluminum can prove problematic for implantable clinical applications. For example, the human body's natural defense mechanism that begins with inflammation coupled with the corrosive effects of biofluids can disrupt the functionality of devices.[84,104] Furthermore, the brittle contact pad nature of silicon leads to a risk of device breakage upon implantation. Another challenge results from the need for sterilization, which is required of any surgical tool or medical device that contacts the body. Although biocompatibility assessment of MEMS materials has been recently reported, there is a paucity of data on the effects of sterilization on the functionality of devices.[63,89] In addition, previous reports on the effects of sterilization of MEMS devices are generally anecdotal without details on operational performance shifts (if any), and often, based on non-standard protocols that would be unacceptable within a clinical environment.[12,51]

Moist heat and radiation sterilization procedures have become widely established in medical institutions for surgical sterilization of implantable devices.[34,88] Other sterilization choices include gas ( ethylene oxide EtO ) and dry heat. Radiation sterilization usually involves exposure of the device to gamma rays from a $^{60}Co$ or $^{137}Cs$ source until a dosage of 1.5–3.5 MRAD is achieved.[33] Moist heat sterilization typically refers to a 20–45 min exposure of the device to dry saturated steam at 121–132°C under pressure.[90] Principal advantages of steam sterilization are the simple sterilization algorithms and rapid processing times,

while gamma sterilization offers a ready alternative for hygroscopic or thermolabile products. In addition, both gamma and steam sterilization procedures do not result in toxic residue, which is an inherent limitation with EtO sterilization.

This paper reports on the effects of steam and gamma sterilization procedures on the functionality of one common class of MEMS devices. Micromachined pressure sensors were selected as the model MEMS device for evaluation because of their wide commercial availability, established performance history, and numerous potential clinical applications. The performance characteristics of commercially available MEMS pressure sensors were determined prior and subsequent to conventional sterilization conditions using a variable pressure testing setup. The results of this investigation should provide guidance to medical device design engineers on their strategies to integrate MEMS components into implantable biomedical systems.

### 6.3. Pressure sensors

Commercially available P529B Novasensor bare silicon pressure sensor die (GE NovaSensor, Freemont, CA) sized at 1.0 ×1.0 ×0.6 $mm_3$ were obtained for the evaluation. The essential sensor elements comprising the pressure sensor include four doped silicon piezoresistors, a bulk micro-machined silicon (Si) membrane, and eight aluminum (Al) contact pads **(Fig. 6.1)**. The silicon membrane is exposed to ambient conditions on its superior surface

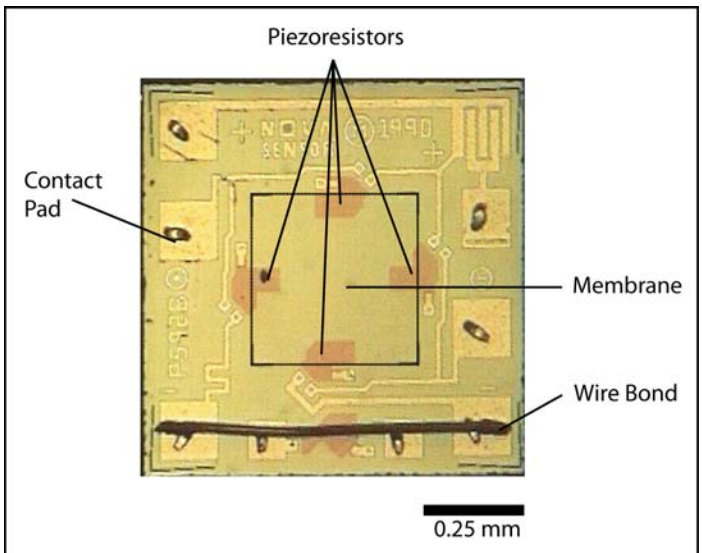


**Figure 6.1** Photograph of a piezoresisive silicon pressure sensor used to evaluate effects of sterilization. The aluminum contact pads are used for external electrical connections to piezoresistors on the silicon membrane. The aluminum bond wire connects two electrical input pads.

while the inferior surface constitutes the roof of a sealed vacuum cavity. According to the manufacturer's datasheet, the device functions as a 0–50 psi (0–345 kPa or 0–2,586 Torr) absolute pressure sensor with a 3 VDC input excitation voltage, which, in turn, provides 60±15 mV full scale output (FSO). The rated temperature coefficient of sensitivity and zero offset are -0.2 %FSO/°C and ±8 mV/V, respectively.

For pressure sensing operation, the four piezoresistors around the silicon membrane were connected into a Wheatstone bridge configuration using five contact pads. Two input (-IN) pads were shorted using aluminum wire and standard wirebonding techniques. Afterwards, the wirebonded pressure sensor was mounted onto a glass slide using biocompatible medical grade (Master Bond, Hackensack, NJ) epoxy adhesive. Altogether, 55 sensors were wirebonded and mounted for subsequent evaluation.

### 6.4 Sterilization Protocols

The pressure sensors were inspected using light and scanning electron microscopy as well as by energy dispersive X-ray spectroscopy (EDS/EDX). The sensors were subsequently divided into two groups for gamma and steam sterilization to achieve sterility assurance level of $10^{-6}$. Gamma sterilization was performed on 21 sensors for a dosage of ~5 MRAD via contract service from STERIS Isomedix Services (Morton Grove, IL). The gamma irradiation was provided by a $^{60}Co$ source and the dosage was selected to simulate 2× exposure of the conventional sterilization dosage of 2.5 MRAD. Steam sterilization was performed on the remaining 34 sensors using a wrap/ gravity algorithm in a standard steam autoclave (Steris/ AMSCO, Mentor, OH) for 25 min at 121°C and 15 psi. The larger sample size of pressure sensors for the evaluation of steam sterilization was based on previous anecdotal evidence that suggested greater likelihood of damage during the handling and sterilization procedure.

## 6.5 Characterization Setup

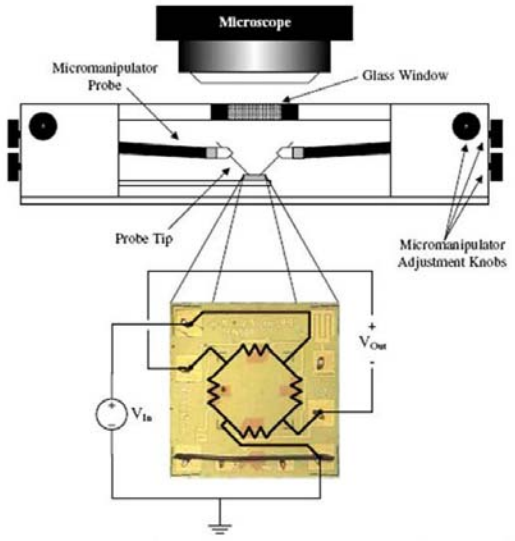


**Figure 6.2** Schematic of the vacuum probe station and circuit diagram of characterization setup to test pressure sensors. Probe tip placement is achieved through manipulaton of adjustment knobs and observed using the optical microscope. Each of the four probes was electrically connected to either the voltage source or and electronic multimeter to measure output change as the chamber pressure was varied.

The pressure sensors were characterized using a MMR LTMP vacuum probe station (MMR Technologies, Mountain View, CA) at room temperature (~25°C). This probe station was originally intended for testing of electronic devices down to cryogenic temperatures and is comprised of four micromanipulators, a pressure control port, a convectron vacuum gauge, and an optical access window **(Fig. 6.2)**. The system was adapted for testing of the micromachined pressure sensors by attaching standard electrical probe tips to the micromanipulators and a mechanical roughing pump to evacuate the test chamber to a base pressure of <100 mTorr A 3 VDC electrical excitation and voltage readout was provided by a Hewlett Packard E3630A Triple Output DC Power Supply and a Keithley 2000 Multimeter, respectively. The characterization setup was situated on a vibration isolation table.

The glass slide mounted with the pressure sensor was placed in the test chamber, which was then evacuated to base pressure. Afterwards, the four probe tips were brought into contact with the sensor pads to complete the Wheat-stone bridge configuration and the output voltage was noted. The pressure valve was subsequently opened until the chamber pressure increased to approximately 100 Torr (13 kPa) and another output voltage was recorded. This procedure was repeated for chamber pressures of approximately 200, 300, 400, and 500 Torr. In order to compare data from the various sensors, the output voltage

characteristic of each pressure sensor was normalized to compensate for zero offset and pressure control variations. Experiments were also conducted to establish the accuracy and reproducibility of the characterization setup.

### 6.6 Data Evaluation.

Each sensor was tested prior and subsequent to sterilization to generate output voltage versus applied pressure data using the characterization setup. The change in output voltage after sterilization at the various applied pressures was calculated for each sensor according to the following equation: **[$\Delta V = V_p - V_s$]** where $\Delta V$ represents the change in sensor output voltage, while $V_p$ and $V_s$ represent the sensor output voltages prior and subsequent to sterilization, respectively. These varia-tions were examined statistically using GraphPad Prism v.3.02 (GraphPad Software, San Diego, CA) software. A one-way analysis of variance (ANOVA) was conducted to determine statistical significance at a 95% confidence interval.

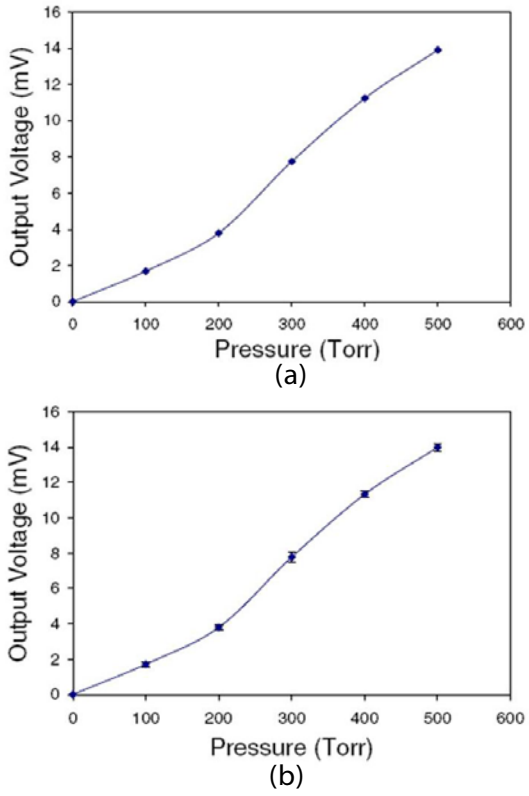


**Figure 6.3** Graphs showing sensor output voltage versus applied pressure data from tests used to validate the characterization setup. The first set of tests (a) was conducted over 15 consecutive pressure cycles. The second set of tests (b) was conducted over five consecutive days with three tests per day.

### 6.7 Results and Discussion

**Figure 6.3** presents a graph of output voltage versus applied pressure for a typical pressure sensor mounted on the

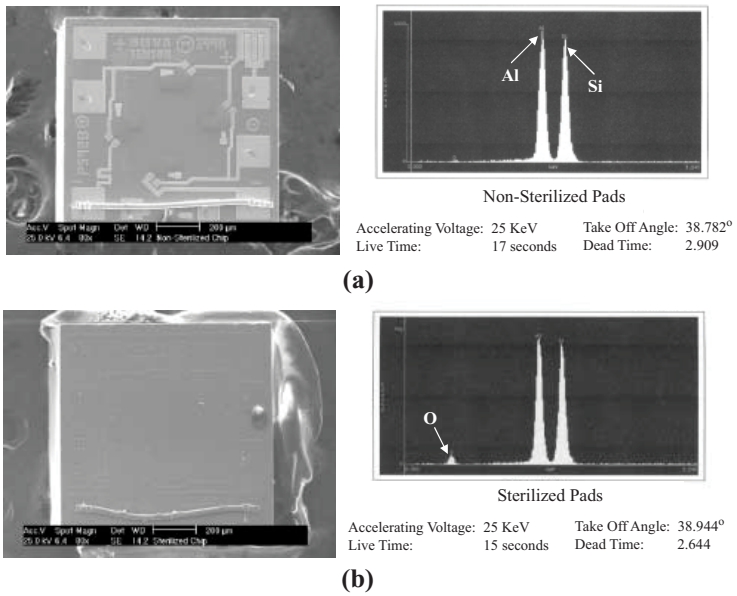


**Figure 6.4** SEM images and corresponding EDX spectra of contact pad regions on a MEMS pressure sensor prior (a) and subsequent (b) to steam sterilization.

probe station. The sensor was tested 15 times over consequent pressure cycles ranging from base pressure (<100 mTorr) to 500 Torr. The maximum variation in test-to-test sensor output was less than 0.40 mV. The apparent nonlinearity of the sensor response is an artifact of the convectron vacuum gauge response. Day-to-day variations were also investigated by comparing output voltage of a sensor that was tested on five consecutive days over three pressure cycles daily. In this case, the maximum variation in sensor output was 0.93 mV.

**Figure 6.4** presents typical scanning electron microscope (SEM) images of non-sterilized and steam-sterilized pressure sensors. Although both images were obtained under identical SEM conditions, the sterilized sensor exhibits a lower contrast, which suggests the presence of an insulating layer. Indeed, analysis of the sensor surface by EDX provides evidence for the formation of an oxide film during the steam sterilization procedure. The SEM image of the sterilized sensor also shows partial reflow of excess epoxy adhesive during the steam sterilization procedure. The extent of epoxy reflow was greater on some sensors such that excess epoxy fouled the silicon membrane. Altogether, epoxy fouling and mishandling resulted in structural damage to ten steam-sterilized sensors. In contrast, all 21 gamma-sterilized sensors were functional and did not exhibit epoxy reflow or the presence of an oxide film.

The 45 (24 steam- and 21 gamma-sterilized) functional pressure sensors were tested using the characterization setup. **Figure 6.5** presents representative output voltage characteristics of two representative sensors prior and subsequent to sterilization. The data confirm that the sensors are functional after sterilization. To further investigate the effect of sterilization on sensor performance, the change in output voltage (ΔV) after sterilization at the various applied pressures was calculated for all 45 sensors. **Table 6.1** and **Fig. 6.6** respectively present a statistical summary and the corresponding graphical depiction of the changes in output voltage due to sterilization. For steam sterilization, mean ΔV decreased with applied pressure

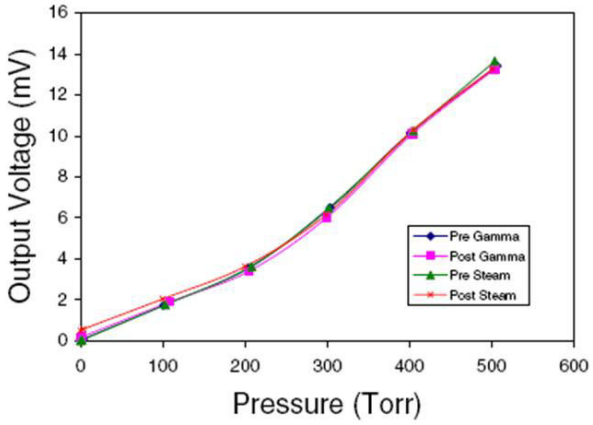


**Figure 6.5** Graph showing representative sensor output voltage versus applied pressure data prior and subsequent to steam and gamma sterilization. The pressure sensors are functional after sterilization.

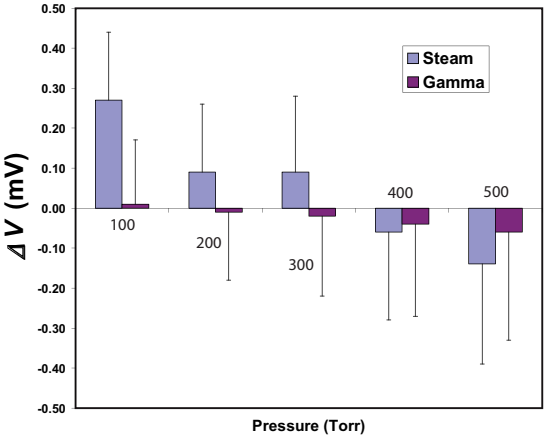


**Figure 6.6** Changes (mean and standard error) in sensor ouput voltage (DV) at various applied pressures due to sterilization. The increased variation in DV for the steam-sterilized sensors is probably due to formation of an oxide film. Nevertheless, the effect of both sterilization procedures on DV is statistically insignificant.

| Pressure (Torr) | Steam sterilization | | Gamma sterilization | |
|---|---|---|---|---|
| | Mean | Standard error | Mean | Standard % error |
| 100 | 0.27 | 0.17 | 0.01 | 0.16 |
| 200 | 0.09 | 0.17 | -0.04 | 0.17 |
| 300 | 0.09 | 0.19 | -0.02 | 0.2 |
| 400 | -0.06 | 0.22 | -0.04 | 0.23 |
| 500 | -0.14 | 0.25 | -0.06 | 0.27 |

**Table 6.1** Summary of changes in sensor output (DV) after sterilization. The mean voltage represents the change in voltage pre and post sterilization.

ranging from +0.27 mV at 100 Torr to -0.14 mV at 500 Torr. In contrast, the corresponding values for gamma-sterilized sensors were lower, decreasing from +0.0 1 mV 100 Torr to -0.06 mV at 500 Torr. The increased variation in $\Delta V$ for the steam-sterilized sensors is probably due to the oxide film, which, in turn, could degrade the electrical characteristics of the piezoresistors and contact pads as well as the deformation behavior of the micromachined membrane. Nevertheless ANOVA revealed that the effect of both sterilization procedures on $\Delta V$ was statistically insignificant ($p \geq 0.05$).

To our knowledge, this is the first report of a systematic investigation into the effects of sterilization on the performance of MEMS devices. The above results indicate that neither steam nor gamma sterilization degrade the performance of MEMS pressure sensors. However, a primary limitation of our investigation is that the sensors were tested only to 500 Torr. Consequently, further experiments are required to verify that the effect of sterilization on $\Delta V$ remains insignificant up to 1,060 Torr, which is the upper limit of typical medical pressure sensors. The selection of micromachined pressures sensors as the model MEMS device for evaluation of sterilization was based on their wide commercial availability, established performance history, and numerous potential clinical applications. Accordingly, the results of our investigation can provide insight into the effects of sterilization on other silicon-based MEMS devices. The effects of sterilization will likely depend on the type of device and its functionality. On the one hand, for most passive (simply mechanical) devices that do not exhibit electrical functionality such as microneedles, it may be safely assumed that performance will not be affected whatsoever. In contrast, for most active (electromechanical) devices such as ultrasound microtransducers and micropumps, the effect on performance will largely depend on the susceptibility of the integrated electrical components to sterilization conditions.

Disinfection of MEMS devices will be critical for their successful deployment in implantable medical applications. Steam and gamma sterilization procedure are currently established as the leading disinfection techniques for processing of medical devices.

Consequently, the compatibility of MEMS devices with these sterilization procedures will enhance their commercialization and clinical implementation.

## 6.8 Conclusion

The performance characteristics of commercially available MEMS pressure sensors prior and subsequent to steam and gamma sterilization were investigated using a variable pressure testing setup. The effects of sterilization were examined as changes in sensor output voltage at various applied pressures. The steam sterilized sensors exhibitied increased variation in output voltage changes compared to sensors exposed to gamma irradiation. Nevertheless, ANOVA revealed that the effect of both sterilization procedures on sensor performance was statistically insignificant.

# CHAPTER VII

# BIOPACKAGING OF MEMS IMPLANTABLE MEDICAL DEVICES

## 7.1 Study Overview

Packaging and coating of implantable devices for long-term implantation is a requirement for any implant to withstand long-term implantation *in vivo*. Multiple studies were conducted to assess various coating and adhesive properties on conventional medical grade metals used for spinal implantation. The mechanical characteristics of a variety of polymeric coatings and adhesives were examined after sterilization to determine electrical continuity, fluid permeability, and adhesive strength.

## 7.2 Introduction

The advent of microelectromechanical systems technology (MEMS) has led to a "second silicon revolution" [102], with the first revolution directed toward the integrated circuit technology originated in the 1950s. The potential for implantable MEMS devices for use in clinical applications is slowly moving into the medical arena and has led to a surge in the development of biomedical applications utilizing MEMS devices. Miniaturization of medical devices shows promise for the future implantation of MEMS sensors and actuators into a living environment. These micro-sized devices are advantageous to the medical industry

due to their general reduction in mass and size, low production cost, low energy consumption, electronic accuracy, easy disposal, wireless transmission capabilities, and durability.[64,65,85,106,108] Such devices will lend to *in vivo* applications (i.e., devices applied for use in a living biological environment) related to the diagnoses and treatment of numerous pathologies. The ability to monitor and measure *in vivo*, real-time fluid pressures, forces, chemistries, temperatures, frequencies, and the internal mechanics of a variety of biological systems through implantable MEMS devices will launch medical science into the technological forefront and make current therapeutic technologies obsolete. The major challenge towards implantable microsensors is the need for rugged packaging that can withstand surgical sterilization initially, and long-term implantation into the harsh fluid environment of a living system for an extended period of time.[61,62,72,125]

Packaging is an essential part of MEMS design and fabrication in order to protect the micro-devices from environmental influences *in vivo*. It involves coating or encasing MEMS devices within chambers that can shield the devices from harsh elements, while maintaining electronic, mechanical, and biofunctionality (i.e., the electromechanical function of the sensors in a biological environment). The functions of packaging are twofold; 1) to protect the device from environmental degradation and, 2) to protect the internal *in vivo* environment from the functioning device so that the environment is not compromised.[61] Although there is no general applicable packaging method for all MEMS based sensors, there are general principles useful in packaging design.[61,62] Protection of devices include the electrical isolation of leads and device structures from moisture and humidity infiltration, mechanical protection to maintain structural integrity of the device, thermal and optical isolation, and chemical and biological isolation from invading elements. To date, MEMS sensors have not been successfully implanted into the human body for the long-term monitoring of various biological parameters due to the challenges the MEMS devices encounter when implanted into a harsh internal biological environment.

Numerous packaging challenges exist with the concept of implantable MEMS devices. Such challenges include the protection of the MEMS devices from foreign body responses within the human environment, low power consumption, delivering and anchoring the MEMS device into targeted regions, biocompatibility of the materials composing each MEMS device, robust design of the sensors and devices for patient safety, and long-term preservation of the electronic viability of the implanted MEMS device. These existing challenges currently limit the capabilities of implantable sensors. Protection from harsh environments involving temperature fluctuations, humidity exposure, changes in chemistry, protein deposition, biofouling, and other foreign body responses limit the functionality of these sensors. Furthermore, there are other existing issues with respect to the wiring of MEMS devices for power and signal transmission. Corrosion and breakage of wires is a common complication once a device is implanted into a living environment for long-term function. The development of a wireless micro-device for signal transmission is the ideal option for optimal performance and survival for long-term implantation.

Once an implantable MEMS device is developed, it will require sterilization prior to implantation into a living environment. Currently, gamma irradiation, steam, or ethylene oxide gas are conventional surgical sterilization processes used to purge implants and surgical tools of any infectious agents or foreign bodies prior to insertion into living tissue. Therefore, the packaging surrounding the device must be able to withstand high temperature and humidity, gamma irradiation, and ethylene oxide gas without degradation to the device or its packaging. It is these challenges that have established the need for the development of novel packaging coatings, chambers, and/or mechanisms that provide protection of an implantable MEMS device from the surrounding internal environment.

MEMS packaging utilizes many processes and toolsets similar to the fabrication of MEMS device, and is just as labor intensive and costly as is the fabrication process. Currently, it is the packaging of a MEMS sensor that is limiting the market potential and applications,

especially for medical use. MEMS devices that are currently used, such as pressure sensors and accelerometers, are marketed for external human use and are therefore, relatively easy to package, making them commercially viable and inexpensive products. However, MEMS packaging is application specific; for example, an implantable pressure sensor for monitoring cardiovascular fluid pressures will require a significantly different packaging process than an implantable MEMS based microarray for monitoring neural signal potentials of the brain. The cardiovascular pressure sensor must remain intact while being inserted into delicate tissue, avoid damaging or puncturing the tissue, and must be able to viably monitor the pressures of the existing environment. On the other hand, the micro-array device must have a means to contact the tissue and may puncture the tissue microscopically to record signals from single neurons in the brain. Both applications require significantly different packaging mechanisms to allow for proper and efficient functioning of each device. Thus it is important that the design of the packaging be concurrent with the development of a MEMS device for a specific application at the time of project conception.[72]

Currently, few studies have investigated the use of wireless implantable sensing devices for the transmission of *in vivo* diagnostics due to the numerous challenges that presently exist with implantable medical devices. Even fewer studies have been performed to examine the biocompatibility of sound packaging agents for the development of implantable MEMS devices into the human body. Commercially available strain gauges have also been implanted for the long-term potential of monitoring strain on spinal stabilizing fixation systems[45], but have remained unsuccessful due to similar challenges experienced by the MEMS devices. Although strain gauges have been used conventionally for many years, few studies have successfully implanted and packaged these gauges for their long-term use as a monitoring system *in vivo*. Similar challenges such as wire breakage and corrosion, loss of fixation, delamination of the gauge, loss of bonding to the host element, and loss of electronic integrity have been experienced once implanted into the harsh human environment. There is existing literature that discusses MEMS packaging and the challenges encountered with non-

implantable MEMS devices, yet none have breached the potential of long-term use inside the human body.

Therefore, the aim of this study was to evaluate numerous adhesives and coatings as potential packaging agents with respect to their mechanical integrity after sterilization. The end result will be to determine optimal coatings and adhesives that could maintain adhesive integrity before and after surgical sterilization, as well as provide protection from harsh elements for the potential use as implantable MEMS devices.

## 7.3 Methods

To evaluate packaging materials and their mechanical responses to various surgical sterilization techniques, commercially available strain gauges were purchased and mounted onto medical grade metals that are currently used in the orthopedic surgical implant industry. Rectangular titanium shams (Ti6Al4V - 5 x 0.5 x 1 cm ) and medical grade stainless steel shams (316L, 1.4 x 1.1 x 3 cm) served as the host materials. Two linear strain gauges of similar resistive ratings (120 Ω or 350 Ω) were mounted onto the surface of each metallic sham and randomly subjected to either ethylene oxide or steam sterilization **(Figure 7.1)**. Specific designated adhesives and coatings were used to affix the gauges and to assess their mechanical integrity and durability post-sterilization.

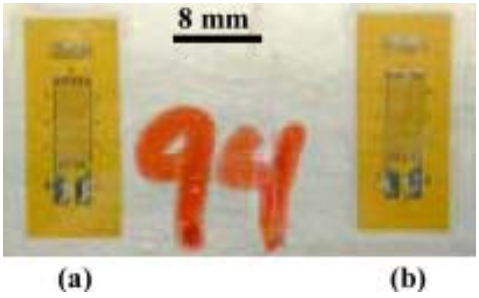


**Figure 7.1:** Digital photograph of the non-coated (a) and thinly coated (b) 120 Ω strain gauge on a titanium sham.

### *7.3.1 Mounting and Coating of the Strain Gauges*

Each sham was prepared in a standard manner for strain gauge mounting. This involved sanding of the metallic surface in a sequential manner using three grades of abrasive grits and degreasing with 100% ethylene alcohol. A conditioner (M-Prep Conditioner A, Measurements Group Inc., Raleigh, NC) was applied using two passes, the first in circular patterns, followed by a single swipe in one direction to dry. The surface was then neutralized using M-Prep Neutralizer 5A, (Measurements Group Inc., Raleigh, NC) in a similar manner following conditioning. The back surface of the strain gauge was placed onto the surface of the glass slide and covered with cellophane tape using a sliding motion over the sensing surface of the guide.

The non-sensing surface of each gauge was mounted using a thin layer of the adhesives listed in **Table 7.1** onto each metallic sham and following the manufacturer's specifications for gauge application. Each specimen was allowed to cure for 24 hours prior to the application of the coating. Two coatings were investigated in this study. The coating was gently applied to each gauge using a syringe containing either epoxy or Ep42ht in liquid form. One small drop was applied over the gauge and allowed to cure for 24 hours for the Phase 1 samples. In Phase 2, the coatings were applied with a small paintbrush in thin layers over the strain gauges and allowed to cure for 24 hours. A four-point resistivity check was conducted on each mounted, but non-coated strain gauge to validate the gauge resistivity prior to and after sterilization. Measurement of the resistivity post-sterilization was necessary to evaluate gauge integrity and to detect possible interruptions in the gauge wiring caused by application of the adhesive. No change in the resistivity indicated there was no degradation or defect in the strain gauge after sterilization. Finally, resistivity measurements were not feasible with the coated gauges due to the lack of access to the metallic resistive pads, nor were they feasible on the significantly thicker stainless steel shams due to geometrical challenges of the host blocks.

### *7.3.2 Sterilization Algorithm*

Ethylene oxide sterilization was conducted through the Animal Surgical Unit at The Cleveland Clinic Foundation (Cleveland, Ohio) following a standard 24 hour sterilization process within an enclosed chamber that allowed for aeration while monitoring the time, temperature, humidity and the concentration of gas sterilant. Steam sterilization was performed on the strain gauges in a standard steam autoclave utilizing a wrap/gravity algorithm for a total cycle of 45 minutes, 25 minutes of steam under 30 psi at 121°C and a 10 minute dry cycle.

### *7.3.3 Determining Adhesive and Coating Integrity*

Coating and adhesive integrity were blindly graded after sterilization. One independent grader conducted a standard peel test to detail the consistency and adhesive integrity of each of the mounted strain gauges. Ample sample sizes were used to concur with the repeatability of the adhesive and/or coating integrities. This involved assessing the peel strength of each gauge. The adhesive strength was graded initially with forcep manipulation post-sterilization, and if the attachment was strong, a scalpel manipulation followed for further strength assessment of the strain gauge attachment to the metallic sham. A grading scale of 1 was deemed equivalent to a strong attachment, and 5 to a weak attachment and bond integrity.

This study was conducted in three phases with the following three study aims listed below:

1. To conduct a preliminary assessment of available coatings and sterilization techniques (Phase 1).
2. To conduct a refined assessment of optimal coatings and adhesives for strain gauge attachment to medical grade materials for the further evaluation of adhesive and coating performance and mechanical integrity after steam sterilization (Phase 2).

3. To conduct a narrower assessment of coating and adhesive integrity; an evaluation of the coating spread and mechanical integrity after steam sterilization on the titanium, 316L medical grade stainless steel, and glass shams (Phase 3)

| Sterilization Process | Adhesive Only | Adhesive & Coating Combination |
|---|---|---|
| ***Ethylene Oxide*** | Strain Gauge 1 | Strain Gauge 2 |
| | **M** | **MP** |
| | | **ME** |
| | **E** | **EP** |
| | | **EE** |
| ***Steam*** | Strain Gauge 1 | Strain Gauge 2 |
| | **M** | **MP** |
| | | **ME** |
| | **E** | **EP** |
| | | **EE** |

*Key: E-Biocompatible Epoxy, P- Biocompatible Polyurethane, M-M600 strain bond*

**Table 7:1:** Phase 1 study design outlining adhesives and coatings for eight titanium shams housing a total of sixteen 350Ω strain gauges. Four shams were exposed to ethylene oxide sterilization and the remaining four shams were exposed to stream sterilization.

## 7.4 Results

### *7.4.1 Phase 1*

The purpose of Phase 1 was to examine possible coatings and adhesives that would prove viable and structurally sound after ethylene oxide or steam sterilization. This phase served as a pilot assessment to detail the advantages and/or disadvantages of ethylene oxide and steam sterilization. It further evaluated a variety of adhesives and coatings and was used to narrow the possibilities.

**ADHESIVE STRENGTH GRADES PRE- AND POST STERILIZATION**

**STEAM STERILIZATION**

| Adhesive | Coating | Pre-sterilization | Post-sterilization |
|---|---|---|---|
| M | | 4 | 5 |
| M | P | 2 | 3 |
| E | | 1 | 2 |
| E | P | 1 | 2 |
| E | | 1 | 3 |
| E | E | 3 | 3 |
| M | | 1 | 1 |
| M | E | 5 | 5 |

**ETHYLENE OXIDE STERILIZATION**

| Adhesive | Coating | Pre-Sterilization | Post-sterilization |
|---|---|---|---|
| M | | 3 | 4 |
| M | P | 2 | 4 |
| E | | 1 | 2 |
| E | P | 3 | 3 |
| E | | 1 | 3 |
| E | E | 2 | 2 |
| M | | 1 | 1 |
| M | E | 2 | 2 |

**Table 7.2:** Phase 1 preliminary results for the ethylene oxide sterilization assessment. Adhesive strength grades are listed, where a grading scale of 1 was deemed equivalent to a strong attachment, and a 5 was deemed equivalent to a weak bond integrity. *(Key: E-Biocompatible Epoxy, P-Biocompatible Polyurethane, M-M600 strain bond).*

**Table 7.1** illustrates the coatings and sterilization techniques used for Phase 1. Four coatings and adhesives were evaluated for adhesive strength after exposure to

either ethylene oxide or steam sterilization. A conventional strain gauge adhesive, M600 (M-Prep Conditioner A, Measurements Group Inc., Raleigh, NC), was used as the adhesive for eight titanium shams with dual mounted gauges (350Ω) that were exposed to ethylene oxide sterilization or steam sterilization. Four of the titanium shams, housing two strain gauges each, were exposed to ethylene oxide sterilization and the remaining four shams with strain gauges were exposed to steam sterilization. Two coatings were used on these shams: 1) polyurethane coating, known as N,N-dimethylacetamide, (Epo-Tek, Epoxy Technology, Billerica, Massachusetts), and 2) Biocompatible epoxy 301(Epo-tech).

**Table 7.2** represents a summary of the adhesive strengths for non-coated and coated strain gauges prior to and after sterilization. Two strain gauges resided on each sham, one with adhesive only, and the second with the same adhesive and a designated coating, as shown. Sterilization consisted of either ethylene oxide or steam sterilization.

For the steam sterilization series on the titanium shams, the biocompatible epoxy as an adhesive performed optimally, and the epoxy combined with a polyurethane coating demonstrated significant bonding to the titanium. However, polyurethane possessed slight osmotic permeability and was therefore, not an ideal candidate for long-term coating of strain gauges due to water infiltration disrupting the coating seal. This was observed microscopically. As an adhesive, the epoxy possessed superior peel strength. When the epoxy was coupled with itself as a coating, it performed reasonably well with a score of 3. However, the placement of a large bolus of epoxy deposited onto a titanium sham accompanied with the stiffer elastic modulus of the epoxy after it was cured, contributed to a reduced adhesive strength to the titanium only when it was coated in the manner described. The adhesive integrity improved when the epoxy was applied in a thin layer with a paintbrush to coat the strain gauges. The M600 adhesive, although not a biocompatible substrate, demonstrated adequate adhesive strength prior to steam sterilization, but performed sub-optimally after steam sterilization.

The ethylene oxide sterilization group demonstrated superior adhesive strength for the biocompatible epoxy. Furthermore, the epoxy provided superior adhesive strength as a coating. The polyurethane did not withstand ethylene oxide sterilization, and puckered upon exposure to it. This was evident by the weak bond attachment and the lack of adhesion to the titanium after sterilization. The M600 performed favorably as an adhesive, but again served only as a control and is not suitable for human use.

Overall, the biocompatible epoxy demonstrated superior adhesive strength to the prepared titanium shams for both types of sterilization processes, and performed optimally as a coating material. As a result, it was further evaluated in phases 2 and 3 of the study, leading to altering the deposition of epoxy for coating purposes in phase 2 due to the stiffer elastic modulus of the cured material. The eventual goal of the epoxy would be to serve as both an adhesive and coating for strain gauges mounted on orthopedic implants for the future *in vivo* long-term monitoring of implant strains. It was clearly evident that brush application of the coating was superior to globular placement with respect to maintaining integrity. Currently, there are novel coatings used on spinal implants that are deposited via plasma spray and remain durable after aggressive mechanical testing. Therefore, the brush application of the coatings, although crude, could be analogous to the plasma spray application. With respect to steam sterilization, it did not perform as ideally as ethylene oxide sterilization. However, there are advantages with this technique including accessibility in numerous medical facilities, durability, ease of use, and inexpensive.

### *7.4.2 Phase 2*

The purpose of Phase 2 was to conduct a further refinement of the preliminary Phase 1 study. Steam sterilization was chosen as sterilization of choice for this phase of the study due to its low cost, ease of use, widespread accessibility, and immediate availability. For this phase, forty-two titanium shams and nineteen stainless steel shams were used to house dually matched strain gauges. One strain gauge per sham was not coated and was used for

resistivity measurement purposes, while the matched gauge was coated. The adhesive and coating combinations are illustrated in **Table 7.3**. A greater number of titanium shams was used due to the widespread use of titanium as the dominant orthopedic implant material. In this phase, a novel biomaterial, a fast curing polymeric system termed Ep42ht, (Master Bond Inc., Hackensack, NJ) with a mix ratio of 10:4 was introduced into the study for investigation. All of the shams in Phase 2 were subjected to steam sterilization and the adhesive integrity and coating appearance were graded.

| Host Material | Adhesive | Coating | Resistance of Strain Gauges (Ω) |
|---|---|---|---|
| Titanium (18) | E | E | 350 |
| Titanium (14) | E | Ep42ht | 120 |
| Titanium (10) | Ep42ht | Ep42ht | 120 |
| | | | |
| Stainless (9) | E | Ep42ht | 120 |
| Stainless (10) | E | Ep42ht | 120 & 350 |

**Table 7.3** The study design, adhesives, coatings, and resistance of the strain gauges evaluated for mechancial integrity after steam sterilization for Phase 2.

The biocompatible epoxy and the fast curing polymer (Ep42ht) and epoxy were evaluated as the adhesives and coatings for this phase. Both 120Ω and 350Ω strain gauges were used for evaluation, and the epoxy and Ep42ht were assessed as an adhesive, as well as a coating. Each sham was steam sterilized following the algorithm detailed previously in phase 1.

| ***Titanium*** | ***120 Ohm Strain Gauges*** | |
|---|---|---|
| **Adhesive / Coating** | **No Coating** | **Coating** |
| E / E | 1 | 1 |
| E / Ep42ht | 3 | 2 |
| Ep42ht / E | 2 | 2 |
| Ep42ht / Ep42ht | 2 | 2 |
| | | |
| ***Stainless Steel*** | ***120 Ohm Strain Gauges*** | |
| **Adhesive / Coating** | **No Coating** | **Coating** |
| E / E | 1 | 2 |
| E / Ep42ht | 1 | 2 |
| Ep42ht / E | 2 | 2 |
| Ep42ht / Ep42ht | 1 | 1 |

**Table 7.4:** Summarized grading of the adhesive durability of 120 Ω strain gauges to the metallic shams post-steam sterilization for Phase 2 of the study.

Coating and adhesive integrity was blindly graded post-sterilization in the same fashion performed in phase 1.

**Table 7.4** lists the adhesive durability grading scores for E and Ep42ht utilized as adhesive and coating agents for 120 Ω strain gauges mounted on titanium and stainless steel shams. Epoxy used in combination as an adhesive and a coating demonstrated the strongest attachment for the titanium shams, while epoxy as an adhesive combined with Ep42ht as a coating agent was the weakest on titanium. Ep42ht as an adhesive, when combined with itself as a coating, did not demonstrate as strong a bond to the titanium, as did the epoxy. However, when used as both an adhesive and coating agent, the Ep42ht was superior to the epoxy on stainless steel.

Phase 1 concluded that application of the coatings as thin layers using a paintbrush application was essential for a strong adhesion. Using a syringe as an applicator for epoxy as an adhesive and coating, created a large bolus of material that did not effectively bond to the titanium or the stainless steel, and was easily peeled off. However, if applied as a thin layer with a paintbrush, the coating material was distributed over a greater surface area of the sham, provided a lower profile, and demonstrated greater bonding strength due to the lower mass of material.

The electronic resistivity of each non-coated gauge was measured before and after steam sterilization and is demonstrated in **Table 7.5**. The results for each non-coated strain gauge mounted to

| Titanium | Pre - steam | Post - steam |
|---|---|---|
| E | 122.9 (0.8) | 120.3 (2.1) |
| EP42hHT | 119.6 (0.2) | 119.7 (0.4) |
| **Stainless Steel** | | |
| E | 119.6 (0.3) | 119.5 (0.4) |
| EP42hHT | 119.4 (0.3) | 126.2 (2.3) |

**Table 7.5:** Summarized table of the electronic resistivity measurements (Ohms) for the non-coated strain gauges on the titanium shams before and after steam sterilization for Phase 2.

titanium was not statistically different after steam sterilization (P>0.05). A total of 27 strain gauges used epoxy as an adhesive and/or coating. A power analysis for a two-tailed analysis with and alpha of 0.05 yielded a sample size of n=20 for this group. Unfortunately, the thicker geometry of the stainless steel shams limited the ability to quantify resistivity due to limitations in the geometrical dimensions of the test stage. The stage displacement was limited and reached maximal displacement that was not suitable for the stainless steel blocks. Additionally, resistivity measurements were similarly limited for coated gauges as well. However, the Phase 2 results concluded that steam sterilization did not alter the electronic performance of the non-coated gauges as indicated by the resistivity measurements in **Table 7.5**. There was very little loss in resistivity, <5%.

### *7.4.3 Phase 3*

The goal of this phase was to evaluate the material spread and mechanical integrity post-steam sterilization for a selected coating on titanium, stainless steel, and glass hosts. Material spread can be defined as the change in the surface area of the epoxy on the host material (titanium, medical grade stainless steel, or glass) subjected to steam sterilization. Bio-compatible epoxy 301 (**Epo-tech)** was chosen as the coating of choice for further assessment. The titanium and stainless steel shams were of similar size and chemical composition as those used in the previous phases. All substrates were cleaned, degreased, and conditioned in a manner identical to Phase 1. The glass substrate consisted of glass slides that are conventionally used to mount biological tissue sections for histological preparations. Each substrate was marked with a circle 1 cm in diameter. This circle served as the boundary guideline for accurate and repeatable placement of the coatings used in this phase of the study.

The biocompatible epoxy was mixed in the prescribed ratio (4:1, mixture to curing agent) and 1 cc of epoxy in its liquid state was gently applied in a controlled manner using

a syringe to each designated circle onto the substrate. Care was taken not to apply the epoxy beyond the boundary area. Each substrate housing two accurately scribed circular regions of epoxy was digitally photographed and the circular regions were measured using a software image analysis system, (Scion Image, National Institutes of Health, Bethesda, Maryland). To obtain actual circular dimensions, each image was calibrated against known dimensions measured from a standard placed in each photograph. Following this, each substrate with the circular epoxy regions were subjected to steam sterilization in the manner discussed above. Digital photography was repeated for all the substrates post-steam sterilization.

Each area of the epoxy regions was digitally analyzed and quantified for the pre and post-steam sterilization conditions. The horizontal and vertical dimensions of each imaged areas were measured, and an elliptical or circular area analysis was conducted. Descriptive statistics and a student's t-test were used to detect statistical differences in the material spread of the epoxy deposits before and after steam sterilization.

The final phase of the study used the results of Phases 1 and 2 and further evaluated material spread and mechanical integrity after exposure to steam sterilization. **Table 7.6** lists the measured areas of the epoxy deposits before and after steam sterilization. An increase in material spread (less than 10%) was noted for the epoxy mounted to the titanium and stainless steel shams. The glass shams demonstrated a larger degree of material spread (23.6%). However, the amount of material spread for all three host materials was not statistically different between the pre and post-steam sterilization conditions ($p \geq 0.05$).

| | Area Pre-sterilization ($cm^2$) | Area Post-sterilization ($cm^2$) | Percent Increase in Spread |
|---|---|---|---|
| **Titanium** | 2.41 (0.61) | 2.59 (0.57) | 7.5 |
| **Stainless Steel** | 3.03 (0.29) | 3.29 (0.44) | 8.6 |
| **Glass** | 1.44 (0.24) | 1.78 (0.61) | 23.6 |

**Table 7.6:** The areas measured of the epoxy deposits before and after steam sterilization to exam material spread. There was no statistically significant difference between epoxy deposit areas before and after steam sterilization.

## 7.5 Conclusion

Overall, no adverse effects in electronic performance, material spread, and mechanical integrity were observed for the adhesives and coatings after exposure to steam sterilization. This form of sterilization was chosen as the conventional method of sterilization due to its high availability, inexpensive cost, ease of use, efficient nature, and negligible effects upon the test materials. Resistivity served as an ideal indicator to examine the electrical and mechanical integrity of the strain gauges and was shown not to be compromised after sterilization.

The assessment of the coatings demonstrated that the biocompatible epoxy performed favorably as a sterilizible adhesive and coating agent for both titanium and 316L medical grade stainless steel. However, when the epoxy was applied with a syringe as a thick bolus for coating purposes, the coating bonded with the adhesive and formed a firm mass that easily lifted from the metallic shams. The Ep42ht fast curing polymer also performed favorably when used as both an adhesive and coating on the stainless steel, but not as well as the epoxy (coating and adhesive) on titanium. A combination of epoxy and Ep42ht for either an adhesive and/or coating was not ideal. The optimal situation was to use each substrate as both an adhesive and a coating agent to protect each mounted gauge, while maintaining a thin layer of coating. The application of thin layers of coating materials by paintbrush or other controlled processes such as plasma spray or vapor deposition will prevent easy removal of the coating material due to the application of multiple thin layers for coating indications.

Biocompatible epoxy served as a superior adhesive and ideal coating agent when applied as a thin layer. The durable exterior and stiffer elastic modulus of epoxy lends itself to fluid impermeability and resistance to the effects of intense temperatures necessary for

surgical sterilization. One limitation to epoxy is the lack of flexibility of the substrate that could lead to issues of cracking and chipping once *in vivo* related to excessive and repetitive stresses. Furthermore, biocompatible epoxy is readily available and practical for *in vivo* use, as opposed to Ep42ht, which tends to be expensive and difficult to obtain in large quantities.

The future of implantable MEMS relies heavily on the packaging of such devices to insure resistance to decay and degradation of the harsh chemical and mechanical environment of a living system. The chemical, electrical, optical, mechanical, and/or biological interfaces which MEMS devices will encounter must be able to maintain electronic, mechanical, and structural integrity for the eventual implantation and long-term monitoring within a living system. Ideally, generic packaging systems should be developed to house single or multiple modes of implantable MEMS devices along with corresponding electronics that drive each system. Coatings can be applied using plasma spray technologies to ensure a uniform distribution of thin protective layers capable of withstanding repetitive motions and excessive forces.

# CHAPTER VIII

# CONCLUSIONS, STUDY LIMITATIONS, AND FUTURE WORK

## 8.1 Conclusions

Spinal fusion with accompanying spinal instrumentation has been the gold standard for stabilization of the degenerative spinal segment. The ideal outcome of a fusion is to create a balanced environment where the spinal instrumentation provides early stage immobilization to allow for bone incorporation at the site of the bone graft.[6,7,59,83] Once bone has fully incorporated and remodeled at the interbody site, the spinal implant no longer bears a significant portion of the axial load, the load is shared with the bone graft and implant until the fusion site is solidified bone, at which point the load is transferred and borne by the fused site. One of the current challenges with fusion surgery is the ability to determine the status of bone healing during the fusion process using conventional radiographic techniques. Often there is a 20% underestimation of the fusion grade by radiographic assessment. Ideally, a system that can measure the real-time bone healing process of a fusion *in vivo* can determine the status of healing with the necessary accuracy that would make radiographic assessment obsolete.

The development of a microsized implantable biosensor using microelectromechanical sensor technology (MEMS) to monitor *in vivo* biomechanical parameters such as tissue healing has the potential to revolutionize the medical industry. The advantages for

implementing MEMS technology in the development of medical devices include; (1) the ability to microsize medical devices for the potential use of *in vivo* applications, (2) the reproducibility of the devices after a prototype has been developed, (3) the electronic accuracy of MEMS devices, and (4) the ability to manufacturer numerous replicas of each device at low cost.

Currently, MEMS technology is in its infancy. Silicon-based MEMS technology is starting to be utilized in the medical field, as few of the materials used for orthopedic and cardiac implant markets are suitable for use in the fabrication of MEMS devices. Therefore, additional work must be performed to fully characterize the safety and efficacy of implantable MEMS sensors into a living system. Tissue healing can generate many responses *in vivo* that have the potential to be measured and quantified. Changes in the local tissue temperature, chemistry, pressures, and loads may all signal a change in the tissue's response to various stimuli. In the spine, changes in intradiscal pressures represent the degenerative nature of the disc, and can correlate with the biomechanical integrity of the disc. Higher pressures within a disc are associated with an increase in disc degeneration identified by compromised disc hydration and a loss of disc height.[69,86] This would make the disc less efficient in load bearing, thus transferring the loads to other regions of the spine, such as the facets, and further augmenting the degenerative cascade of the motion segment and adjacent segments. Furthermore, bone is a viscoelastic tissue that responds to mechanical stimuli and can be measured in terms of loads and pressures.[91,113, 114, 115]

This dissertation presents the reserach necessary to validate the concept of measuring *in vivo* biomechanical parameters, and the feasibility of using implantable telemetric sensor technology to monitor changes in pressures and axial forces during bone healing. Initially, an *in vitro* model was established to address the feasibility of measuring altered biomechanical parameters during early bone healing. A simulated *in vitro* bone healing model utilizing polymethylmethacrylate (PMMA), (an orthopedic cement that possesses an elastic modulus similar to bone), demonstrated changes in the graft site pressures and axial

loads along the ventral cervical plate that was used to immobilize the fusion site during a conventional anterior cervical fusion procedure. Noticeable differences in the pressure and force trends were observed for different stages of the simulated stages of healing. However, the *in vitro* study described in Chapter 3 demonstrated that pressure served as a better indicator of bone healing due to the direct contact and vicinity of the pressure sensors placed at the location of the bone healing site. The ventral cervical plate that functioned as an active force transducer to monitor the loads along the spine was placed ventral to the bone graft and bone healing site and had divergent fixed screw fixation at this margin. This would have placed a localized compressive load at the ventral margin of the vertebral cortex, thus demonstrating localized compressive loads in the plate that may not be mimicked by the pressures measured at the bone graft healing site. Theoretically, the pressures measured at the bone graft site should increase with simulated bone healing (as observed) and the forces along the ventral plate should decrease with bone healing (not observed). The localized compressive forces related to the divergent screws and accompanying subsidence measured across the bone graft site may have masked the 'offloading' of the plate once bone started to heal and share in the axial support.

The *in vivo* evaluation of monitoring pressure at the bone graft site demonstrated that monitoring altered biomechanical pressures such as pressures and forces in a wireless fashion was feasible within a living system. Although a solid fusion was not achieved at the bone graft site after six months in the goat cervical spines due to unforeseen complications, the pressures measured at the bone graft site did reveal the presence of the pseudarthrosis. Erratic pressures were observed following the initial subsidence phase of healing, during which interface pressures were elevated. This erratic pressure fluctuation was intuitively associated with motion and pseudoarthrosis. If stability were present, motion at the graft site would not have occurred and fluctuations of pressure at this site would similarly not be observed. Erratic fluctuations of pressure were consistent with pseudoarthrosis, as demonstrated radiographically, while elevations of pressure were consistent with early healing

and inflammation. A cascade of events occurred with the ensuing non-union. A rise in pressure was observed during the early stages of bone healing, however, once the bone graft started to fail and early signs of a non-union were forming, the pressures revealed erratic patterns indicative of excessive motions across the graft site. As the bone graft started to resorb during the pseudarthrosis cascade, the motions across the bone graft increased and the pressures grew irregular. Overall, the *in vivo* study established a model that provided a living environment that was capable of monitoring altered biomechanical parameters over time, and have the potential to serve as markers to determine the status of tissue, whether it is a positive or negative outcome.

It appears that both pressure and load can serve as indicators for bone healing and fusion incorporation. The later chapters (5-7) in this work evaluate the feasibility of incorporating MEMS technology into the fabrication of microchips for long-term implantation into living systems. Due to the complications associated with conventional telemetric medical devices, the future potential of developing a microscopic, wireless, implantable biosensor is an attractive prospect for orthopedic applications. However, general concepts of feasibility for implanting MEMS sensors such as; packaging, sterilization, and biocompatibility must be assessed to determine the potential of long-term implantation and surrounding tissue reaction to MEMS based biosensors. The electronic integrity of MEMS pressure sensors post-sterilization was evaluated to ensure that conventional sterilization techniques (steam or ethylene oxide) will not damage the electronic capacity of the microchips, but will provide a sterile sensor with minimal risk of infection. The epoxy and Ep42ht polymeric coatings examined for packaging force transducers and potential MEMS sensors served as suitable adhesive and coating materials that were not compromised by conventional sterilization means, whereas, polyurethane coatings demonstrated permeability to fluids and would not be an ideal coating material. Finally, biocompatibility was evaluated by implanting a series of MEMS fabrication materials and MEMS pressure sensors into the intervertebral disc and vertebral bone for a maximum of six months. Histological analysis

after six-months of implantation into a series of goat models did not reveal evidence of any adverse foreign body response, inflammation, infection, or excessive fibrous tissue reaction in the caprine spinal tissue to the implanted MEMS materials and MEMS pressures sensors.

## 8.2 Study Limitations

There were limitations with respect to the work presented in this dissertation. The *in vivo* goat study provided the greatest challenges. The current lack of a commercially available, viable, wireless telemetric pressure sensor that could withstand long-term implantation limited the capabilities of recording pressure alterations for long term bone healing. Additionally, radiographic identification of a microscopically sized MEMS chip posed significant challenges. The radiographic capabilities of MEMS sensors and MEMS materials were investigated and demonstrated that the microscopic nature of the sensors did not provide a dense enough material to be detected by radiographic means **(Figures 8.1 and 8.2)**. The MEMS materials (10mm x 10mm x 0.5μm) were placed in saline beakers and radiographed, followed by placement of the MEMS sensors into the intervertebral disc with repeated radiographic imaging. A top view of the sensors and MEMS materials were not visible radiographically. A sagittal (lateral) view of an implanted spinal segment did reveal the presence of the MEMS chip (silicon 10mm x 10mm x 0.5μm), however, this would not suffice for post-surgical assessment of sensor placement.

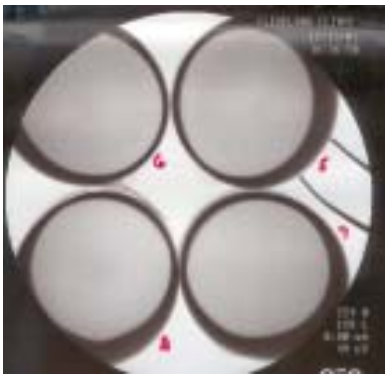

**Figure 8.1:** Top View: MEMS chips in a saline bath did not demonstrate visibility radiographically.

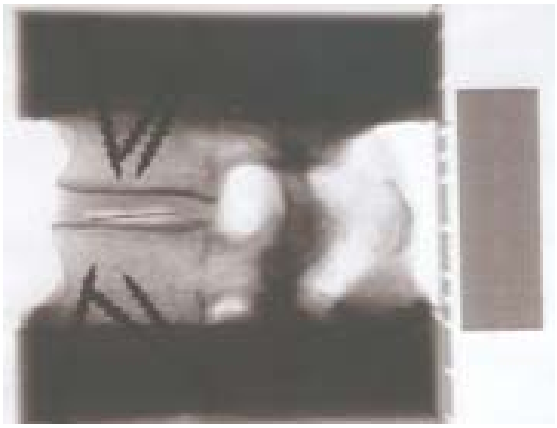

**Figure 8.2:** Side View: Placement of a MEMS chip in the intervertebral disc of a human cadaveric lumbar segment. The side of the chip is visible due to the density of the chip in that view.

Realistically, MEMS sensors will be significantly smaller than the 10mm x 10mm x 0.5µm sized MEMS wafer chips used in this radiographic evaluation. Therefore, sagittal visualization capabilities will be inadequate for post-surgical assessment of chip location. The sensors must potentially be visible in the oblique and anteroposterior radiographic planes for tracking chip positioning during tissue healing, as this would be essential to ensure the warranted measurements are being accurately monitored.

The available telemetric technology used in this dissertation demonstrated the feasibility of *in vivo* recordings, yet the adverse reactions of the local tissue to the catheter and gel-based sensor technology interfered with the tissue healing process. Furthermore, the telemetric ventral cervical plate that utilized strain gauges to form a load transducer for recording load transmission along the cervical plate also exhibited challenges with respect to potential wire breakage and gauge delamination if used for long-term *in vivo* implantation. Once implanted into the goat model, there was cracking of the polymeric coating (parylene and silastic coatings) within one week of implantation **(Figures 8.3A and 8.3B)**.

This resulted in immediate fluid infiltration and failure of the ventral plate electronics housed in the goat neck. Although, the load transducer along the ventral cervical plate

demonstrated in the *in vitro* study that load transmission along the plate can be quantified, the current means of implantable technology with respect to pliable coatings is still inadequate to resist cracking and biodegradation, resulting in failure to sustain long term implantation. Thus, there is a current void in availability of compliant biocompatible device coatings and adhesives that will prevent cracking, crazing, biodegradation, delamination, and wire breakage for MEMS devices and that would prevent fluid infiltration into the electronics. However, it could be concluded that the parylene and silicone combination used in the present study was not ideal for this application.

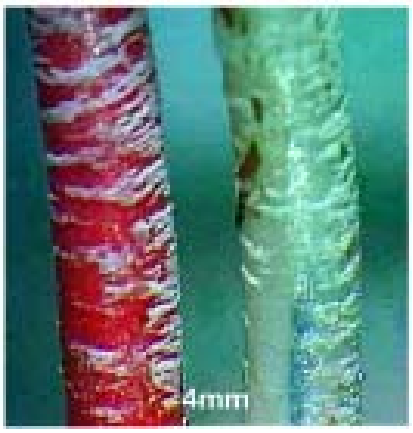


**Figure 8.3A:** Checking and crazing of the parylene and silastic coating on the wires leading to the ventral plate.

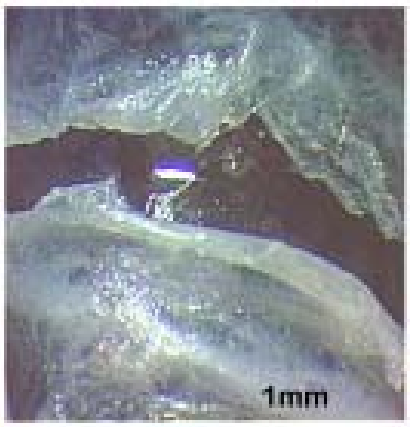


**Figure 8.3B:** Large cracks observed in the coating exposing the wire leading to the battery pack.

## 8.3 Future Work

Nevertheless, the 'proof of concept' goal of this study, that is the ability to monitor in vivo, altered biomechanical parameters (pressure and force) related to early bone healing, was achieved. The limitations discussed above further reiterate the need for additional research to develop a completely wireless encapsulated microsized biosensor that can be implanted long-term to further evaluate implant performance for numerous technologies, including motion preserving orthopedic devices. Improved and efficient clinical methods for telemetrically

assessing *in vivo* pressures are eagerly anticipated, thus leading to the development of a microsized implantable biosensor using MEMS technology. An ideal implantable coating of these sensors that resist long term biodegradation, crazing, and cracking during implantation that does not cause adverse tissue reactions requires additional research. Novel polymeric coatings that possess the compliant properties to respond to varied loading rates are on the forefront of development and are not yet commercially available for human use. The challenges discussed for radiographic assessment of the MEMS chips post-operatively require additional innovation. Deposition of metallic markers of a substantial size that will suit radiographic visibility could alleviate this limitation. Currently, the orthopedic implant industry incorporates tantalum markers in their polymeric implants that are less than 1mm in diameter and allow for post-surgical radiographic visibility. Finally, optimization of the electronic capabilities and data transmission of an implantable MEMS sensor are needed to accommodate various implantation depths and allow for multiple sites of tissue recordings.

Overall, this dissertation work contributed the necessary groundwork to validate the potential for *in vivo* monitoring of bone healing. The concept of measuring the mechanics associated with real-time tissue healing can eliminate the need for conventional post-symptomatic diagnostic technologies (i.e. radiographs, MRI, CT). Further evaluation of the MEMS materials combined with novel compliant coatings and optimized electronics used for the potential fabrication of such biosensors is needed to increase the lifespan of implantable microsized biosensors.

A series of peer reviewed publications were generated from the work presented in this dissertation. The feasibility of incorporating MEMS into miniature sensing platforms to monitor in vivo tissue healing was validated by the early in vitro and in vivo studies previously discussed in Chapters 3 and 4, which were published in the Journal of Neurosurgery, Spine 2007 and the Spine Arthoplasty Society Journal, 2008.[35,36] Once it had been determined that the concept of using implantable sensors to monitor fusion healing was feasible, the factors that can affect MEMS lifespan during long-term implantation were

investigated as reported in Biomedical Microdevices in 2003 and 2007.[37,38] Clearly, MEMS technology offers the miniaturization necessary to develop small sensing platforms that will not negatively impact the surrounding tissue environment, while utilizing biocompatible materials to fabricate small sensors that can be sterilized for long-term tissue implantation.

## BIBLIOGRAPHY


1. Adams MA, Dolan P: A Technique For Quantifying the Bending Moment Acting on the Lumbar Spine In Vivo. J. Biomechanics 24:117-126, 1991.

2. Ahn CH, Choi JW, Beaucage G, Nevin JH, Lee JB, Puntambekar A, and Lee JY: "Disposable smart lab on a chip for point-of-care clinical diagnostics," Proceedings of IEEE, vol. 92, pp. 154-173, 2004.

3. Akamaru T, Kawahara N, Yoon ST, Minamide A, Kim KS, Tomita K, and Hutton WC: Adjacent Segment Motion after a Simulated Lumbar Fusion in Different Sagittal Alignments. Spine 28(14), 1560-1566. 2003.

4. Al Hami S: Cervical monosegmental interbody fusion using titanium implants in degenerative, intervertebral disc disease. Minim. Invasive Neurosurg 42:10-17, 1999.

5. Benzel E, Ferrara L, Roy S, Fleischman A: Biomaterials and implantable devices: discoveries in the spine surgery arena. Clinical Neurosurgery 49:209-225, 2002.

6. Benzel E, Ferrara L: Cervical interbody fusion: J. Neurosurgery 94:180, 2001.

7. Benzel E, Lastra J, Kalfas I, Bak K, Ferrara L: The biomechanics of interbody fusion and the shortcomings of lumbar fusion with cages and interbody bone dowels. Clinical Neurosurgery 47:557-588, 2000.

8. Benzel, E, Ferrara, L, Roy, S, and Fleischman: A: Micromachines in Spine Surgery. Spine 15(29), 6-601. 3-15-2004.

9. Bishop, RC and Moore, KA: Anterior Cervical Interbody Fusion Using Autogeneic and Allogeneic Bone Graft Substrate: A Prospective Comparative Analysis. J Neurosurg (Spine) 85, 206-210. 1996.

10. Black J: The Inflammatory Process, in Black J (ed): Biological Performance of Materials: Fundamentals of Biocompatibility, ed 3. New York: Marcel Dekker, Inc.; pp. 131-154, 1999.

11. Blumenthal S, Gill K: Can lumbar spine radiographs accurately determine fusion in postoperative patients? Correlation of routine radiographs with a second surgical look at lumbar fusions. Spine 18:1186-1189, 1993.

12. Bragin A, Hetke J, Wilson CL, Anderson D.J, Engel Jr. J, and Buzsaki G: "Multiple site silicon-based probes for chronic recordings in freely moving rats: implantation, recording and histological verification," Journal of Neuroscience Methods, vol. 98, pp. 77-82, 2000.

13. Brighton C: Principles of Fracture Healing. St. Louis, C.V. Mosby, pp 60-82, 1984.

14. Brodsky A, Kovalsky E, Khalil M: Correlation of radiologic assessment of lumbar spine fusions with surgical exploration. Spine S261-S265, 1991.

15. Burny F, Donkerwolcke M, Moulart F, Bourgois R; Puers R, Van Schuylenbergh, Barborosa M, Paiva O, Rodes F, Begueret JB, Lawes P: Concept, design, fabrication of smart orthopaedic implants. Medical Engineering & Physics 22:469-479, 2000.

16. Burr DB, Milgrom C, Milgrom C, Fyhrie D, Forwood M, Nyska M, Finestone A, Hoshaw S, Saiag E, Simkin A: In Vivo Measurement of Human Tibial Strains during Vigorous Activity. Bone 18:405-410, 1996.

17. Burr DB, Schaffler MB, Yang KH, Fyhrie D, Yang, KH, Wu, DD, Lukoschek, M, Kandzari, D, Sivaneri, N, Blaha, JD, Radin, EL: The Effects of Altered Strain Environments on Bone Tissue Kinetics. Bone 10:215-221, 1989.

18. Carter, DR, Blenman, PR, and Beaupre, GS; Correlations between Mechanical Stress History and Tissue Differentiation in Initial Fracture Healing. J Orthopaedic Research 6, 736-748. 1988.

19. Chatzandroulis S, Tsoukalas D, Neukomm P: A Miniature Pressure System with a Capacitive Sensor and a Passive Telemetry Link for Use in Implantable Applications. Journal of Microelectromechanical Systems 9:18-23, 2000.

20. Choi, MG, Koh, HS, Kluess, D, O'Connor, D, Mathur A, Truskey GA, Rubin J, Zhou DXF, and Sung KL: Effects of Titanium Particle Size on Osteoblast Functions In Vitro and In Vivo. Proc Natl Acad Sci U S A 102(12), 4578-4583. 3-22-2005.

21. Chow DH, Luk KD, Evans JH, Leong JC: Effects of Short Term Anterior Lumbar Interbody Fusion on Biomechanics of Neighboring Unfused Segments. Spine 21, 549-555. 1996.

22. Claes, L, Augat, P, Suger, G, and Wilke, HJ: Influence of Size and Stability of the Osteotomy Gap on the Success of Fracture Healing. J. Orthop Res 15, 577-584. 1997.

23. Cowin S: Bone Mechanics. Boca Raton: CRC Press, Inc., pp 260-262, 1989.

24. Cowin, S. Bone Stress Adaptation Models. J. Biomechanical Eng 115, 528-533, 2005.

25. Cunningham, B, Orbegoso, CM, Dmitriev, AE, Hallab, J, Sefter, J C, Asdourian, P, and McAfee, PC: The Effect of Spinal Instrumentation Particulate Wear Debris: An In Vivo Rabbit Model and Applied Clinical Study of Retrieved Instrumentation Cases. The Spine Journal 3, 19-32. 2003.

26. Cunningham, B, Orbegoso, CM, Dmitriev, AE, Hallab, J, Sefter, and McAfee, P C: The effect of titanium particulate on development and maintenance of a posterolateral spinal arthrodesis. Spine 27(18), 1971-1981, 2002.

27. Dario P, Carrozza MC, Benvenuto A, et al: Microsystems in biomedical applications. J Micromech Microeng 10:235-244, 2000.

28. Dekutoski MB, Schendel MJ, Ogilview JW, Olsewski JM, Wallace LJ, Lewis JL: Comparison of An In Vivo and In Vitro Adjacent Segment Motion after Lumbar Fusion. Spine 19, 1745-1751. 1994.

29. DiAngelo, DJ, Foley, KT, Vossel, KA, Rampersaud, YR, and Jansen, TH: Anterior Cervical Plating Reverses Load Transfer through Multi-level Strut-grafts. Spine 25(7), 783-795. 4-1-2000.

30. Donaldson PEK: Twenty Years of Neurological Prosthesis-Making. J.Biomed.Eng. 9:290-298, 1987.

31. Edell DJ, Toi VV, McNeil VM, Clark, LD: Factors influencing the biocompatibility of insertable silicon microshafts in cerebral cortex. IEEE Trans Biomed Eng 39:635-643, 1992.

32. Elfstrom, G, Eng, et al: Telemetry Recordings of Forces in the Harrington Distraction Rod: A Method for Increasing Safety in the Operative Treatment of Scoliosis Patients. Clinical Orthopaedics and Related Research 93:158-172, 1973.

33. Fairand BP: Radiation sterilization for healthcare products: x-ray, gamma, and electron beam. Boca Raton, FL: CRC Press, 2002.

34. Fay (Ferrara) L, Kao H, Yuan D, Cassidy J, McLeod W, Edwards W: Evaluation of a new fixation technique for posterior cervical fusion in an in vivo sheep model. Journal of Long-term Effects of Medical Implants 4:88-93, 1994.

35. Ferrara LA, Gordon I, Fleischman A, Schlenk R, Bauer T, Togawa D, Roy S, Benzel EC, In Vivo Assessment of Bone Graft/Endplate Contact Pressure in a Caprine Interbody Pseudarthrosis Model: A Preliminary Biomechanical Characterization of the Fusion Process for the development of a MEMS Biosensor, SAS Journal, Winter 2008, Vol. 2, Issue 1.

36. Ferrara LA, I. Gordon I, Coquillette M, Milks R, Fleischman AJ, Roy S, Goel VK, Benzel EC, A preliminary biomechanical evaluation in a simulated spinal fusion model. Laboratory investigation, Journal of Neurosurgery Spine., November, Vol. 7 (5), Issue 5, 2007, pp:542-548.

37. Ferrara L, Fleischman A, Tokogawa D, Bauer, T, Zorman, C, Benzel, E, Roy, S, Effects Of Biomedical Sterilization Processes on Performance Characteristics of MEMS Pressure Sensors Biomedical Microdevices 9:809, 2007.

38. Ferrara LA, Fleischman AJ, Togawa D, Bauer TW, Benzel EC, and Roy S, "An in vivo biocompatibility assessment of MEMS materials for spinal fusion monitoring," Biomedical Microdevices, vol. 5, pp. 297-302, 2003.

39. Fleischman AJ, Modi R, Nair, Talman AJ, Lockwood G, and Roy S: "Miniature high frequency focused ultrasonic transducers for minimally invasive imaging procedures," Sensors and Actuators, A: Physical, vol. 103, pp. 76-82, 2003.

40. Flick B, Orglmeister R: A Portable Microsystem-Based Telemetric Pressure and Temperature Measurement Unit. IEEE Transactions on Biomendical Engineering 47:12-16, 2000.

41. Foley KT, DiAngelo DJ, Rampersaud YR, Vossel KA, and Jansen TH.: The In Vitro Effects of Instrumentation on Multilevel Cervical Strut-Graft Mechanics. Spine 24(22), 2366-2376, 1999.

42. Ghalambor N, Cho DR, Goldring SR, Nihal A, and Trepman, E: Microscopic metallic wear and tissue response in failed titanium hallux metatarsophalangeal implants: two cases. Foot and Ankle International 23(2), 158-163, 2002.

43. Goodman, S. B., Huie, B., and Song, Y. Loosening and Osteolysis of Cemented Joint Arthroplasties. Clin.Orthop. 337, 149-163, 1997.

44. Goodship AE and Kenwright J: The Influence of Induced Micromovement Upon the Healing of Experimental Tibial Fractures. J.Bone Joint Surg 67B, 650-655, 1985.

45. Graichen F, Bergmann G, Rohlmann A: Patient monitoring system for load measurement with spinal fixation devices. Med Eng Phys 18:167-174, 1996.

46. Grass M., Kohler, TH, and Proksa, R: 3D cone-beam CT reconstruction for circular trajectories. Phys Med Biol 45, 329-327. 2000.

47. Grayson ACR., Shawgo R S., Johnson AM, Flynn NT, Li Y, Cima MJ, and R. Langer, "A BioMEMS review: MEMS technology for physiologically integrated devices," Proceedings of IEEE, vol. 92, pp. 6-21, 2004.

48. Gutwein LG, and Webster TJ: Increased viable osteoblast density in the presence of nanophase compared to conventional alumina and titanium particles. Biomaterials 25, 4175-4183. 2004.

49. Haher T, Valdevit A, and Nucci R: The Subsidence of Intervertebral Spacer Devices Due to Cyclic Loading. World Spine III, Rio de Janeiro, Brazil, 8-2-2005.

50. Hampson L, Goodship A, Shah J, Lanyon LS: Bone deformation recorded in vivo from strain gauges attached to the human tibial shaft. Acta orthop.scand.256-268, 1975.

51. He E, Meng YC, Tai CM, Rutherglen J, Erickson, and J Pine: “Parylene neuro-cages for live neural networks study,” Proceedings of the 2003 International Conference on Solid State Sensors, Actuators and Microsystems (Boston, MA), pp. 995-998, 2003.

52. Health Research International and Division of Personal Medical Systems Inc. Opportunities in the US Fusion Spinal Market. 104-1-US-0203. 2003.

53. Hydbring E, Cvek K, Olsson K: Telemetric registration of heart rate and blood pressure in the same unrestrained goats during pregnancy, lactation and the non-pregnant, non-lactating period. Acta Physiol Scand 165:141, 2003.

54. Hydbring E, Macdonald E, Olsson K: Radiotelemetrically recorded blood pressure and heart rate changes in relation to plasma catecholamine levels during parturation in the conscious, unrestrained goat. Acta Physiol Scand 161:295-302, 1997.

55. Ito M, Fay (Ferrara) L, Ito Y, Yuan MR, Edwards W, Yuan H: The effect of pulsed magnetic fields on instrumented posterolateral spinal fusion and device-related stress shielding. Spine 22:382-388, 1997.

56. Ji J, Cho ST, Zhang Y, Najafi K, and Wise KD, “An ultraminiature CMOS pressure sensor for a multiplexed cardiovascular catheter,” Proceedings of the 1991 International Conference on Solid-State Sensors and Actuators (San Francisco, CA), pp. 1018-1020, 1991.

57. Junqueira LC, Carneiro J: Basic Histology, 10th edition Text and Atlas, ed 10. New York: Lange Medical Books McGraw-Hill, pp 95-100, 2003.

58. Kaden B, Schramm J, Fuhrmann G, Hoffmann CH: Titanium intervertebral disc and instrumentation for fusion in anterior cervical discectomy. Technical note. Neurosurg Rev. 18:25-29, 1995.

59. Kanayama M, Cunningham B, Weis J: Maturation of the posterolateral spinal fusion and its effect on load-sharing of spinal instrumentation. J.Bone Joint Surg (Am) 1710-1720, 1997.

60. Ko W: Packaging of Microfabricated Devices and Systems. Materials Chemistry and Physics 42:169-175, 1995.

61. Ko W: The future of sensor and actuator systems. Sensors and Actuators A 56:193-197, 1996.

62. Ko WH, Meyrick CW, and Rekate HL: “Cerebrospinal fluid control system,” Proceedings of the IEEE, vol. 76, pp. 1226-1235, 1988.

63. Kotzar G, M. Freas M, Abel P, Fleischman A, Roy S, C. Zorman C, Moran JM, and Melzak J: “Evaluation of MEMS materials of construction for implantable medical devices,” Biomaterials, vol. 23, pp. 2737, 2002.

64. Kricka LJ: Miniaturization of Analytical Systems. Clinical Chemistry 44:2008-2014, 1998.

65. Lang, W: Reflexions on the future of microsystems. Sensors and Actuators 72:1-15, 1999.

66. Lanyon LE, Hampson WG, Goodship AE, Shah, JS: Bone Deformation Recorded In Vivo From Strain Gauges Attached to the Human Tibial Shaft. Acta orthop. scand. 46:256-268, 1975.

67. Latson, L, Kuban, B, Bryan, J, Stredney, D, Davros, Midura, R, Apte, S, and Powell, K. X-ray Micro-Computed Tomography System: Novel Applications in Bone Imaging. Engineering Medicine and Biology Society International Meeting. 10-2-2003.

68. Ledet E, Sachs B, Brunski J, Gatto C, Donzelli P: Real-Time In Vivo Loading in the Lumbar Spine. Spine 25:2595-2600, 2000.

69. Lee SH, Derby, R, Chen, R, Seo, KS, and Kim, MJ: In Vitro Measurement of Pressure in Intervertebral Discs and Annulus Fibrosus with and without Annular Tears during Discography. The Spine Journal 4, 614-618. 2004.

70. Leoni L, Desai TA: Nanoporous biocapsules for the encapsulation of insulinoma cells: biotransport and biocompatibility considerations. IEEE Trans Biomed Eng 48:1335-1341, 2001.

71 Liew LA and Bright VM: “Disposable CMOS catheter-tip pressure sensor for intracranial pressure measurement,” presented at 2000 IEEE-EMBS International Special Topic Conference on Microtechnologies in Medicine and Biology, Lyon, France, 2000.

72. Malshe AP, O’Neal C, Singh SB: Challenges in the Packaging of MEMS. The International Journal of Microcircuits and Electronic Packaging 22:233-239, 1999.

73. Mata AJ, Fleischman AJ, Roy S, Biomedical Microdevices 7, 28 1-293 (2005).

74. McAfee P C, Cunningham B, Dmitriev A E, Hu N, Woo KS, Cappuccino A, and Pimenta L: Cervical Disc Replacement-porous Coated Motion Prosthesis: A Comparative Biomechanical Analysis Showing the Key Role of the Posterior Longitudinal Ligament. Spine 28(20), S176-S185. 2003.

75. McAllister DV, Allen MG, Prausnitz MR: Microfabricated microneedles for gene and drug delivery. Annu Rev Biomed Eng 2:289-313, 2000.

76. Meadows TH, Bronk JT, Chao EYS, and Kelly PJ. Effect of Weight-Bearing on Healing of Cortical Defects in the Canine Tibia. J.Bone Joint Surg (Am) 72A, 1074-1080. 1990.

77. Medtech Insight and Health Research International. Advances in Spinal Fusion and Dynamic Stabilization Products A308, 1-179. 2007.

78. Millenium Research Group. US Markets for Spinal Implants 5413. 2006.

79. Nachemson A, Elfstrom G: Intravital Wireless Telemetry of Axial Forces in Harrington Distraction Rods in Patients with Idiopathic Scoliosis. The Journal of Bone and Joint Surgery 53-A:445-465, 1971.

80. Nachemson A: The load on lumbar discs in different positions of the body. Clinical Orthopaedics 45:107, 1966.

81. Najafi N, and Ludomirsky A: “Initial animal studies of a wireless, battery-less, MEMS implant for cardiovascular applications,” Biomedical Microdevices, vol. 6, pp. 61-64, 2004.

82. O’Sullivan, ME, Chao, EYS, and Kelly, PJ: Current Concepts Review: The Effects of Fixation on Fracture Healing, J. Bone Joint Surg 71A, 306-310. 1989.

83. Oktenoglu T, Ozer A, Ferrara L, Andalkar N, Sarioglu A, Benzel E: Effects of cervical spine posture on axial bearing ability: A biomechanical study. Spine 94:108-114, 2001.

84. Pan JY: “Reliability considerations for the BioMEMS designer,” Proceedings of IEEE, vol. 92, pp. 174-184, 2004.

85. Petersen K: From microsensors to microinstruments. Sensors and Actuators A 56:143-149, 1996.

86. Polga DJ, Beaubien BP, Kallemeier PM, Schellhas KP, William D, Buttermann GR, and Wood KB: Measurement of In Vivo Intradiscal Pressure in Healthy Thoracic Intervertebral Discs. Spine 29(12), 1320-1324. 6-15-2004.

87. Pospiech J, Stolke D, Wilke H, Claes L: Intradiscal Pressure Recordings in the Cervical Spine. Neurosurgery 44:379-384, 1999.

88. Rand JA, An KN, and Chao EYS Kelly PJ: A Comparison of the Effect of Open Intramedullary Nailing and Compression-Plate Fixation on Fracture Site Blood Flow and Future Union. J.Bone Joint Surg 63A, 427-442. 1981.

89. Rebello KJ: “Applications of MEMS in surgery,” Proceedings of IEEE, vol. 92, pp. 43-55, 2004.

90. Reichert M, and Young JH: “Sterilization technology for the health care facility,” 2nd ed. Gaithersburg, MD: Aspen Publishers, 1997.

91. Rohlmann A, Zander T, and Bergmann G: Effects of fusion-bone stiffness on the mechanical behavior of the lumbar spine after vertebral body replacement. Clin.Biomech. 21(3), 221-227. 2006.

92. Rohlmann A, Graichen F, Bergmann G: Loads on an Internal Spinal Fixation Device During Physical Therapy. Physical Therapy 82:44-51, 2002.

93. Rohlmann A, Ulrike A, Graichen F: Loads on an internal spinal fixation device during sitting. Journal of Biomechanics 34:989-993, 2001.

94. Rohlmann A, Bergmann G, Graichen F, Weber, U: Changes in the loads on an internal spinal fixator after iliac-crest autograft. Journal of Bone and Joint Surgery 82-B:445-449, 2000.

95. Rohlmann A, Graichen F, Bergmann G: Influence of load carrying on loads in internal spinal fixators. Journal of Biomechanics 33:1099-1104, 2000.

96. Rohlmann A, Graichen F, Weber U, Bergmann G: Monitoring In Vivo Implant Loads with a Telemetrized Internal Spinal Fixation Device. Spine 25:2981-2986, 2000.

97. Rohlmann A, Calisse J, Bergmann G: Internal Spinal Fixator Stiffness Has Only a Minor Influence on Stresses in the Adjacent Discs. Spine 24:1192-1196, 1999.

98. Rohlmann A, Bergmann G, Graichen F: Comparison of loads on internal spinal fixation devices measured in vitro and in vitro. Med Eng Phys 19:539-546, 1997.

99. Rohlmann A, Bergmann G, Graichen F: Loads on an Internal Spinal Fixation Device during Walking, J. Biomechanics 30:41-47, 1997.

100. Rohlmann A, Riley LH, III, Bergmann G, Graichen, F: In vitro load measurement using an instrumented spinal fixation device. Med Eng Phys 18:485-488, 1996.

101. Rohlmann A, Bergmann G, Mayer HM: Telemeterized Load measurement Using Instrumented Spinal Internal Fixators in a Patient with Degenerative Instability. Spine 20:2683-2689, 1995.

102. Romig AD, Dressendorfer PV, Palmer DW: High Performance Microsystem Packaging: A Perspective. Microelectron.Reliab. 37:1771-1781, 1997.

103. Ross, T, Capen, D, and Hayes, W: Clinical Significance of Graft Subsidence in Smith-Robinson Anterior Cervical Discectomy and Fusion. 10th Annual Conference of the North American Spine Society, Washington D.C. 1995.

104. Roy S, and Fleischman AJ: “Cytotoxicity evaluation for microsystems materials using human cells,” Sensors and Materials, vol. 15, pp. 335-40, 2003.

105. Roy S, Ferrara L, Fleischman A, Benzel E: Microelectromechanical systems and Neurosurgery: A new era in a new millennium. Neurosurgery 49:779-798, 2001.

106. Salzberg A, Bloom M, Mourlas N: Microelectrical Mechanical Systems in Surgery and Medicine. J Am Coll Surg 194:463-476, 2002.

107. Sarmiento A, Sobol PA, Hoy AL, Ross SDK, Racette WL, and Tarr RR:. Prefabricated Functional Braces for the Treatment of Fractures of the Tibial Diaphysis. J. Bone Joint Surg 66A, 1328-1339. 1984.

108. Seeley RS: The future of medical microelectromechanical systems. Medical electronics manufacturing. 2003. Ref Type: Internet Communication.

109. Serhan H, Slivka M, Albert T: Is galvanic corrosion between titanium alloy and stainless steel spinal implants a clinical concern? Spine J 4:379-387, 2004.

110. Service R: Can Sensors Make a Home in the Body. Science 297:962-963, 2002.

111. Shubavyev FI, Branemark R, Steinauer BS, and Myers RR: Titanium Implants Induce Expression of Matrix Metalloproteinases in Bone During Osseointegration. Journal of Rehabilitation Research and Development 41(6A), 757-766. 2004.

112. Smit T: The use of a quadruped as an in vivo model for the study of the spine - biomechanical considerations. Eur Spine J. 11:137-144, 2002.

113. Spencer DL, Ray, RD, Spigos DG, and Kanakis C: Intraosseous Pressure in the Lumbar Spine. Spine 6(2), 159-161. 1981.

114. Szivek J, Roberto R, Slack J, Majeed B: An Implantable Strain Measurement System Designed to Detect Spine Fusion. Spine 27:487-497, 2002.

115. Szivek J, Magee F: A Long-Term In Vivo Bone Strain Measurement Device. Journal of Investigative Surgery 2:195-206, 1989.

116. Torpey BM, Dormans JP, Drummond DS: The use of MRI-compatible titanium segmental spinal instrumentation in pediatric patients with intraspinal tumor. J Spinal Disord 8:76-81, 1995.

117. Turkof E, Bellolo H, Monsivais J: The anatomy of the vertebral column of the Nubian goat: a peculiarity of the arcus vertebrae C5, C6, and C7 forming large spatia interarcualia. Can J Vet Res. 58:156, 1994.

118. Turner JN, Shain W, Szarowski DH: Cerebral Astrocyte response to Micromachined silicon implants. Exp. Neurol 156:33-49, 1999.

119. Tye GW, Graham RS, Broaddus WC, and Young HF: Graft Subsidence After Instrument-assisted Anterior Cervical Fusion. J Neurosurg (Spine) 2(97), 186-192, 2002.

120. Uppal, G, Akmakjian, J, and Clarke, L: Instrumented Decompression and Fusion of the Cervical Spine. 25th Annual Meeting of the Cervical Spine Research Society, Rancho Mirage, California 1997.

121. Vazquez-Seoane P, Yoo J, Zou D: Interference screw fixation of cervical grafts: a combined in vitro biomechanical and in vivo animal study. Spine 18:946-954. 1993.

122. Von Knoch M, Jewison DE, Sibonga JD: The effectiveness of polyethylene versus titanium particles in inducing osteolysis in vivo. J Orthopaedic Research 22:237-243, 2004.

123. Voskerician G, Shawgo RS, Hiltner PA: In vivo inflammatory and wound healing effects of gold electrode voltammetry for MEMS micro-reservoir drug delivery device. IEEE Trans Biomed Eng 51:627-635, 2004.

124. Voskerician G, Shive MS, Shawgo RS: Biocompatibility and biofouling of MEMS drug delivery devices. Biomaterials 24:1959-1967, 2003.

125. Wagner B: Principles of Development and Design of Microsystems. End Surg. 3:204-209, 1995.

126. Wang JC, Zou D, Yuan H, and Yoo J: A Biomechanical Evaluation of Graft Loading Characteristics for Anterior Cervical Discectomy and Fusion: A Comparison of Traditional and Reverse Grafting Techniques. Spine 23(22), 2450-2454. 1998.

127. Wang JL, Panjabi MM, and Isomi T: The Role of Bone Graft Force in Stabilizing the Multilevel Anterior Cervical Spine Plate System. Spine 25(13), 1649-1654. 2000.

128. What are the Mediators (Cellular, Molecular) of the Local and Systemic Biologic Reactions to Wear Debris?, Ed. American Association of Orthopedic Surgeons, pp 71-85, 2001.

129. Wise KD, Anderson DJ, Hetke JF, Kipke DR and Najafi K, “Wireless implantable microsystems: high-density electronic interfaces to the nervous system,” Proceedings of IEEE, vol. 92, pp. 76-97, 2004.

130. Wittenberg RH, Shea M, Kramer J, and Hayes WC: Biomechanical studies of bisegmental lumbosacral stabilization using the internal fixator or PMMA-simulated fusion. Z Orthop Ihre Grenzgeb 133(2), 123-129. 1995.

131. Wolff J: Des Gesetz der transformation der knocken. Berlin: 1884.

132. Wuisman DM, Smit T: Resorbable cages for spinal fusion: an experimental goat model. J Neurosurg (Spine) 4:433-439, 2002.

133. Yamaguchi K, Konishi H, Hara S: Biocompatibility studies of titanium-based alloy pedicle screw and rod system: histological aspects. Spine J 1:260-268, 2001.

134. Yang, K and King, A: 1984 Volvo award in biomechanics: Mechanisms of facet load transmission as a hypothesis for low-back pain. Spine 9(6), 557. 1984.

135. Zdeblick T, Cooke M, Wilson D, Kunz, DN, McCabe, RP: Anterior Cervical Discectomy, Fusion, and Plating: A Comparative Animal Study. Spine 18:1974-1983, 1993.

136. Zdeblick T, Cooke M, Wilson D, Kunz, DN, McCabe RP, Ulm M.J. Vanderby R: Anterior Cervical Discectomy and Fusion. Spine 17:S418-S426, 1992.

137. Zdeblick T, Ghanayem A, Rapoff A, Swain, C, Bassett T, Cooke M, Markel M: Cervical Interbody Fusion Cages: An Animal Model With and Without Bone Morphogenetic Protein. Spine 23:758-766, 1998.